Geodynamo theory and simulations

Paul H. Roberts

Institute of Geophysics and Planetary Physics, University of California, Los Angeles, California 90095

Gary A. Glatzmaier

Department of Earth Sciences, University of California, Santa Cruz, California 95064

80 years ago, Joseph Larmor planted the seed that grew into today's imposing body of knowledge about how the Earth's magnetic field is created. His simple idea, that the geomagnetic field is the result of dynamo action in the Earth's electrically conducting, fluid core, encountered many difficulties, but these have by now been largely overcome, while alternative proposals have been found to be untenable. The development of the theory and its current status are reviewed below. The basic electrodynamics are summarized, but the main focus is on dynamical questions. A special study is made of the energy and entropy requirements of the dynamo and in particular of how efficient it is, considered as a heat engine. Particular attention is paid to modeling core magnetohydrodynamics in a way that is tractable but nevertheless incorporates the dynamical effects of core turbulence in an approximate way. This theory has been tested by numerical integrations, some results from which are presented. The success of these simulations seems to be considerable, when measured against the known geomagnetic facts summarized here. Obstacles that still remain to be overcome are discussed, and some other future challenges are described.

CONTENTS

I. GROUNDWORK

A. Objectives

The Chinese were the first to discover, probably several millennia ago, that the Earth is magnetic, but the reason for this remained a puzzle until quite recently. Theory first started along the right lines early in the 20th century and has now reached the stage at which the favored mechanism of field production has been simulated with considerable success. It is our pleasant task to try to explain the status of the subject as it stands today to physicists having no specialized knowledge of geomagnetism, and who may well believe that a subject based on 19th-century physics cannot possibly be interesting. In trying to convince them otherwise, we shall simplify the subject in two ways that may disturb the professional geophysicist. On the one hand, we shall ignore known geophysical facts that would complicate our arguments without adding anything essential to the physics. (The arguments are already complicated enough.) On the other hand, we shall try to avoid prevarication by making dogmatic assertions even when certainty is geophysically unjustified.

B. A rudimentary model of the Earth

The Earth is an almost spherical body of mean radius $r_E = 20\,000/\pi$ km, consisting concentrically of a solid inner core, a fluid outer core, a rocky mantle, and the thin crust on which we live. It is sketched in Fig. 1, where the following abbreviations, used throughout this review, appear:

SIC=solid inner core;

FOC=fluid outer core;

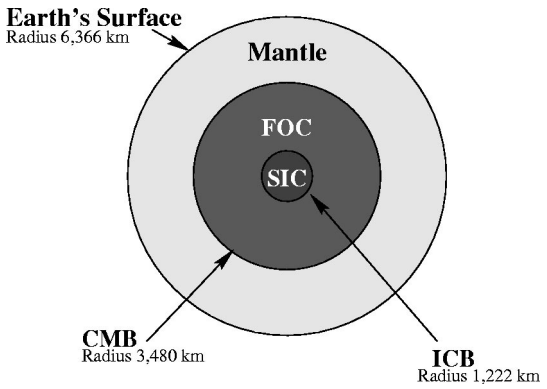

FIG. 1. Rudimentary sketch of the Earth's internal structure: SIC, solid inner core; ICB, inner core boundary; FOC, fluid outer core; CMB, core-mantle boundary.

ICB=inner core boundary (mean radius $\overline{r}_{\mathrm{ICB}} \approx 1221.5\,\mathrm{km}$);

CMB=core-mantle boundary (mean radius $r_{\mathrm{CMB}} \approx 3480\,\mathrm{km}$).

The Earth is in approximate hydrostatic equilibrium in an effective gravitational field $\overline{\mathbf{g}}$ that is mostly its own (Newtonian) self-gravity but is also partly the centrifugal acceleration created by its rotation $\mathbf{\Omega}$, which makes it slightly oblate. We have

$$\nabla \overline{P} = \overline{\rho}\,\overline{\mathbf{g}}, \tag{1.1}$$

$$\overline{\mathbf{g}} = -\nabla \overline{U}, \tag{1.2}$$

where P is pressure, ρ is density, and U is the effective gravitational potential. The overbar is used here to indicate horizontally averaged quantities (or more precisely quantities averaged over surfaces of constant U; see Sec. IV.B). Later, the overbar will also refer to the large-scale component of the quantity under it. Table I gives some idea of how $\overline{P}$ and $\overline{\rho}$ increase with depth. (The suffix $_M$ on the diffusivities listed there indicates that they are the "molecular" values, to distinguish them from turbulent values that will appear later.) There is a discontinuity $\Delta\rho = 600\ \mathrm{kg\,m^{-3}}$ in density at the inner core boundary.

The core has a density comparable to, but less than, what iron would have at core pressures, and it is probably an iron-rich alloy, made of an "uncertain mixture of all the elements" (Birch, 1952). The percentage by weight of iron is perhaps 85–90 %. It is not even known what the principal alloying element is, silicon, sulfur, oxygen, and hydrogen all having been proposed. To remove the ambiguity, it is supposed here that the core is made of FeX, where X stands for the principal, but unknown, light constituent. The last four entries of Table I are about right if X=S or Si; see Braginsky and Roberts (1995), from which we draw most of our data. The inclusion of further light elements would greatly complicate the theory without adding significant enlightenment.

To model seismic data successfully, it is necessary to assume that the core is isentropic and chemically homogeneous:

$$\nabla \overline{S} = \mathbf{0}, \tag{1.3}$$

$$\nabla \overline{\xi} = \mathbf{0}. \tag{1.4}$$

Here S is the specific entropy and ξ is the mass fraction of element X. From elementary thermodynamics and Eqs. (1.1)–(1.4) it follows that

$$\nabla \overline{\rho} = \overline{\rho}\,\overline{\mathbf{g}}/\overline{u_S^2}, \tag{1.5}$$

$$\nabla \overline{T} = \overline{\alpha^S}\,\overline{\mathbf{g}}, \tag{1.6}$$

$$\nabla \overline{\mu} = \overline{\alpha^\xi}\,\overline{\mathbf{g}}. \tag{1.7}$$

Here T is temperature, μ is chemical potential, u_S is the speed of sound,

$$\alpha^S = -\frac{1}{\rho}\left(\frac{\partial \rho}{\partial S}\right)_{P,\xi} = \rho\left(\frac{\partial T}{\partial P}\right)_{S,\xi} = \frac{\alpha T}{c_P} \tag{1.8}$$

is the *entropic expansion coefficient*, and

$$\alpha^\xi = -\frac{1}{\rho}\left(\frac{\partial \rho}{\partial \xi}\right)_{P,S} = \rho\left(\frac{\partial \mu}{\partial P}\right)_{S,\xi} \tag{1.9}$$

is the *compositional expansion coefficient*. The coefficient α^S is more useful than the more familiar thermal expansion coefficient α, to which it is related by the last term in Eq. (1.8), c_P being the specific heat at constant pressure. The coefficients $\overline{\alpha^S}$ and $\overline{\alpha^\xi}$ will occur frequently below; values are given in Table I.

In the general case, which is briefly touched on in Sec. IV, Eq. (1.1) shows that $\overline{\rho}$ and $\overline{P}$ and therefore all thermodynamic variables are constant over each equipotential surface, $\overline{U}$=constant. We shall usually ignore centrifugal forces. The model Earth then has a spherically symmetric structure, and $\overline{\rho}$, $\overline{P}$, $\overline{T}$, $\overline{\mu}$, $\overline{\alpha^S}$, $\overline{\alpha^\xi}$ ... are functions only of radial distance r from the geocenter O. (We shall denote $\partial/\partial r$ by ∂_r, and similarly for other differentials.) Since $\nabla\cdot\overline{\mathbf{g}} = -4\pi G\overline{\rho}$ where G is the gravitational constant, Eq. (1.2) gives

$$\nabla^2 \overline{U} = 4\pi G\overline{\rho}. \tag{1.10}$$

In principle, a model of the Earth's interior can be constructed from the seismically determined $\overline{u_S}$ by solving Eqs. (1.5) and (1.10) self-consistently for $\overline{\rho}$ and $\overline{U}$. Then $\overline{P}$ is obtained by solving Eq. (1.1) subject to $\overline{P}(r_E) = 0$. Similarly, $\overline{T}$ and $\overline{\mu}$ are obtained, apart from integration constants, from Eqs. (1.6) and (1.7). For example, if we assume that $\overline{\alpha^S}$ and $\overline{\alpha^\xi}$ are constant, we obtain

$$\overline{T} - \overline{T}_{\mathrm{CMB}} = -\overline{\alpha^S}(\overline{U} - \overline{U}_{\mathrm{CMB}}), \tag{1.11}$$

$$\overline{\mu} - \overline{\mu}_{\mathrm{ICB}} = \overline{\alpha^\xi}(\overline{U}_{\mathrm{ICB}} - \overline{U}). \tag{1.12}$$

Equation (1.6) defines the *adiabatic gradient* $-\partial_r \overline{T}$, which is less than $1\ \mathrm{K\,km^{-1}}$; see Table I. The implied outward heat flux, $\overline{\mathbf{I}}_r^{\mathrm{ad}} = -K_M \partial_r \overline{T}$ (where K_M is the thermal conductivity), is about $0.015\ \mathrm{W\,m^{-2}}$ at the inner core

TABLE I. Notation and magnitudes.

Well-determined parameters	
$\Omega = 7.292\times10^{-5}\ \mathrm{s}^{-1}$	Angular velocity of the Earth
$\overline{P}_{\mathrm{CMB}} = 135.75\ \mathrm{GPa}$	Pressure at the CMB
$\overline{P}_{\mathrm{ICB}} = 328.85\ \mathrm{GPa}$	Pressure at the ICB
$\rho_0 = 10.9\times10^{3}\ \mathrm{kg\,m}^{-3}$	Mean density of the FOC
$\overline{\rho}_{\mathrm{CMB}} = 9.9\times10^{3}\ \mathrm{kg\,m}^{-3}$	Density of the FOC at the CMB
$\overline{\rho}^{+}_{\mathrm{ICB}} = 12.166\times10^{3}\ \mathrm{kg\,m}^{-3}$	Density of the FOC at the ICB
$\overline{\rho}^{-}_{\mathrm{ICB}} = 12.764\times10^{3}\ \mathrm{kg\,m}^{-3}$	Density of the SIC at the ICB
$\Delta\overline{\rho} = (\overline{\rho}_{\mathrm{ICB}})^{-}_{+} = 0.6\times10^{3}\ \mathrm{kg\,m}^{-3}$	Density jump at the ICB
$\overline{g}_{\mathrm{CMB}} = 10.68\ \mathrm{m\,s}^{-2}$	Acceleration due to gravity at the CMB
$\overline{g}_{\mathrm{ICB}} = 4.40\ \mathrm{m\,s}^{-2}$	Acceleration due to gravity at the ICB
$\overline{U}_{\mathrm{CMB}} - \overline{U}_{\mathrm{ICB}} = 2.55\times10^{7}\ \mathrm{m}^2\,\mathrm{s}^{-2}$	Gravitational potential difference across FOC
$\overline{u}_{S,\mathrm{CMB}} = 8.065\times10^{3}\ \mathrm{m\,s}^{-1}$	Seismic velocity in FOC at the CMB
$\overline{u}_{S,\mathrm{ICB}} = 10.356\times10^{3}\ \mathrm{m\,s}^{-1}$	Seismic velocity in FOC at the ICB
Thermodynamic properties	
$\overline{T}_{\mathrm{CMB}} = 4000\ \mathrm{K}$	Temperature of the CMB
$\overline{T}_{\mathrm{ICB}} = 5300\ \mathrm{K}$	Temperature of the ICB
$\overline{T}_0 = 4590\ \mathrm{K}$	Mean temperature of the FOC
$-(\partial_r \overline{T})_{\mathrm{ICB}} = 0.28\ \mathrm{K\,km}^{-1}$	Adiabatic gradient at ICB
$-(\partial_r \overline{T})_{\mathrm{CMB}} = 0.89\ \mathrm{K\,km}^{-1}$	Adiabatic gradient at CMB
$\overline{\alpha}_{\mathrm{CMB}} = 1.8\times10^{-5}\ \mathrm{K}^{-1}$	Thermal expansion coefficient at the CMB
$\overline{\alpha}_{\mathrm{ICB}} = 1.0\times10^{-5}\ \mathrm{K}^{-1}$	Thermal expansion coefficient at the ICB
$\overline{c}_{P,\mathrm{CMB}} = 866\ \mathrm{J\,kg}^{-1}\,\mathrm{K}^{-1}$	Specific heat at constant P at the CMB
$\overline{c}_{P,\mathrm{ICB}} = 842\ \mathrm{J\,kg}^{-1}\,\mathrm{K}^{-1}$	Specific heat at constant P at the ICB
$\overline{\alpha}^{S}_{\mathrm{CMB}} = 8.5\times10^{-5}\ \mathrm{kg\,J}^{-1}\,\mathrm{K}$	Entropic expansion coefficient at CMB
$\overline{\alpha}^{S}_{\mathrm{ICB}} = 6.3\times10^{-5}\ \mathrm{kg\,J}^{-1}\,\mathrm{K}$	Entropic expansion coefficient at ICB
Relevant but less well-determined quantities	
$\overline{\eta} = 2\ \mathrm{m}^2\,\mathrm{s}^{-1}$	Magnetic diffusivity
$(\overline{K}_M)_{\mathrm{CMB}} = 40\ \mathrm{W\,m}^{-1}\,\mathrm{K}^{-1}$	Thermal conductivity at CMB
$(\overline{K}_M)_{\mathrm{ICB}} = 53\ \mathrm{W\,m}^{-1}\,\mathrm{K}^{-1}$	Thermal conductivity at ICB
$\overline{\kappa}_M = 5\times10^{-6}\ \mathrm{m}^2\,\mathrm{s}^{-1}$	Thermal diffusivity of FOC
$\overline{D}_M = 10^{-9}\ \mathrm{m}^2\,\mathrm{s}^{-1}$	Compositional diffusivity of FOC
$\overline{\nu}_M = 10^{-6}\ \mathrm{m}^2\,\mathrm{s}^{-1}$	Kinematic viscosity of FOC
$\overline{\alpha}^{\xi} = 0.7$	Compositional expansion coefficient
$h = 10^{6}\ \mathrm{J\,kg}^{-1}$	Latent heat of crystallization
$\overline{\xi} = 0.16$	Mass fraction of light constituents in FOC
$\overline{\xi}_{\mathrm{SIC}} = 0.1$	Mass fraction of light constituents in SIC
$\Delta\overline{T}_m = 700\ \mathrm{K}$	Depression of melting point through alloying

boundary and $0.036\ \mathrm{W\,m}^{-2}$ at the core-mantle boundary. Multiplying by the area of these surfaces, we find that the adiabatic heat flow is

$$\mathcal{H}_{\mathrm{ICB}} = 0.3\ \ \mathrm{TW}, \tag{1.13}$$

$$\mathcal{H}_{\mathrm{CMB}} = 5.4\ \ \mathrm{TW}. \tag{1.14}$$

Being highly metallic, the electrical conductivity σ_M of the core is large. Taking $\sigma_M = 4\times10^{5}\ \mathrm{S\,m}^{-1}$ in the fluid outer core, we see that the more useful magnetic diffusivity $\overline{\eta} = 1/\mu_0\sigma_M$ is $2\ \mathrm{m}^2\,\mathrm{s}^{-1}$, a value we adopt for the solid inner core also. Because $\overline{T}$ is so large, we take the magnetic permeability to be that of free space, $\mu_0 = 4\pi\times10^{-7}\ \mathrm{H\,m}^{-1}$.

C. What needs to be explained

Sufficiently far from the Earth, its external magnetic field $\hat{\mathbf{B}}$ is dipolar. In mathematical terms,

$$\hat{\mathbf{B}} = -\boldsymbol{\nabla} V, \tag{1.15}$$

$$\nabla \cdot \hat{\mathbf{B}} = 0, \tag{1.16}$$

where

$$V \sim -\mathbf{m} \cdot \nabla r^{-1}, \text{ for } r \to \infty. \tag{1.17}$$

Here $\mathbf{m}(t)$ is the strength of the "centered dipole" at time t; currently $m \approx 7.835 \times 10^{22}$ A m^2. Its direction is inclined to the geographic axis Oz by only about 11° at the present time, or perhaps we should say "169°," since the dipole axis is almost *antiparallel* to the Earth's angular velocity $\mathbf{\Omega}$, the South magnetic pole being close to the North geographic pole. It is this proximity of the poles that makes the magnetic compass needle such a boon to seafarers. The fact that $\hat{\mathbf{B}}$ is represented by a field that diminishes with distance from the Earth lends support to the conjecture made by William Gilbert in 1600 that the origin of the Earth's magnetism lies within it.

The dipole (1.17) is merely the first term in an expansion of V that includes quadrupoles, octupoles, etc. and is more economically represented by an expansion in spherical harmonics, $P_l^m(\theta)\cos m\phi$ and $P_l^m(\theta)\sin m\phi$, where the P_l^m are Legendre functions, θ is colatitude, and ϕ is longitude. (Colatitude differs from latitude by $\frac{1}{2}\pi$, the North pole being $\theta = 0$ and the South pole $\theta = \pi$.) The full expansion of $V(r,\theta,\phi,t)$ is

$$V = r_E \sum_{l=0}^{\infty} \sum_{m=0}^{l} \left(\frac{r_E}{r}\right)^{l+1} P_l^m(\theta)[g_l^m(t)\cos m\phi + h_l^m(t)\sin m\phi]. \tag{1.18}$$

The coefficients g_l^m and h_l^m are named after Gauss, who in 1839 was the first to analyze the geomagnetic data in this way. In addition to the interior harmonics proportional to $(r_E/r)^{l+1}$ appearing in Eq. (1.18), Gauss also included the exterior harmonics, which are proportional to $(r/r_E)^l$. He showed that these are so weak as to be effectively nonexistent. Equations (1.15) and (1.18) are tenable only because the electric current density at and above $r = r_E$ is essentially zero.

Gauss's analysis supported Gilbert's conjecture, but also suggested more. Let the mean magnetic energy density on the spherical surface of radius r be $W(r,t)$. For $r > r_E$, this may be expressed as the sum of contributions from each spherical harmonic:

$$W(r,t) = \sum_l W_l(r,t). \tag{1.19}$$

The set of values W_l is called the *power spectrum* of the field. Two approximate relations are found for the Earth's present surface field (Langel and Estes, 1982):

$$\log_{10} W_l(r_E) \approx \begin{cases} -3.270 - 0.569l, & \text{for } 2 \leqslant l \leqslant 12, \\ -10.83 - 0.0114l, & \text{for } 16 \leqslant l \leqslant 23. \end{cases} \tag{1.20}$$

For $13 \leqslant l \leqslant 15$ the spectrum makes a transition between these two linear relations. The largeness of the constant 0.569 in the first relation indicates (but does not prove) that the sources of these terms lie far below the Earth's surface. They create the *main geomagnetic field*, or simply (as we shall call it) the "main field." This is the object of our study. The smallness of the constant 0.0114 in the second relation indicates (but does not prove) that the sources of these terms lie close to the Earth's surface; they are attributed to the permanent magnetism of the crust. The crustal sources in the sum (1.18) swamp the main field sources for $l > 12$, thus destroying all the short-wavelength information about the main field; for our purposes, the sum can be truncated at $l = 12$. This sets a limit of about 5 nT on the accuracy to which we can know the main field at the Earth's surface.[1]

Since the lth harmonic of $\hat{\mathbf{B}}$ is proportional to $(r_E/r)^{l+2}$, we have

$$W_l(r) = W_l(r_E)(r_E/r)^{2l+4}, \tag{1.21}$$

so that, if applied at the core surface, the first relation (1.20) would give

$$\log_{10} W_l(r_{\mathrm{CMB}}) \approx -2.221 - 0.044l, \text{ for } 2 \leqslant l \leqslant 12. \tag{1.22}$$

The fact that the coefficient of l is negative means that, if taken to $l = \infty$ (the crustal sources having been removed), the series (1.20) would converge at the core surface. This suggests that there are no further sources of magnetism in the mantle and in particular no electric currents flowing there. The mantle is certainly a poor conductor compared with the core, and we shall usually assume it is insulating. Obviously, the expansion (1.20) has no meaning below the core surface where Eq. (1.15) is drastically violated, but the fact that the constant 0.044 in Eq. (1.22) is so small is unexpected and suggests that there is abundant small-scale structure on the core surface.[2]

Figure 2 shows typical magnetic energy spectra at the core surface $[W_l(r_{\mathrm{CMB}})]$ through degree 12 for the Earth in 1980 according to Langel and Estes (1985) and through degree 95 for a snapshot from our simulation (Sec. VI below). In both cases, the energy in the dipole ($l = 1$) exceeds that in any other harmonic. We shall call this *dipole dominance*. Since the dipole part of the field decreases the least rapidly with distance from the core, the dipole dominates even more strongly at the Earth's surface. This is illustrated in Fig. 3, where the radial component of the field is plotted in equal area projections. The three panels on the left are projections on the Earth's surface; the three on the right are for the core-mantle boundary. The top panels depict the real geomagnetic field truncated at $l = 12$; the center panels show

[1] Since crustal sources, if they change at all, do so on time scales much longer than the core's, one could in principle derive information about the time rate of change of the Gauss coefficients of the main field for $l > 12$.

[2] The fact that the power spectrum of the field is nearly flat at the core surface led Hide (1978) to propose that the core radii of other planets and satellites in the solar system that generate their own magnetic fields could be determined by analyzing their fields (as determined in flybys) into spherical harmonics and then extrapolating these to the depth at which the power spectrum becomes flat. See also Hide and Malin (1979, 1981).

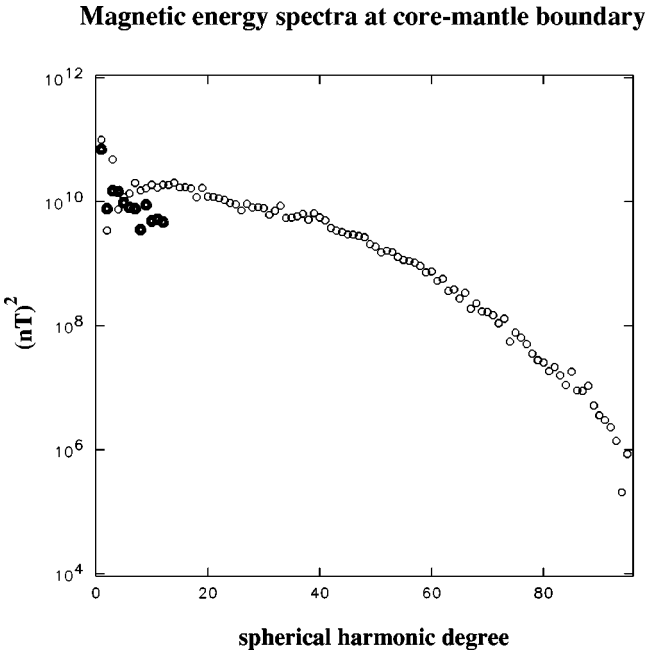

FIG. 2. Magnetic energy density $W_l(r_{\mathrm{CMB}})$ at the core-mantle boundary as a function of spherical harmonic degree l for (solid symbols) the Earth in 1980 and (open symbols) a snapshot from the Glatzmaier-Roberts simulation. Values of W_l have been multiplied by $2\mu_0$.

our simulation, also truncated at $l=12$, while the bottom panels show the same fields at the maximum truncation level of the simulation, $l=95$. One can see that, although including degrees 13–95 produces no detectable difference in the surface field, it makes a significant difference in the structure of the field at the core-mantle boundary. The intense concentrations of magnetic flux (core spots) seen in the simulated field at this boundary, which are essentially undetectable from the (filtered) geomagnetic-field measurements at the Earth's surface, are somewhat similar to sun spots on the solar surface. These figures graphically illustrate the difficulty in inferring the field at the core-mantle boundary from the observed field at the Earth's surface.

Although the power spectrum at the core surface is unknown for the real Earth beyond $l=12$, it cannot be absolutely white, as that would imply an infinite W and an infinite magnetic energy $\hat{\mathcal{E}}^B$ outside the core. If we adopt law (1.22) for all $l\geqslant 2$, and add in the contribution from the dipole (which is more than 70% of the whole), we find that $\hat{\mathcal{E}}^B\approx 6.9\times 10^{18}$ J. If there were no field sources, this energy would be carried by the Poynting flux back into the core and be dissipated there through ohmic heating in a time of order $(r_{\mathrm{CMB}}/\pi)^2/\overline{\eta}\approx 2\times 10^4$ yr. This is the longest efolding time for the decay modes of field in a stationary sphere of radius r_{CMB}; it belongs to the $l=1$ harmonic. We may write it as

$$\tau_\eta=\overline{\mathcal{L}}^2/\overline{\eta}, \tag{1.23}$$

with $\overline{\mathcal{L}}=r_{\mathrm{CMB}}/\pi\approx 10^3$ km. The efolding times of all other harmonics are shorter and, to make an allowance for this, we shall take as our estimate of the characteristic length scale of fields in the core

$$\overline{\mathcal{L}}=500 \text{ km}. \tag{1.24}$$

The overbar indicates that this refers to the large scales of core magnetohydrodynamics (MHD). The *electromagnetic time constant* (1.23) from the estimate (1.24) is 4×10^3 yr and corresponds roughly to $l=3$. To maintain the external magnetic energy $\hat{\mathcal{E}}$, the power delivered by the sources must exceed $\hat{\mathcal{E}}^B/\tau_\eta\approx 45$ MW. This considerably underestimates the total energy requirements; we shall find in Sec. II.A that the magnetic field in the core (which we shall denote by $\mathbf{B}$ to distinguish it from the field $\hat{\mathbf{B}}$ in and above the mantle) makes larger energy demands than 45 MW.

In reality the main field is not constant, but varies slowly in time, t, a phenomenon called the *secular variation*. It has many time scales. These range[3] from secular variation impulses or "jerks" (Le Mouël and Courtillot, 1981; Le Mouël *et al.*, 1982) that are completed in about one year to total reversals of the polarity of the field, the last of which occurred about 7.8×10^5 yr ago. Knowledge of the field over such long times is derived from archeomagnetic and paleomagnetic data. Paleomagnetism is the study of the main field from Precambrian times to the present, as revealed by the field recorded by rocks and sediments at their birth. Archeomagnetism provides similar information from historic and prehistoric times from the field imprinted on manmade artifacts such as shards of pottery and the bricks from the kilns that made it. We shall not describe here the processes by which ancient fields are trapped, nor the techniques and pitfalls of extracting reliable geomagnetic information from samples. We simply report conclusions that are relevant to our theme. More detailed information can be found in Merrill *et al.* (1996).

Perhaps the most striking facts that have emerged from paleomagnetism are that the Earth has possessed a field for more than 3×10^9 yr and that, except during a polarity reversal (a process that is typically completed in a few thousand years), its intensity has not varied by a factor of more than about 3 over most of geological time (Kono and Tanaka, 1995). The age of the field therefore greatly exceeds τ_η, and it is necessary to find an energy source for it. The field and currents cannot be relics of the Earth's creation.

We have little to say about secular variation impulses. They are small but have not yet been convincingly explained. They seem to be worldwide phenomena and to have their origin in the core. Two observations suggest this. First, the jerks seem to be correlated to changes in the westward drift rate (Le Mouël *et al.*, 1981; Gire *et al.*,

[3]There are probably also much shorter time scales, but these are shielded from observation by electrical conduction in the mantle, which has an electromagnetic time constant of order 1 yr. See, for example, Gubbins and Roberts (1987).

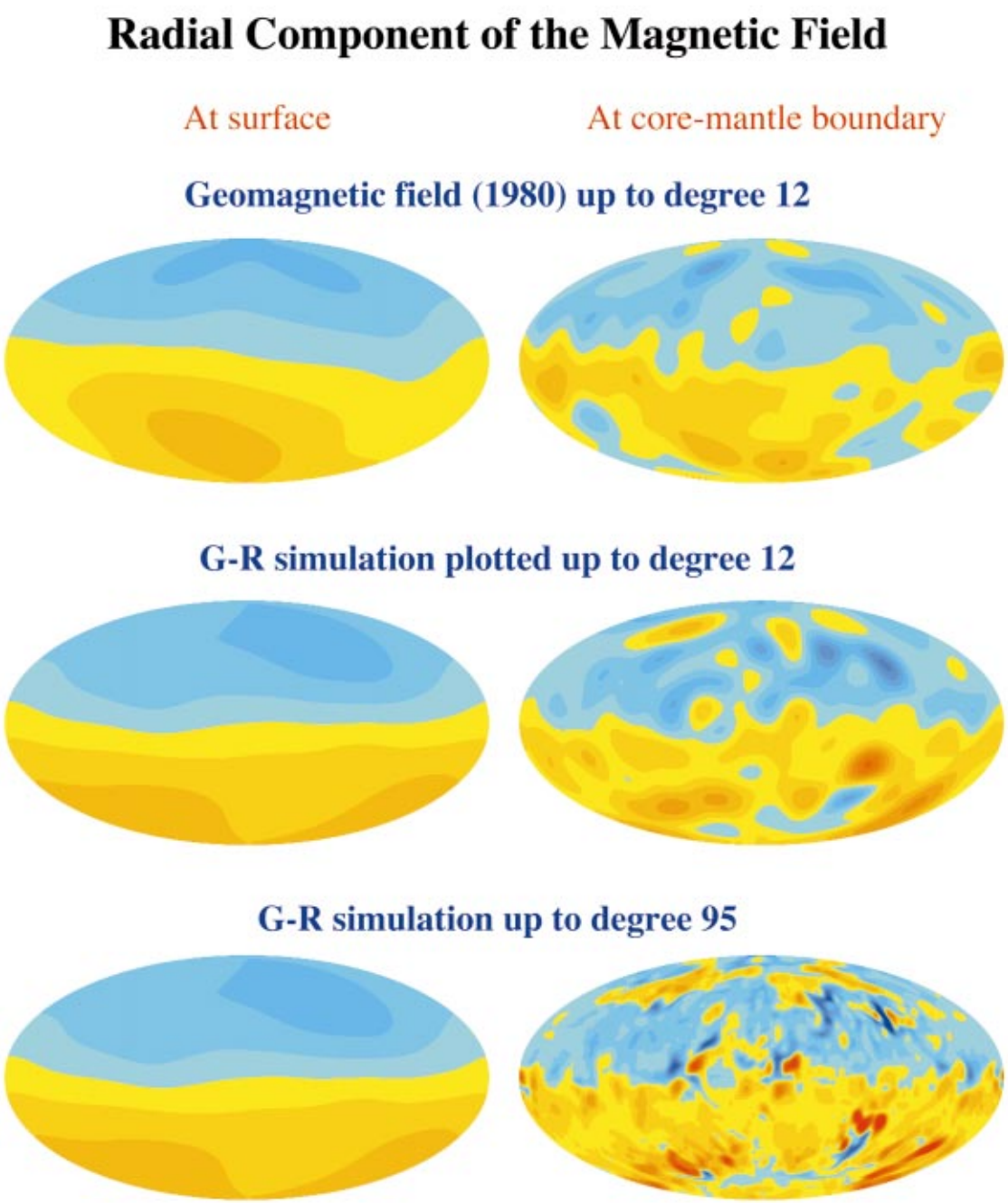

FIG. 3. Radial component of the magnetic field (reds for outward directed and blues for inward) plotted at the Earth's surface and at the core-mantle boundary. The surface fields are multiplied by 10 to obtain comparable color contrast. The Earth's field is plotted out to spherical harmonic degree 12. A snapshot from the Glatzmaier-Roberts simulation is plotted out to degree 12 (for comparison) and out to degree 95 [Color].

1983). Second, they also seem to be correlated with equally rapid variations in the length of the day. It has long been known that the Earth is not a perfect time keeper and that the length of the day can change by as much as 5 ms in 10 yr during so-called decade variations. The magnitude of these changes is too large to be explained by a transfer of angular momentum between the mantle and the atmosphere. The global wind system would have to more than reverse or more than double to explain it. The rapidity of the changes shows that the fluctuating unbalanced torque acting on the mantle is typically of order[4] 10^{18} N m, and this also is too great to be provided by the atmosphere or oceans. The exchange of angular momentum must be between mantle and

[4]The axial moment of inertia of the mantle is 7.12×10^{37} kg m^2, so that a fluctuation of 1 ms, corresponding to a change in angular velocity Ω of the mantle of $\delta\Omega\approx8.4\times10^{-13}$ s^{-1}, is associated with a change in angular momentum of 5.07×10^{25} kg m^2 s^{-1}. The torque required to bring this about in a year is 1.6×10^{18} N m.

core. Correlations between westward drift and mantle rotation have long been suspected (see, for example Le Mouël *et al.*, 1981), and there are indications (Jackson *et al.*, 1993; Jault *et al.*, 1988) that changes in the angular momentum of the mantle are accompanied by equal and opposite changes in the angular momentum of the core associated with a ''torsional wave''; see Sec. V.C below.

The secular variation operates on many time scales intermediate between the two extremes described above. Because of the historical importance of the geomagnetic field to mariners, the field has been increasingly well studied since the fifteenth century, and many maps have been constructed that describe its structure at the Earth's surface and its variation over the last 400 years (see Langel, 1987). One striking phenomenon is the westward drift of the field patterns, a phenomenon discovered by Halley, who presciently attributed it to fluid motions inside the Earth. The drift is latitude dependent and irregular. Its typical value in midlatitudes is commonly used to estimate $\overline{\mathcal{U}}$, the characteristic large-scale velocity in the core:

$$\overline{\mathcal{U}}=5\times10^{-4}\ \mathrm{m\,s^{-1}}. \tag{1.25}$$

Three other paleomagnetic facts will be of interest to us later. First, consider Fig. 4, which shows the location of the South geomagnetic pole in the northern hemisphere at various times during the past 5 Myr. (More precisely, Fig. 4 shows the virtual geomagnetic pole, or VGP, which is computed at a site from a measurement of the direction of the prevailing magnetic field. This pole represents the position that the south magnetic pole would have were the field precisely dipolar at the site.) Figure 4 suggests that the present angle of about 10° between the geographic and geomagnetic axes is not uncharacteristic of the past, but archeomagnetic data (not shown here) from the past 1000 years indicates that the average angle is roughly 5°. When averaged over a time of order 10^4 yr, the geographic and geomagnetic axes coincide.[5] Several points shown in Fig. 4 lie far from the North geographic pole, and very often in the past the South geomagnetic pole has actually moved to the southern hemisphere and remained there until later another fluctuation has returned it to the northern hemisphere. These are geomagnetic field reversals and they bring us to our second interesting fact: there is no firm evidence that the Earth prefers to be in one polarity state rather than the other. If there is a bias, it is too small to be convincing. Our third interesting fact is the irregularity of reversals. Figure 5 shows the reversal frequency during the past 165 Myr. It may be seen that during a period of about 35 Myr during the Cretaceous (144-66 Myr ago) the field remained of one polarity state. It is also known that, during 50 Myr in the Permo-Carboniferous, the field did not reverse. At the present time, however, the field is reversing roughly 4–5 times per Myr. When a constant-polarity interval endures for more than 10^5 yr, it defines a *polarity epoch*, otherwise it is called a *polarity event*. When a magnetic pole moves further from the nearest geographic pole than 45°, but then returns, a *polarity excursion* has occurred. There is evidence that 14 of these have so far occurred in the present polarity epoch (Lund *et al.*, 1998). On occasions, called ''cryptochrons,'' a pair of back-to-back reversals occur in quick succession, restoring the initial polarity state. Sometimes the magnetic field may appear to reverse at one site where the data was collected but not at another, suggesting that the nondipole field dominates the dipole field during this time.

The geomagnetic facts just summarized raise many challenging questions, and we aim to answer in at least a qualitative way virtually all of them.

II. CORE CONVECTION

A. Energy balance of the core

The temperature T beneath the crust exceeds the Curie point of all known materials; permanent magnetism does not exist anywhere in the Earth, except the crust. The obvious explanation of the Earth's magnetism is therefore untenable; the main field is created by electric currents flowing mainly in the core.[6] Several possible origins of these currents have been proposed,[7] but all except one have been found wanting. The favored idea today is that they are generated by self-excited dynamo action associated with the motion of core fluid, a suggestion first made by Larmor (1919). We discuss the foundations of dynamo theory in Sec. III.

What drives core motions? It is obvious that, by Lenz's law, the Lorentz force created by currents induced by core motion oppose that motion and bring it to rest, unless an energy source is available to drive the motion. Looked at another way, the fluid motions must supply the Joule heat losses of the electric currents. If they fail to do so, the field will diminish until dynamo action ceases. How large are these losses? Let us estimate the Joule losses $\mathcal{Q}^J$ from $\overline{\mathbf{B}}$ as $\mathcal{Q}^J=(\overline{\mathcal{J}}^2/$

[5]Over time scales longer than 5 Myr, the mean geomagnetic poles appear to move over the Earth's surface in ''polar wander'' paths. This provides the main tool used to infer how continents have moved relative to one another over geological time. Further discussion of this fascinating topic, and the related subject of sea floor spreading, would take us too far from our present objectives; see, for example, McElhinny (1973) and Merrill *et al.* (1996).

[6]We ignore the by now discredited idea that all rotating bodies produce a field because of their rotation (Blackett, 1947).

[7]For example, some geophysicists have argued that the currents are driven by thermoelectric potential differences between rising and falling convection currents or between the core and the mantle. According to others, the currents have an electrochemical origin, as in a battery. The Nernst-Ettinghauser effect has also been suggested. Like the Blackett proposal, all these theories find it impossible to explain polarity reversals and the apparent indifference of the field to its polarity state, i.e., the sign of $\hat{\mathbf{B}}$.

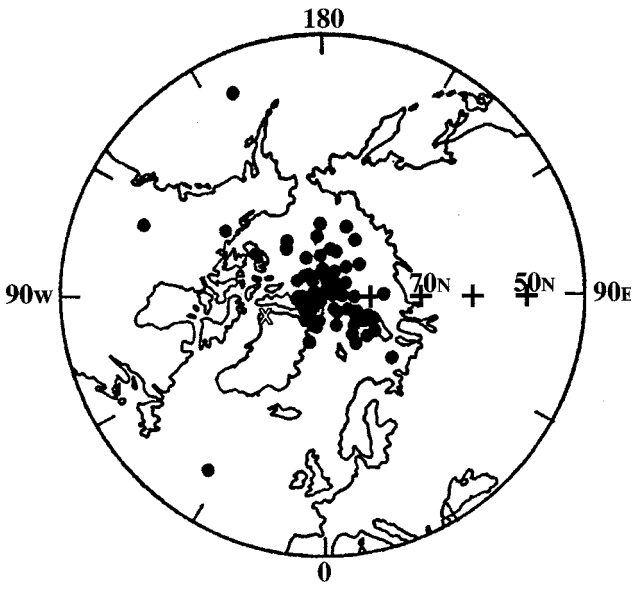

FIG. 4. Paleomagnetic poles north of 40° N during the past 5 Myr in polar stereographic projection; the white diagonal cross is the present South magnetic pole. From McElhinny, 1973.

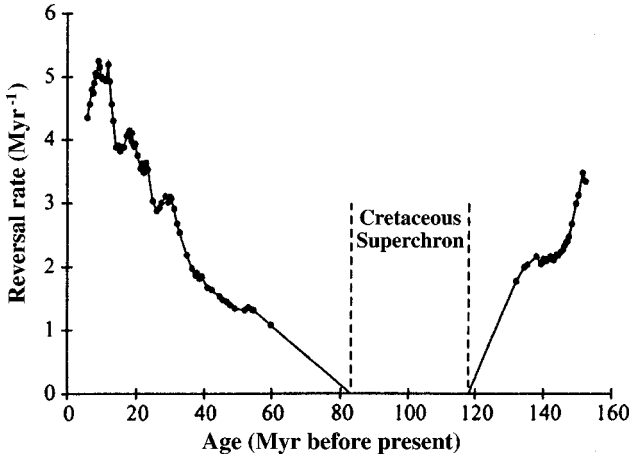

FIG. 5. Estimated reversal rate of the geomagnetic field over the past 160 Myr. From Merrill *et al.*, 1996.

$\sigma_M)V_{\rm core}$, where $V_{\rm core}\approx 1.77\times 10^{24}$ m^3 is the volume of the core. Using Ampère's law [see Eq. (3.4) below], we estimate the characteristic current density $\overline{\mathcal{J}}$ for a typical field strength of $\overline{\mathbf{B}}$ as $\overline{\mathcal{J}}\approx\overline{\mathcal{B}}/\mu_0\overline{\mathcal{L}}$. In Sec. V.A we shall assess $\overline{\mathcal{B}}$ by equating the Coriolis force $2\Omega\overline{\rho}\overline{\mathbf{V}}\approx 2\Omega\rho_0\overline{\mathcal{U}}$, where $\mathbf{V}$ is fluid velocity, to the Lorentz force $\overline{\mathbf{J}\times\mathbf{B}}\approx\overline{\mathcal{J}}\overline{\mathcal{B}}$, so that $\overline{\mathcal{B}}\approx\sqrt{(2\Omega\rho_0\mu_0\overline{\mathcal{U}}\overline{\mathcal{L}})}\approx 20$ mT, $\overline{\mathcal{J}}\approx 0.04$ A m^{-2}, and $\mathcal{Q}^J\approx 1$ TW. These values are probably overestimates. In the simulations described in Sec. VI, the maximum field strength is of order 20 mT and the typical field strength is closer to 5 mT, and it is found that

$$\mathcal{Q}^J\approx 0.3\,\text{TW}. \tag{2.1}$$

It is hard to be confident about estimate (2.1), which is clearly sensitive to the assumed $\overline{\mathcal{B}}$ and $\overline{\mathcal{L}}$. It is even harder to assess the energy dissipation rate $\mathcal{Q}^t$ of core turbulence, which may be at least as large as $\mathcal{Q}^J$, though the energy dissipation rate $\mathcal{Q}^\nu$ from the large-scale flow is likely to be much smaller; see Secs. IV and V. The turbulent energy loss is mainly through Joule dissipation of the small-scale currents, and only slightly from the viscous dissipation of the small-scale motions; see Sec. IV.D. The problem of estimating the total dissipation rate,

$$\mathcal{Q}^D=\mathcal{Q}^J+\mathcal{Q}^\nu+\mathcal{Q}^t, \tag{2.2}$$

will be the principal concern of Sec. II.C.

The source of $\mathcal{Q}^J$ has been argued about for most of the last 50 years, and by now the main consensus is that the flow is convectively driven. The only alternative explanation that has not been ruled out is that the motions are powered by the luni-solar precession of the Earth's rotation axis; see Bullard (1949), Malkus (1963, 1968), and Vanyo (1991). In this review we go with the majority and assume that core motions are driven by buoyancy. The rate of working $\mathcal{Q}^C$ of the buoyancy forces must balance the dissipative losses:

$$\mathcal{Q}^C=\mathcal{Q}^D\equiv\mathcal{Q}^J+\mathcal{Q}^\nu+\mathcal{Q}^t. \tag{2.3}$$

This statement, like Eqs. (2.9) and (2.33) below, should be interpreted as an average, since the quantities involved fluctuate over time; see Sec. 7 of Braginsky and Roberts (1995) for a detailed derivation. An expression for $\mathcal{Q}^C$ is given in Eq. (2.15) below.

If we use $\overline{\mathcal{B}}=5$ mT and the estimate (1.25) for $\overline{\mathcal{U}}$ to calculate the magnetic energy density as $\overline{\mathcal{B}}^2/2\mu_0$ and the kinetic energy density (of core motions relative to the mantle) as $\frac{1}{2}\rho_0\overline{\mathcal{U}}^2$, we obtain 10 J m^{-3} and 1.4 mJ m^{-3}, respectively. The ratio of the magnetic energy $\mathcal{E}^B\approx 1.8\times 10^{21}$ J of the Earth to the kinetic energy of core motions $\mathcal{E}^V\approx 2.4\times 10^{17}$ J is therefore large: $\mathcal{E}^B/\mathcal{E}^V\approx 7500$; see Sec. V.

B. Sources of energy

What is the origin of the buoyancy? Most geochemists argue that there is no significant radioactivity in the core to heat it; see, for example, Stacey (1992).[8] It is now thought that the buoyancy arises from processes driven by the slow cooling of the Earth over geological time. The Earth continually radiates heat into space. This heat comes partly from radioactive sources in the crust and mantle, but the Earth loses more heat than that, i.e., the temperature of the Earth is dropping. Within the Earth, the heat is carried outwards mainly by thermal conduction down the adiabatic temperature gradient (1.6). But this state is convectionally unstable; see Sec. II.C. Both mantle and (probably) core also carry heat outward by convection, though, because their viscosities are so very different, mantle motions are measured in cm/yr,

[8]For a recent reassessment of the radiogenic heat release in the core, see Chabot and Drake (1999).

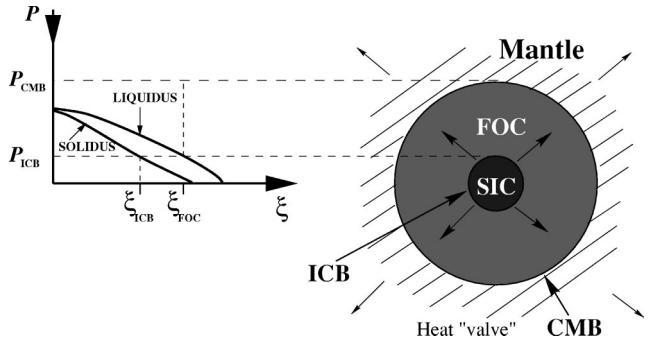

FIG. 6. Phase diagram (left) for the binary alloy representing the core and its relationship (right) to core structure. The arrows from the solid inner core (SIC) represent the outward fluxes of heat and light component of the alloy from the inner core boundary as it freezes; the arrows in the mantle represent the heat flux from core to mantle, which acts as a "valve" controlling core convection.

whereas those in the fluid core are about six orders of magnitude greater, i.e., a few mm/s. Correspondingly, the overturning time τ_c of core convection is measured in hundreds of years and that of the mantle τ_m in hundreds of millions of years.

The downward temperature gradient created in a fluid layer cooled sufficiently strongly from the top may cause it to lose convective stability, but this is not an efficient way to make it convect. For given buoyancy sources, stronger motions arise when the sources are deep in the layer rather than distributed volumetrically throughout it. Best of all, they should be at the base of the layer. The core achieves this in an interesting way (Braginsky, 1963). For simplicity, let us (as is commonly done; see Sec. I.B) model the core as a binary, iron-rich alloy. A phase diagram usually displays the solidus and liquidus of the alloy as curves in ξT-space, where ξ is the mass fraction of the (unknown) light constituent. This is because freezing is usually discussed in contexts where variations in pressure P are unimportant. In reality, the liquidus and solidus depend on the thermodynamic state of the material. They should therefore appear as surfaces in, say, ξPT-space. The traditional diagrams are merely projections of these surfaces onto the appropriate constant-P plane. For the core it makes more sense to plot the solidus and liquidus in ξPS-space and to project them onto the appropriate constant-S plane. The result is a ξP plot, such as that shown in Fig. 6.

On descending through the fluid core from the core-mantle boundary, we eventually encounter the inner core boundary (ICB), where solid freezes from the overlying melt. In fact, the core is a body of fluid that is cooled from the top but freezes from the bottom! This may seem paradoxical, but only because we are not familiar with such processes in everyday life on Earth's surface. The paradox is inevitable whenever the melting point of a material increases more rapidly with increasing pressure than the ambient temperature does. Although the ICB is a freezing front, the material lying below it is unlikely to be completely solid. Rather, it will be a mixed-phase region, where liquid and solid coexist (Loper and Roberts, 1981); this is often called a "mush" in the metallurgical literature. This idea is corroborated by seismically determined estimates of the Q of the solid inner core (SIC), which are fairly low; Vidale and Earle (2000) give values between 244 and 450. The mush beneath the ICB is called the "solid" inner core, but the adjective is appropriate because the mass fraction φ of solid is likely to increase rapidly with depth and become close to 1 within a few meters of the ICB. There are two reasons for this. First, the fluid that percolates through the channels of the mush deposits solid on them and gradually closes them up. Second, a mush is of low mechanical strength and will easily compact in the prevailing pressure gradient. The upper layers of the SIC, in which φ differs significantly from 1, impart a "fuzziness" to the ICB that we shall disregard in the remainder of this review. The mechanical weakness of the SIC suggests that it cannot sustain significant internal nonhydrostatic stresses. It is therefore close to being in hydrostatic equilibrium and the ICB is close to being an equipotential surface, a fact used in Sec. IV.

The idea that the SIC is only a solidified form of the fluid lying above it, and that the inner core surface is a freezing front that advances slowly into the fluid as the Earth cools, was first suggested by Jacobs (1953) and is now generally accepted. If the SIC has added to its mass $\mathcal{M}_{\rm SIC}\approx 9.7\times 10^{22}$ kg at a uniform rate over most of its age, which (for consistency with other estimates made below) we take to be $\overline{\tau}=1.2$ Gyr, the rate of increase in its mass is 2.5×10^{6} kg s^{-1}, corresponding to a rate of advance of the ICB currently of $\dot{\bar{r}}_{\rm ICB}\approx 10$ pm s^{-1} or 0.3 mm yr^{-1}. Verhoogen (1961) pointed out that the latent heat released at the inner surface as it freezes provides a *thermal buoyancy* source to stir the core. The heat release at the ICB is

$$\mathcal{Q}^L=\overline{T}_{\rm ICB}\Delta\overline{S}\dot{\mathcal{M}}_{\rm SIC}, \tag{2.4}$$

where $\Delta\overline{S}=\overline{S}^{+}-\overline{S}^{-}$ is the jump in $\overline{S}$ at the SIC. This is closely related to the latent heat of crystallization h, which is usually defined as the discontinuity in enthalpy: $h=T\Delta S+\mu\Delta\xi$. Since h is rather uncertain, there is little point in distinguishing between $\overline{T}_{\rm ICB}\Delta\overline{S}$ and h. From our estimate of $\dot{\bar{r}}_{\rm ICB}$ above and Table I, we find that

$$\mathcal{Q}^L\approx 2.5 \text{ TW}. \tag{2.5}$$

Braginsky (1963) remarked that the difference in the compositions ξ of the liquidus and solidus (see Fig. 6) means that the inner core is richer in iron than the outer core, and that this largely accounts for the observed density jump $\Delta\overline{\rho}=\overline{\rho}^{-}-\overline{\rho}^{+}$ at the ICB, i.e., the density jump is due less to the contraction of a material as it freezes (an effect we do not include) than to a discontinuity $\Delta\overline{\xi}=\overline{\xi}-\overline{\xi}_{\rm ICB}^{-}$ in $\overline{\xi}$. This also implies, he noted, that some of the light component of the alloy is released as the inner core freezes and that this provides a second, *compositional buoyancy* source to stir the core. Suppose that the core fluid is 16% by weight of light component and that it retains 40% of this when it freezes onto the surface of the SIC. The remainder provides an average

mass flux $I_r^{\xi}=\overline{\rho}_{\rm ICB}\Delta\overline{\xi}\dot{\overline{r}}_{\rm ICB}$ of light component away from the ICB of approximately $8.7\times10^{-9}\,{\rm kg\,m^{-2}\,s^{-1}}$ and a rate of increase of $\overline{\xi}$ in the fluid outer core (FOC) of $\dot{\overline{\xi}}\approx8.9\times10^{-20}\ {\rm s^{-1}}$. (In reality, $\dot{\overline{r}}_{\rm ICB}$, $\overline{I}^{\xi}_{\rm ICB}$, and $\overline{I}^{S}_{\rm ICB}$ vary over the ICB but, since each depends on the rate of freezing, they are everywhere proportional to one another; see Sec. IV.E.) If ξ were ever to approach the eutectic, compositional forcing would cease.

The fact that the solid core is growing and is richer in iron than the fluid core means that the Earth is continually becoming more centrally condensed as it cools. In addition, therefore, to the release of internal energy, of which the latent heat is the most significant part, there is a release of gravitational energy $\mathcal{Q}^G$, which we may estimate by the following argument. A change $\delta\overline{\xi}$ in $\overline{\xi}$ creates a fractional change in outer core density of $-\overline{\rho\alpha^{\xi}}\delta\overline{\xi}$, which is the same everywhere in the FOC if (as we shall temporarily assume for simplicity) $\overline{\alpha^{\xi}}$ is constant. We compute the change in gravitational energy by imagining that the mass $(\overline{\alpha^{\xi}}\delta\overline{\xi})\overline{\rho}d^3x$ in a volume element d^3x is moved directly to the ICB, to form part of the mass $4\pi\overline{r}^2_{\rm ICB}\delta\overline{r}_{\rm ICB}\Delta\rho=\mathcal{M}_{\rm FOC}\overline{\alpha^{\xi}}\delta\overline{\xi}$ added to the SIC through freezing. The gravitational energy released is $\overline{\alpha^{\xi}}\delta\overline{\xi}(\overline{U}-\overline{U}_{\rm ICB})\overline{\rho}d^3x$. Summing over the FOC and supposing that the increase $\delta\overline{\xi}$ in $\overline{\xi}$ happens in time δt, we obtain in the limit $\delta\overline{\xi}/\delta t\to\dot{\overline{\xi}}$

$$\mathcal{Q}^G=-\overline{\alpha^{\xi}}\dot{\overline{\xi}}\int_{\rm FOC}(\overline{U}_{\rm ICB}-\overline{U})\overline{\rho}d^3x. \tag{2.6}$$

Using $\dot{\overline{\xi}}\approx8.9\times10^{-20}\ {\rm s^{-1}}$, we find that

$$\mathcal{Q}^G\approx1.3\,{\rm TW}. \tag{2.7}$$

Equation (1.12) allows us to express $\mathcal{Q}^G$ differently:

$$\mathcal{Q}^G=-\dot{\overline{\xi}}\int_{\rm FOC}(\overline{\mu}_{\rm ICB}-\overline{\mu})\overline{\rho}d^3x, \tag{2.8}$$

and this is the appropriate form for $\mathcal{Q}^G$ if the assumption of constant $\overline{\alpha^{\xi}}$ is lifted.

The average heat balance of the FOC is expressed by[9]

$$\mathcal{Q}_{\rm CMB}=\mathcal{H}_{\rm ICB}+\mathcal{Q}^L+\mathcal{Q}^G+\mathcal{Q}^S+\mathcal{Q}^R, \tag{2.9}$$

where $\mathcal{H}_{\rm ICB}$ has been estimated in Eq. (1.13), the subscript CMB refers to the core-mantle boundary, $\mathcal{Q}^R$ is the rate of energy input from core radioactivity (if any), and $\mathcal{Q}^S$ is the heat loss through the cooling of the FOC:

$$\mathcal{Q}^S=-\dot{\overline{S}}\int_{\rm FOC}\overline{T}\overline{\rho}d^3x. \tag{2.10}$$

Equation (2.10) may also be written as $\mathcal{Q}^S=-\overline{T}_0\dot{\overline{S}}\mathcal{M}_{\rm FOC}$ where $\overline{T}_0$ is the mass-weighted average of $\overline{T}$ in the FOC; see Table I. We give later, in Eq. (4.66), a means of computing $\dot{S}$ (which is proportional to $\dot{\overline{r}}_{\rm ICB}$), and this gives $\dot{S}\approx-3.7\times10^{-16}\,{\rm W\,kg^{-1}\,K^{-1}}$. Since $\mathcal{M}_{\rm FOC}=1.8367\times10^{24}$ kg, we now have

$$\mathcal{Q}^S\approx3.1\ {\rm TW}. \tag{2.11}$$

Assuming that $\mathcal{Q}^R=0$, we find from Eq. (2.9) that $\mathcal{Q}_{\rm CMB}=7.2$ TW.

Since $\mathcal{Q}^L$, $\mathcal{Q}^G$, and $\mathcal{Q}^S$ are proportional to $\dot{\overline{r}}_{\rm ICB}$, we can easily explore other possibilities, such as the following:

(a) if $\mathcal{Q}_{\rm CMB}=\mathcal{H}_{\rm CMB}$ and $\mathcal{Q}^R=0$, then $\overline{\tau}=1.6$ Gyr;

(b) if $\overline{\tau}=4$ Gyr and $\mathcal{Q}_R=0$, then $\mathcal{Q}_{\rm CMB}=2.4$ TW $<\mathcal{H}_{\rm CMB}$, so that convection pumps heat downward; see Sec. II.C;

(c) if $\mathcal{Q}^R>\mathcal{Q}_{\rm CMB}-\mathcal{H}_{\rm ICB}$, then the SIC would start to remelt ($\dot{\overline{r}}_{\rm ICB}<0$).

C. Convection in a compressible fluid; CO density

Convection experiments in the laboratory usually involve thin layers of fluid that are almost uniform in density, but the compressibility of a thick shell of fluid like the fluid outer core cannot be ignored, since (see Sec. I.B) the adiabatic increase of $\overline{T}$ with depth results in a heat loss $\mathcal{H}_{\rm CMB}$ from the core far exceeding the energy demands $\mathcal{Q}^D$ of the dynamo.

Let us consider first the case of a chemically homogeneous fluid in which $\overline{\xi}$ is constant so that compositional buoyancy is absent. Suppose that the fluid is in a hydrostatic equilibrium in which the specific entropy $\overline{S}$ depends on depth, and apply a "test parcel" argument (see also Sec. 4 of Landau and Lifshitz, 1987). Imagine that a small parcel of fluid is infinitesimally displaced downwards so fast that heat has no time to change its entropy content but so slowly that its internal pressure adjusts to that of its new surroundings. Its density will therefore increase by $\delta\rho=\delta\overline{P}/\overline{u}_S^2$. The density of the new surroundings is greater than that of the old surroundings by $\delta\overline{\rho}=\delta\overline{P}/\overline{u}_S^2-\overline{\rho\alpha^S}\delta\overline{S}$, where $\overline{\alpha^S}>0$. If $\delta\rho>\delta\overline{\rho}$, the parcel is denser than its new surroundings and will tend to sink further. The equilibrium is then said to be *convectively unstable* (although, strictly speaking, the argument ignores thermal conduction and viscosity, both of which tend to stabilize the equilibrium; see Sec. V). If $\delta\rho<\delta\overline{\rho}$, the buoyancy force will drive it upwards towards its original position; this defines *convective stability*; $\delta\rho=\delta\overline{\rho}$ signifies neutral stability. Stated another way, the fluid is unstable if $\overline{S}$ increases downwards anywhere, and it is stable if $\overline{S}$ decreases downwards everywhere (as, for example, happens if the fluid is isothermal). The downward temperature gradient in the isentropic state of uniform $\overline{S}$ and neutral stability is the adiabatic (temperature) gradient defined in Sec. I.B.

When the heat flow $\mathcal{Q}_{\rm CMB}$ from the top of the layer exceeds $\mathcal{H}_{\rm CMB}$ given by Eq. (1.14), the layer convects

[9]The form (2.9) differs from Eq. (7.32) of Braginsky and Roberts (1995), who give $\mathcal{Q}_{\rm CMB}=\mathcal{Q}^L+\mathcal{Q}^G+\mathcal{Q}^S_{\rm total}+\mathcal{Q}^R_{\rm total}$, where $\mathcal{Q}^S_{\rm total}$ and $\mathcal{Q}^R_{\rm total}$ also include the solid inner core. The form (2.9) excludes the SIC by supposing that the heat flux from SIC to FOC arises only from the adiabatic gradient in the SIC, which is assumed to be continuous across the ICB. Again, Eq. (2.9) should be interpreted as an average over the convective time scale.

and the difference $\mathcal{Q}_{\rm CMB}^{\rm conv}$ is the convective heat flowing from core to mantle. To estimate $\mathcal{Q}_{\rm CMB}^{\rm conv}$, we suppose that the convective velocities $\mathcal{U}\sim 5\times 10^{-4}\,{\rm m\,s^{-1}}$ are of the order inferred in Sec. I.C and that the temperature difference between the rising and falling convective streams is of order only $\delta T\sim 10^{-4}$ K. (We shall find in Secs. V.B and VI.B that this estimate of δT is realistic for the core.) The outward convective heat flux $I_r^{\rm conv}\sim\rho_0\overline{c}_P\mathcal{U}\delta T$ then significantly exceeds $\overline{I}_r^{\rm ad}$, and the fluid may be said to be convecting strongly. Vigorous convection homogenizes all extensive properties of the fluid, so that $\overline{S}$ becomes almost uniform everywhere, except in boundary layers. As we saw in Sec. I.B, the success of models of the Earth's interior, based on seismic and other data, depends on the assumption that the core is close to being in an isentropic state, and this success is a strong indication that it is convecting vigorously.

Let us now ask if and how compositional buoyancy changes any of these conclusions. Suppose that $\overline{S}$ *and* $\overline{\xi}$ depend on depth and that the parcel retains both its S and ξ contents when it sinks. The increase in its density is again $\delta\rho=\delta\overline{P}/\overline{u}_S^2$, but that of the surroundings is now $\delta\overline{\rho}=\delta\overline{P}/\overline{u}_S^2-\overline{\rho}(\overline{\alpha}^S\delta\overline{S}+\overline{\alpha}^\xi\delta\overline{\xi})$. Again the sign of $\delta\rho-\delta\overline{\rho}$ is all important. Stability means that $-\overline{\mathbf{g}}\cdot(\overline{\alpha}^S\boldsymbol{\nabla}\overline{S}+\overline{\alpha}^\xi\boldsymbol{\nabla}\overline{\xi})>0$ everywhere, but if

$$-\overline{\mathbf{g}}\cdot(\overline{\alpha}^S\boldsymbol{\nabla}\overline{S}+\overline{\alpha}^\xi\boldsymbol{\nabla}\overline{\xi})<0 \tag{2.12}$$

anywhere, the fluid is unstable. If the resulting convection is sufficiently vigorous, it will homogenize both $\overline{S}$ *and* $\overline{\xi}$ everywhere, except in boundary layers.[10]

If $\overline{\alpha}^S$ and $\overline{\alpha}^\xi$ are constants, we may rewrite inequality (2.12) as

$$\overline{\mathbf{g}}\cdot\boldsymbol{\nabla}\overline{C}<0, \tag{2.13}$$

where

$$C=-\alpha^S S-\alpha^\xi\xi \tag{2.14}$$

is the CO *density*, which stands for the convection-originating density (although strictly speaking it is a relative density).[11] This name underscores its virtue: the buoyancy force arising from the density differences created by changes in S and ξ produces convective circulations, but those created by a change in P do not; its buoyancy force can be absorbed into the gradient of a reduced pressure (see Sec. IV.C). The CO density neatly splits off the important from the unimportant. The rate at which buoyancy supplies energy to the flow is

$$\mathcal{Q}^C=\int_{\rm FOC}C\mathbf{V}\cdot\overline{\mathbf{g}}\,\overline{\rho}\,d^3x. \tag{2.15}$$

It is obvious from inequality (2.12) that, if $d\overline{\xi}/dr$ is sufficiently negative, the fluid is unstable even when $d\overline{S}/dr$ is positive. And, as Loper (1978) observed, if the outward compositional flux I_r^ξ is sufficiently large and positive, convection will occur through compositional buoyancy, irrespective of whether the outward heat flux I_r^q exceeds the adiabatic flux $\overline{I}_r^{\rm ad}$ or not. The heat $\mathcal{Q}_{\rm CMB}$ leaving the core may be greater or less than the heat $\mathcal{H}_{\rm CMB}$ conducted down the adiabat; compositional buoyancy can be so strong that vigorous mixing occurs that homogenizes $\overline{S}$ and $\overline{\xi}$ even though heat is being pumped downwards by hot descending fluid and cold rising currents! Nevertheless, most simulations of core convection and the geodynamo assume that the convective heat flow $\mathcal{Q}_{\rm CMB}^{\rm conv}$ at the core-mantle boundary is positive (but see Glatzmaier and Roberts, 1997). The reason is simple: a downward entropy flux reduces the vigor of convection and is detrimental to dynamo action.

The mantle and core should ideally be studied as a coupled system. This, however, is impractical; because of their very different viscosities, the mantle and core operate on vastly different time scales. Usually therefore they are considered separately, the thermal state of the one providing a boundary condition at the CMB for the other. The mobility of the core allows it to carry heat readily from one area of the CMB to another, so equalizing their temperatures; this boundary is therefore an isothermal surface. Its temperature prescribes the bottom boundary condition for mantle convection. The heat flux $I_{\rm CMB}^q(\theta,\phi)$ per unit area is then found as a function of (θ,ϕ) by solving the mantle convection equations.[12] This $I_{\rm CMB}^q(\theta,\phi)$ prescribes the upper boundary condition on the solution of the core convection equations. In this way, convection in the mantle is affected by heating from the core, and the core is cooled by the overlying mantle. Convection in the mantle resembles a valve controlling the heat flux $I_{\rm CMB}^q$ from the core. Core convection and the geodynamo are completely at the mercy of this valve. Unless the valve is set to allow enough heat through (i.e., unless mantle convection is sufficiently strong), the dynamo will fail and

[10]The scenario envisaged here for the core is very different from that of the oceans, where $-\xi$ would correspond to the salt content of sea water. The resulting thermohaline convection is usually modeled using a Boussinesq approximation, so that in place of Eq. (2.12), for instance, the criterion for instability is $-\overline{\mathbf{g}}\cdot(\overline{\alpha}\boldsymbol{\nabla}\overline{T}+\overline{\alpha}_T^\xi\boldsymbol{\nabla}\overline{\xi})<0$, where α_T^ξ is the isothermal coefficient of compositional expansion; see Sec. IV.F. Vertical mixing in the oceans is not sufficiently effective to homogenize $\overline{T}$ and $\overline{\xi}$. Similarly, a stably stratified layer may exist at the top of the FOC (Braginsky, 1999).

[11]The CO density has been widely used for convection in Boussinesq (i.e., almost incompressible) fluids, but Braginsky and Roberts (1995), who invented the acronym, seem to have been the first to show that the same idea works for compressible fluids. For a discussion of the history of the idea, see Braginsky and Roberts (2000).

[12]Cold subducting lithospheric plates may descend to a graveyard of plates at the base of the mantle where, until their temperature rises, they cause the heat flux from the core to the mantle to increase locally. See, for example, Ricard *et al.* (1993).

core convection may even shut down. In the reference frame moving with the mantle, the setting of the valve changes only very slowly, on the convective time scale $\tau_m \sim 10^8$ yr of the mantle. The character of core convection and the geodynamo respond on the same τ_m time scale. This provides the most plausible explanation of the variations in reversal frequency shown in Fig. 5.

D. Thermodynamic efficiency

Even if energy is available to satisfy the balance (2.3), is it obvious that the dynamo will function? A further complication was first noticed by Braginsky (1964d), who, regarding the dynamo as a heat engine, questioned whether enough buoyant power would be available to maintain the field. The issue of thermodynamic efficiency was taken further by several authors, most recently by Braginsky and Roberts (1995), whose article gives references to earlier work. This subsection aims to estimate the efficiency of the geodynamo.

There are significant points of difference between the geodynamo and the heat engine considered in texts on thermodynamics. To understand the former better, let us start from the classic heat engine operating steadily in the well-known Carnot cycle. The heat input $\mathcal{Q}_{\rm in}$ is provided at a higher temperature $T_{\rm in}$ than the temperature $T_{\rm out}$ at which heat $\mathcal{Q}_{\rm out}$ is extracted. In a perfect machine, the difference $\mathcal{Q}_{\rm in}-\mathcal{Q}_{\rm out}$ is all useful work, but in practice a part $\mathcal{Q}^D$ of this energy is dissipated uselessly as heat. The rate at which the machine does useful work is therefore

$$\mathcal{A}=\mathcal{Q}_{\rm in}-\mathcal{Q}_{\rm out}-\mathcal{Q}^D. \tag{2.16}$$

The Efficiency of the engine η_E is defined as

$$\eta_E \equiv \frac{\mathcal{A}}{\mathcal{Q}_{\rm in}}=1-\frac{\mathcal{Q}_{\rm out}}{\mathcal{Q}_{\rm in}}-\frac{\mathcal{Q}^D}{\mathcal{Q}_{\rm in}}. \tag{2.17}$$

For simplicity, let us suppose that $\mathcal{Q}^D$ is expended at a single moment during the cycle, when the temperature T_D is within the operating temperature range: $T_{\rm out}<T_D<T_{\rm in}$ of the machine. The entropy balance is then

$$\frac{\mathcal{Q}_{\rm in}}{T_{\rm in}}=\frac{\mathcal{Q}_{\rm out}}{T_{\rm out}}+\frac{\mathcal{Q}^D}{T_D}. \tag{2.18}$$

Equations (2.16)–(2.18) imply that

$$\eta_E=f_F\eta_C, \tag{2.19}$$

$$\eta_C=1-T_{\rm out}/T_{\rm in}. \tag{2.20}$$

Here η_C is the Carnot efficiency and $f_F=1-(\mathcal{Q}^D/\mathcal{Q}_{\rm in}\eta_C)(1-T_{\rm out}/T_D)$ is a frictional factor, lying between 0 and 1 and representing a reduction in the efficiency of the machine below the theoretical maximum η_C.

We now abandon the classical heat engine and attempt to apply similar ideas to Earth's core. There are new and significant features. First, the definition of the "useful work" $\mathcal{A}$ done by the engine is largely arbitrary. Let us suppose that it is the rate of production of large-scale magnetic energy; we do this even though that energy is eventually ohmically degraded into heat at the same rate $\mathcal{Q}^J$. The engine must also make good the remaining frictional losses, $\mathcal{Q}^F$ (say), such as $\mathcal{Q}^\nu$ and $\mathcal{Q}^\iota$ in Eq. (2.2). It follows that

$$\mathcal{A}=\mathcal{Q}^J, \tag{2.21}$$

$$\mathcal{Q}^D=\mathcal{Q}^J+\mathcal{Q}^F. \tag{2.22}$$

A second difference is that, since both $\mathcal{Q}^J$ and $\mathcal{Q}^F$ reappear within the fluid, they must be regarded as part of the energy source driving the engine. The energy balance replacing Eq. (2.16) is therefore simply

$$\mathcal{Q}_{\rm in}=\mathcal{Q}_{\rm out}. \tag{2.23}$$

The entropy balance is expressed by

$$\frac{\mathcal{Q}_{\rm in}}{T_{\rm in}}+\frac{\mathcal{Q}^D}{T_D}=\frac{\mathcal{Q}_{\rm out}}{T_{\rm out}}. \tag{2.24}$$

To be slightly more sophisticated, we may suppose that $\mathcal{Q}^J$ is dissipated at one temperature T_J and $\mathcal{Q}^F$ at another, T_F; then T_D is a compromise between T_J and T_F defined by

$$\frac{\mathcal{Q}^D}{T_D}=\frac{\mathcal{Q}^J}{T_J}+\frac{\mathcal{Q}^F}{T_F}. \tag{2.25}$$

By Eq. (2.23), we may rewrite Eq. (2.24) as

$$\mathcal{Q}^D=\mathcal{Q}_{\rm in}T_D\left(\frac{1}{T_{\rm out}}-\frac{1}{T_{\rm in}}\right). \tag{2.26}$$

It may be seen from Eqs. (2.23) and (2.24) that heat is needed not to maintain the energy balance but to preserve the entropy balance. This limits the efficiency of the device in producing magnetic power. It suggests that, in analogy with the oft encountered phrase "the available energy," it is useful to call $\mathcal{Q}^D$ "the available dissipation," of which only the fraction f_F goes into useful work, $\mathcal{Q}^J$.

The dynamo Efficiency is

$$\eta_E \equiv \frac{\mathcal{Q}^J}{\mathcal{Q}_{\rm in}}=\frac{\mathcal{Q}^J}{\mathcal{Q}^D}\cdot\frac{\mathcal{Q}^D}{\mathcal{Q}_{\rm in}}=f_F\eta_I, \tag{2.27}$$

where the "frictional factor," $f_F=\mathcal{Q}^J/(\mathcal{Q}^J+\mathcal{Q}^F)$, is the fraction of $\mathcal{Q}^D$ that is "useful dissipation," while the factor

$$\eta_I=T_D\left(\frac{1}{T_{\rm out}}-\frac{1}{T_{\rm in}}\right) \tag{2.28}$$

is the Ideal efficiency, which cannot be exceeded, even when there is no internal friction. Since $T_{\rm out}\leqslant T_D\leqslant T_{\rm in}$, it follows from Eq. (2.28) that

$$\eta_C\leqslant\eta_I\leqslant\eta_B, \quad \text{where} \quad \eta_B=(T_{\rm in}/T_{\rm out})-1. \tag{2.29}$$

The argument is now further modified by recognizing the third significant difference between the classical heat engine and the Earth's core: the former is a machine that works steadily, but the core is a slowly evolving system that, apart possibly from some radioactivity, receives all its energy from cooling and gravitational settling. We shall confine this nonstationarity to the refer-

ence state and shall consider the superimposed convection as cyclic, i.e., one that, when averaged over the time scale τ_c of the convection, varies only on the time scale of the slow evolution of the core $\overline{\tau}$. We define the ideal dynamo efficiency η_D as

$$\eta_D = \mathcal{Q}^J / \mathcal{Q}_{\rm CMB}. \tag{2.30}$$

The reciprocal St of η_D was introduced by Stevenson (1984), who pointed out that $St>1$ is a necessary condition for dynamo action.

In considering the average entropy balance of the FOC, we define [in the spirit of our earlier discussion; see Eq. (2.25)] effective temperatures T_R and T_D for radioactivity and dissipation:

$$\mathcal{Q}^D/T_D = \int_{\rm FOC} (q^D/\overline{T}) d^3x, \quad \mathcal{Q}^R/T_R = \int_{\rm FOC} (q^R/\overline{T}) d^3x, \tag{2.31}$$

where q^D and q^R are the volumetric sources that give rise to $\mathcal{Q}^D$ and $\mathcal{Q}^R$ on integration; see Sec. IV. We also encounter the term

$$\int_{\rm FOC} \dot{\bar{S}} \overline{\rho} d^3x = \mathcal{M}_{\rm FOC} \dot{\bar{S}} = -\frac{\mathcal{Q}_S}{\overline{T}_0}, \tag{2.32}$$

by Eq. (2.10). The entropy balance then assumes the form

$$\frac{\mathcal{Q}_{\rm CMB}}{T_{\rm CMB}} = \frac{\mathcal{H}_{\rm ICB} + \mathcal{Q}^L}{T_{\rm ICB}} + \Sigma + \frac{\mathcal{Q}^D}{T_D} + \frac{\mathcal{Q}^S}{\overline{T}_0} + \frac{\mathcal{Q}^R}{T_R}. \tag{2.33}$$

The left-hand side is the entropy flow out of the fluid outer core across the CMB and the first term on the right-hand side is the flow into the fluid outer core across the ICB; Σ is the entropy source from conduction of heat down the adiabat:

$$\Sigma = \int_{\rm FOC} \overline{K}_M (\boldsymbol{\nabla} \overline{T}/\overline{T})^2 d^3x. \tag{2.34}$$

From the model described in Sec. IV.B below, we find that

$$\Sigma \approx 190 \ \ {\rm MW\,K^{-1}}. \tag{2.35}$$

According to Eqs. (2.9) and (2.33), we have

$$\mathcal{Q}^D = \mathcal{Q}^G + \mathcal{Q}^H, \tag{2.36}$$

where

$$\mathcal{Q}^H = (\mathcal{H}_{\rm ICB} + \mathcal{Q}^L)\left(1 - \frac{T_D}{T_{\rm ICB}}\right) + \mathcal{Q}_{\rm CMB}\left(\frac{T_D}{T_{\rm CMB}} - 1\right) + \mathcal{Q}^S\left(1 - \frac{T_D}{\overline{T}_0}\right) + \mathcal{Q}^R\left(1 - \frac{T_D}{T_R}\right) - T_D\Sigma. \tag{2.37}$$

Taking $\overline{T}_0$ as a rough but plausible estimate of T_D (see Table I and Sec. II.A) and assuming that $\mathcal{Q}^R=0$, we obtain

$$\mathcal{Q}^H \approx 0.6 \ \ {\rm TW}, \quad \mathcal{Q}^D \approx 1.9 \ \ {\rm TW}. \tag{2.38}$$

Thus all the gravitational energy released is available for dissipation but (as anticipated from the earlier discussion) only a part, proportional to $\Delta T/T$ for some ΔT, of each thermal contribution to $\mathcal{Q}^D$ is available; in the case of Σ this is evident from its definition (2.34). Recalling that $\mathcal{Q}^\nu$ is probably an insignificant part of $\mathcal{Q}^D$, we see from Eqs. (2.3) and (2.38) that the turbulent dissipation is about six times the large-scale Joule losses (2.1).

By Eq. (2.36), the efficiency (2.30) of the dynamo is $\eta_D = f_F \eta_G$ where η_G is the ideal Geodynamo efficiency,

$$\eta_G \equiv \frac{\mathcal{Q}^D}{\mathcal{Q}_{\rm CMB}}, \tag{2.39}$$

and $f_F = \mathcal{Q}^J/\mathcal{Q}^D$ is the frictional factor. Our estimates of these are

$$\eta_G \approx 28\%, \ \ \eta_D \approx 4\%, \ \ f_F \approx 0.15. \tag{2.40}$$

A similar conclusion follows from an expression derived by Braginsky and Roberts (1995):

$$\eta_G \approx \frac{1}{\mathcal{Q}_{\rm CMB}}\left[\mathcal{Q}^G + \frac{\Delta T_0}{T_{\rm CMB}}(\mathcal{Q}^{\rm conv}_{\rm CMB} + \mathcal{H}_{\rm ICB} + \mathcal{Q}^L)\right], \tag{2.41}$$

where $\Delta T_0 = \overline{T}_0 - T_{\rm CMB}$; this is also about 28%. The heat conducted down the adiabat does not drive convection and is conspicuous by its absence from Eq. (2.41). The two remaining thermal terms are also diminished in usefulness by the factor $\Delta T_0/T_{\rm CMB} \approx 0.13$.

The importance of the issue of thermodynamic efficiency was first raised by Braginsky (1964d), who argued that the efficiency of a thermally driven dynamo would be proportional to ΔT_0 and therefore small. He also foresaw that the compositionally driven dynamo would be 100% efficient. This led him to the conclusion that the geodynamo is primarily compositionally driven. This is supported by our present estimates, which suggest that $\mathcal{Q}^G$ is about twice $\mathcal{Q}^H$.

From an assumed $\mathcal{Q}_{\rm CMB}$, the efficiency η_G determines $\mathcal{Q}^D$ and therefore an upper bound on $\mathcal{Q}^J$. Two other examples of this are the following:
(a) If $\mathcal{Q}^{\rm conv}_{\rm CMB} = \mathcal{Q}^R = 0$, then $\eta_G \approx 24\%$ and $\mathcal{Q}^D \approx 1.3$ TW;
(b) If $\overline{\tau} = 4$ Gyr and $\mathcal{Q}^R = 0$, thermal buoyancy opposes compositional buoyancy, and $\eta_G \approx 2\%$, which implies that $\mathcal{Q}^D \approx 0.04$ TW.
Example (b) touches on a perplexing question of how a thermally driven geodynamo, which is the only type of dynamo that can operate before the birth of the solid inner core, can maintain a field having an intensity much the same as at present, as the paleomagnetic evidence requires (Sec. II.C). Are the estimates made above so greatly in error? Is the assumption that $\mathcal{Q}^R$ was negligible in the remote past (or even now) unjustified?

III. BASIC DYNAMO THEORY

A. The induction equation

This section describes solutions of

$$\partial_t \mathbf{B} = \boldsymbol{\nabla} \times (\mathbf{V} \times \mathbf{B} - \overline{\eta} \boldsymbol{\nabla} \times \mathbf{B}), \tag{3.1}$$

$$\boldsymbol{\nabla} \cdot \mathbf{B} = 0. \tag{3.2}$$

These are the equations governing the magnetic field **B** in the conducting volume $\mathcal{V}$ (=FOC+SIC) of the core. Equation (3.1) is called the *induction equation*. In this subsection we sketch its origins. Further details can be found in most texts on MHD.

We start from the pre-Maxwell equations, i.e., the Maxwell equations with the displacement current neglected because $\overline{\mathcal{U}}$ is tiny compared with the speed of light. These include Eq. (3.2) together with

$$\partial_t \mathbf{B} = -\nabla \times \mathbf{E}, \tag{3.3}$$

$$\mathbf{J} = \nabla \times \mathbf{B}/\mu_0, \tag{3.4}$$

where **E** is the electric field. Implicit in Eq. (3.4) is the assumption that the permeability μ_0 is that of free space, so that the magnetizing force **H** is simply $\mathbf{B}/\mu_0$. The source of **B** and **E** is the electric current density **J**, which for a dense fluid such as the Earth's core is given by Ohm's law, in the form appropriate for a moving, dense, electrical conductor:

$$\mathbf{J} = \sigma_M(\mathbf{E} + \mathbf{V} \times \mathbf{B}), \tag{3.5}$$

where σ_M is the electrical conductivity. Equations (3.4) and (3.5) imply[13]

$$\mathbf{E} = -\mathbf{V} \times \mathbf{B} + \overline{\eta} \nabla \times \mathbf{B}, \tag{3.6}$$

where (see Sec. I.B) $\overline{\eta} = 1/\mu_0 \sigma_M$. Equation (3.1) follows at once from Eqs. (3.3) and (3.6) and, if σ_M is constant, it may be written alternatively as

$$\partial_t \mathbf{B} = \nabla \times (\mathbf{V} \times \mathbf{B}) + \overline{\eta} \nabla^2 \mathbf{B}. \tag{3.7}$$

Pre-Maxwell theory is Galilean invariant and not Lorentz invariant; **B**, and therefore **J**, are frame invariant, though plainly **E** is not. Also, although ∂_t and **V** depend on the reference frame, Eq. (3.1) does not.

For simplicity, let us ignore electrical conduction everywhere in the exterior $\hat{\mathcal{V}}$ of $\mathcal{V}$, including the mantle. The electromagnetic field again obeys Eqs. (3.2)–(3.4), but Eq. (3.5) is replaced by $\hat{\mathbf{J}} = \mathbf{0}$, so that $\hat{\mathbf{B}}$ is a potential field [see Eqs. (1.15) and (1.16)]. And

$$\mathbf{B} = \hat{\mathbf{B}}, \quad \text{on the core-mantle boundary.} \tag{3.8}$$

[13]This form of Ohm's law highlights the fact that, in contrast to full Maxwell theory, **E** and **B** are not on an equal footing in the pre-Maxwell approximation: **B** is the master and **E** the slave. If desired, **E** can be obtained from Eq. (3.6) after **B** has been determined. The energy density of the electric field is negligible compared with that of the magnetic field, and the electric stresses are negligible compared with the magnetic stresses. The free charge density is in general nonzero but exerts a force on the conductor that is negligible compared with the Lorentz force. If $\overline{\eta}$ and/or $\mathbf{r} \times \mathbf{V}$ is assumed to be discontinuous on the inner core boundary, **E** makes a fleeting reappearance, since it is necessary to ensure that $\mathbf{r} \times \mathbf{E}$ is continuous. Because of the surface charge density generally present on a surface of discontinuity of material properties, there is a jump in the normal component of **E** there, but (since $\overline{\eta} \neq 0$) all components of **B** are continuous.

B. Kinematic dynamos, Cowling's theorem

The dynamos we study in this review are often called "homogeneous dynamos," to distinguish them from the manmade dynamos that are deliberately constructed to be inhomogeneous and that obviously work. It is not so evident that a continuous simply connected mass of fluid can create field efficiently (or at all).

The *dynamo problem* arises when we require that there be no sources of magnetic field in $\hat{\mathcal{V}}$ even "at infinity." This demand is crucial, since it is always possible to maintain a field in a conductor by applying one from the outside. Sources in $\hat{V}$ at a finite distance from the conductor, arising from electric currents or permanent magnetism, are excluded by Eqs. (1.15) and (1.16), and sources at infinity are eliminated by the requirement (1.17) that the field be dipolar at great distances:

$$\hat{\mathbf{B}} = O(r^{-3}), \quad \text{as} \quad r \to \infty. \tag{3.9}$$

We shall refer to this as the "dynamo condition." A successful dynamo is one that actively maintains **B** for as long as energy sources exist to maintain **V**:

$$\mathbf{B} \not\to \mathbf{0}, \quad \text{as} \quad t \to \infty. \tag{3.10}$$

In practical terms, $t \to \infty$ can simply mean $t \gg \tau_\eta$ (see below).

There are two kinds of dynamos: the *kinematic dynamo* and the *MHD dynamo*.[14] The kinematic dynamo problem is, Given **V**, find **B**. The MHD dynamo problem is, Given an energy source such as buoyancy, find **B** *and* **V**. Evidently, the MHD problem contains the kinematic problem. The kinematic problem is linear in the unknown **B** and is therefore considerably easier to solve than the MHD problem, which is nonlinear in **B** and **V**. The linearity of kinematic dynamo theory is also its principal weakness. It predicts that **B** either grows without limit for the given **V**, or dies inexorably, or rests on a knife edge between. This unreality disappears when momentum balance is demanded. The Lorentz force $\mathbf{J} \times \mathbf{B}$ regulates **V** so that the knife edge becomes the norm for a successful dynamo, at least when averaged over time. We may regard kinematic theory as being realistic for studying the growth of a weak "seed field" until (or if) that seed field becomes so strong that its Lorentz force alters **V**.

When **V** is time independent, the kinematic dynamo defines a linear eigenvalue problem for the growth rate λ of the field $[\mathbf{B}(t) = \mathbf{B}(0)\exp(\lambda t)]$. Because the eigenvalue problem is not self-adjoint, λ is usually complex. If $\mathrm{Im}(\lambda) \neq 0$, the solution oscillates, corresponding to field reversal, but on a time scale of order τ_η, which is too short to have a direct bearing on the geomagnetic field (although it is of interest in the modeling of magnetic activity in the Sun and other lower main-sequence stars).

[14]Sometimes the MHD dynamo is called the "self-consistent dynamo." We refrain from using this term, to avoid the unfortunate implication that the kinematic theory is inconsistently formulated.

By condition (3.10), dynamo action requires that $\mathrm{Re}(\lambda) \geqslant 0$ for at least one eigenvalue, with $\mathrm{Re}(\lambda)=0$ for that eigenvalue defining the *marginal state*. There is no guarantee that, if $\mathbf{V}$ is a dynamo motion, $-\mathbf{V}$ is one also.

When $\mathbf{V}$ is periodic in time with period P, dynamo action requires that a solution exist in which $\mathbf{B}(t+P) = \mathbf{B}(t)\exp(\lambda P)$ with $\mathrm{Re}(\lambda)\geqslant 0$. When $\mathbf{V}$ is time dependent but not periodic (as can happen when solving the MHD problem—see Sec. VI), the claim of dynamo action is not so easily made precise but, if $\mathbf{B}$ has persisted without noticeable diminution over a time long compared with τ_η (so that transients from the initial state have disappeared), it is reasonable to claim that a dynamo has been found. A less stringent definition of dynamo action has been proposed by Hughes (1993). But both definitions of a dynamo differ from what is usually meant by this term when describing the reversed-field pinch in plasma research (see, for example, Fowler, 1999; Kabantsev *et al.*, 1999).

In this section we consider only kinematic theory; the remainder of the article deals with MHD dynamos. By taking the scalar product of Eq. (3.1) with $\mathbf{B}/\mu_0$ and integrating over the core $\mathcal{V}$, we find that

$$-\partial_t \mathcal{E}^B = \mathcal{Q}^B + \mathcal{Q}^J, \tag{3.11}$$

where

$$\left.\begin{aligned} &\mathcal{E}^B = \frac{1}{2\mu_0}\int_{\mathcal{V}+\hat{\mathcal{V}}} \mathbf{B}^2 d^3x, \quad \mathcal{Q}^B = \int_{\mathcal{V}} \mathbf{V}\cdot(\mathbf{J}\times\mathbf{B}) d^3x, \\ &\mathcal{Q}^J = \mu_0 \int_{\mathcal{V}} \overline{\eta}\mathbf{J}^2 d^3x. \end{aligned}\right\} \tag{3.12}$$

Equation (3.11) has a simple interpretation: the left-hand side is the rate of decrease of magnetic energy $\mathcal{E}^B$; the first term on the right-hand side is the rate $\mathcal{Q}^B$ at which the Lorentz force converts magnetic energy into kinetic energy; the final term is the Ohmic dissipation $\mathcal{Q}^J$, which is positive. In a successful dynamo, the first term on the right-hand side is negative and creates magnetic energy from kinetic energy at a rate greater than the rate $\mathcal{Q}^J$ at which electrical resistance can transform it into heat. By dimensional analysis of Eq. (3.1), we see that a necessary condition for this to happen is[15] $Rm \gtrsim O(1)$, where

$$Rm = \overline{\mathcal{UL}}/\overline{\eta} \tag{3.13}$$

is the magnetic Reynolds number. According to estimates (1.24) and (1.25), this is about 125 for the Earth. A long-standing challenge to experimenters has been to exhibit convincingly a homogeneous fluid dynamo in the laboratory where, even with the use of liquid metals, $O(1)$ values of Rm are hard to attain because of the comparatively small values of $\overline{\mathcal{L}}$ available; see Roberts and Jensen (1993), Busse (2000). Very recent reports suggest that this challenge has now been met; see Gailitis *et al.* (2000), Stieglitz and Müller (2000).

Unfortunately, the condition $Rm \gtrsim O(1)$, though necessary, is not sufficient for dynamo action, and it is easy to construct examples in which Rm is large and the magnetic energy $\mathcal{E}^B$ grows strongly at first, but ultimately tends to zero. Cowling (1933) was responsible for a major setback in the subject:

Cowling's theorem: *an axisymmetric* $\mathbf{B}$ *cannot be sustained by dynamo action*.

[A field is said to be axisymmetric if it is the same in every meridional plane about the symmetry axis; this does not mean that its zonal component is zero. In our application, the polar axis Oz defines axisymmetry; see Eq. (3.20) below.] It took 25 more years before the existence of homogeneous dynamos was unequivocally established. By now there are several simple examples, based on the observation that, although Cowling's theorem rules out axisymmetric $\mathbf{B}$, it does not rule out kinematic[16] dynamos with axisymmetric $\mathbf{V}$. The simplest example of all (Ponomarenko, 1973) operates in a space-filling conductor which is stationary apart from an infinite cylinder ($s<a$) that is in helical motion:

$$\mathbf{V} = \omega s \mathbf{1}_\phi + U\mathbf{1}_z, \tag{3.14}$$

where (s,ϕ,z) are cylindrical coordinates, unit vectors in the direction of coordinate q increasing are denoted by $\mathbf{1}_q$, and U and ω are nonzero constants. Ponomarenko's model is obviously remote from geophysics, but it does dispel any gloomy thoughts Cowling's theorem might provoke. And simple axisymmetric models have been devised (Dudley and James, 1989) that resemble the Ponomarenko model but that fit into a sphere. The Ponomarenko model and the Dudley and James models maintain asymmetric $\mathbf{B}$, thus evading Cowling's theorem. The field travels as a wave around the axis of symmetry, a wave that grows in amplitude if Rm exceeds a critical value Rm_c but that diminishes to zero if $Rm < Rm_c$.

With the Earth in mind and with symmetry dictated by the polar axis (because of the importance of Coriolis forces; see Sec. V), we should focus on working dynamos in which $\mathbf{B}$ possesses a nonzero axisymmetric part $\tilde{\mathbf{B}}$. In what follows, we shall write

$$\mathbf{B} = \tilde{\mathbf{B}} + \mathbf{B}', \quad \mathbf{V} = \tilde{\mathbf{V}} + \mathbf{V}', \tag{3.15}$$

and define the emf (electromotive force) due to the asymmetries by

$$\boldsymbol{\mathcal{E}} \equiv \mathbf{V}'\times\mathbf{B}' = \tilde{\boldsymbol{\mathcal{E}}} + \boldsymbol{\mathcal{E}}'. \tag{3.16}$$

Dividing Eq. (3.7) into axisymmetric and asymmetric parts, we obtain

[15] A fascinating branch of kinematic dynamo theory concerns the fast-dynamo limit, $Rm\to\infty$. The geodynamo operates on the "slow" diffusive time scale τ_η, and we shall therefore not discuss fast dynamos, but see Childress and Gilbert (1995).

[16] It does, however, prevent MHD dynamos from being axisymmetric in $\mathbf{V}$. Kinematic dynamos with axisymmetric $\mathbf{V}$ create asymmetric $\mathbf{B}$. The concomitant asymmetry in the Lorentz force adds asymmetry to $\mathbf{V}$.

$$\partial_t \tilde{\mathbf{B}} = \boldsymbol{\nabla}\times(\tilde{\mathbf{V}}\times\tilde{\mathbf{B}} + \tilde{\boldsymbol{\mathcal{E}}}) + \overline{\eta}\nabla^2\tilde{\mathbf{B}}, \tag{3.17}$$

$$\partial_t \mathbf{B}' - \boldsymbol{\nabla}\times(\tilde{\mathbf{V}}\times\mathbf{B}' + \boldsymbol{\mathcal{E}}') - \overline{\eta}\nabla^2\mathbf{B}' = \boldsymbol{\nabla}\times(\mathbf{V}'\times\tilde{\mathbf{B}}). \tag{3.18}$$

A transparent way of establishing Cowling's theorem was devised by Braginsky (1964a) and requires $\tilde{\mathbf{V}}$ to be an incompressible flow ($\boldsymbol{\nabla}\cdot\tilde{\mathbf{V}}=0$).[17] First $\tilde{\mathbf{V}}$ and $\tilde{\mathbf{B}}$ are divided into their (axisymmetric) zonal and meridional parts,

$$\tilde{\mathbf{V}} = s\zeta(s,z,t)\mathbf{1}_\phi + \mathbf{V}_p(s,z,t), \tag{3.19}$$

$$\tilde{\mathbf{B}} = B(s,z,t)\mathbf{1}_\phi + \mathbf{B}_p(s,z,t), \tag{3.20}$$

where $_p$ is used for the "meridional" or "poloidal" component; this can be represented by a vector potential, e.g.,

$$\mathbf{B}_p = \boldsymbol{\nabla}\times[A(s,z,t)\mathbf{1}_\phi]. \tag{3.21}$$

Then Eq. (3.17) gives

$$\frac{1}{s}\left[\frac{\partial}{\partial t} + \mathbf{V}_p\cdot\boldsymbol{\nabla}\right]sA - \overline{\eta}\Delta A = \tilde{\mathcal{E}}_\phi, \tag{3.22}$$

$$s\left[\frac{\partial}{\partial t} + \mathbf{V}_p\cdot\boldsymbol{\nabla}\right]\frac{B}{s} - \overline{\eta}\Delta B = s\mathbf{B}_p\cdot\boldsymbol{\nabla}\zeta + (\boldsymbol{\nabla}\times\tilde{\boldsymbol{\mathcal{E}}})_\phi, \tag{3.23}$$

where $\Delta = \nabla^2 - s^{-2}$. In $\hat{\mathcal{V}}$, we have

$$\Delta\hat{A} = \hat{B} = 0, \ \hat{A}\to 0 \ \text{ as } \ r\to\infty, \tag{3.24}$$

and Eq. (3.8) requires that

$$A = \hat{A}, \ \frac{\partial A}{\partial r} = \frac{\partial \hat{A}}{\partial r}, \ B = \hat{B}, \ \text{ on the CMB.} \tag{3.25}$$

If $\boldsymbol{\mathcal{E}}\equiv\mathbf{0}$, it follows from Eqs. (3.22)–(3.25) that

$$\tfrac{1}{2}\,\partial_t\int_{\mathcal{V}}(sA)^2 d^3x = -\overline{\eta}\int_{\mathcal{V}+\hat{\mathcal{V}}}[\boldsymbol{\nabla}(sA)]^2 d^3x < 0, \tag{3.26}$$

$$\tfrac{1}{2}\,\partial_t\int_{\mathcal{V}}\left(\frac{B}{s}\right)^2 d^3x = -\overline{\eta}\int_{\mathcal{V}}\left[\boldsymbol{\nabla}\left(\frac{B}{s}\right)\right]^2 d^3x + \int_{\mathcal{V}}\frac{B}{s^2}[\boldsymbol{\nabla}(sA)\times\boldsymbol{\nabla}\zeta]_\phi d^3x. \tag{3.27}$$

By Eq. (3.26), $A\to 0$ as $t\to\infty$, so that the second term on the right-hand side of Eq. (3.27) ultimately disappears too. The right-hand side of Eq. (3.27) is then negative, so that $B\to 0$ also. In short, $\boldsymbol{\mathcal{E}}\equiv\mathbf{0}$ implies that $\tilde{\mathbf{B}}\to 0$ as $t\to\infty$. This is Cowling's result: A working dynamo necessarily maintains a $\mathbf{B}$ having an asymmetric part $\mathbf{B}'$. Perhaps this is why the geomagnetic and geographic axes are persistently inclined to one another (see Sec. I.C).

This proof of Cowling's theorem shows that to establish dynamo action it is never sufficient to show that $\mathcal{E}^B$ initially increases in time. Equation (3.27) demonstrates that, until A becomes small, the rate of increase of the magnetic energy stored in the zonal field may be positive if ζ is large enough. The term $s\mathbf{B}_p\cdot\boldsymbol{\nabla}\zeta$ in Eq. (3.23) responsible for this can be interpreted by

Alfvén's frozen-flux theorem: *Flux tubes in a perfectly conducting fluid are carried by the fluid in its motion, just as though they were frozen to it.*

The freezing is imperfect when Rm is large but not infinite. The theorem nevertheless provides a useful and qualitatively correct way of visualizing induction processes, except in regions where the field gradients are large and where a locally defined Rm is uncharacteristically small, thus allowing the severing and reconnection of field lines that would be forbidden when $Rm=\infty$. In the present case, the zonal shear ζ stretches the lines of force ($sA=$const) of the meridional field $\mathbf{B}_p$ along lines of latitude to create $\tilde{B}_\phi$. Often (though not here) $\tilde{V}_\phi/s$ is denoted by ω rather than ζ, and this mechanism for creating B became known as the "ω effect".

C. Turbulent helicity and the α effect

For given $\tilde{\mathbf{B}}$ and $\mathbf{V}$, Eq. (3.18) is an inhomogeneous linear equation for $\mathbf{B}'$, its right-hand side being then a known source. Solving Eq. (3.18) for $\mathbf{B}'$, we can then obtain $\tilde{\boldsymbol{\mathcal{E}}}$ from Eq. (3.16). Thus $\mathbf{B}'(\tilde{\mathbf{B}})$ and $\tilde{\boldsymbol{\mathcal{E}}}(\tilde{\mathbf{B}})$ are linear functionals of $\tilde{\mathbf{B}}$, and Eq. (3.17) becomes a closed equation for $\tilde{\mathbf{B}}$.

At first sight, this method of solving the kinematic dynamo does not recommend itself. The functionals $\mathbf{B}'(\tilde{\mathbf{B}})$ and $\tilde{\boldsymbol{\mathcal{E}}}(\tilde{\mathbf{B}})$ depend on $\tilde{\mathbf{B}}$ and $\mathbf{V}$ at all points $\mathbf{x}$ in the fluid and at all earlier times t. To determine them seems to be a task every bit as daunting as solving Eq. (3.1) itself. Simplifications arise, however, when the conducting fluid is in turbulent motion: we separate $\mathbf{V}$ and $\mathbf{B}$, not as in Eq. (3.15) according to their symmetry, but into their large-scale (which we often call the "macroscale" below) and small-scale ("microscale") parts, the former being the average over the turbulence (denoted by angle brackets) and the latter being the fluctuating remnant, for example,

$$\mathbf{V} = \langle\mathbf{V}\rangle + \mathbf{V}^t, \ \text{ where } \ \langle\mathbf{V}^t\rangle = \mathbf{0}. \tag{3.28}$$

In this subsection (but not later) we shall have particularly in mind situations of large magnetic Reynolds number, $Rm^t = \mathcal{L}^t\mathcal{V}^t/\eta$; these are relevant in many astrophysical contexts.

The emf due to the turbulence is similar to Eq. (3.16):

$$\boldsymbol{\mathcal{F}} \equiv \mathbf{V}^t\times\mathbf{B}^t = \langle\boldsymbol{\mathcal{F}}\rangle + \boldsymbol{\mathcal{F}}^t. \tag{3.29}$$

Separating Eq. (3.7) into its macroscale and microscale parts, we obtain, as in Eqs. (3.17) and (3.18),

$$\partial_t\langle\mathbf{B}\rangle = \boldsymbol{\nabla}\times(\langle\mathbf{V}\rangle\times\langle\mathbf{B}\rangle + \langle\boldsymbol{\mathcal{F}}\rangle) + \overline{\eta}\nabla^2\langle\mathbf{B}\rangle, \tag{3.30}$$

$$\partial_t\mathbf{B}^t - \boldsymbol{\nabla}\times(\langle\mathbf{V}\rangle\times\mathbf{B}^t + \boldsymbol{\mathcal{F}}^t) - \overline{\eta}\nabla^2\mathbf{B}^t = \boldsymbol{\nabla}\times(\mathbf{V}^t\times\langle\mathbf{B}\rangle). \tag{3.31}$$

[17] This assumption was not made by Cowling in one of his original proofs, but this proof was not totally satisfactory. Ivers and James (1984) provided the mathematically most general demonstration of Cowling's theorem.

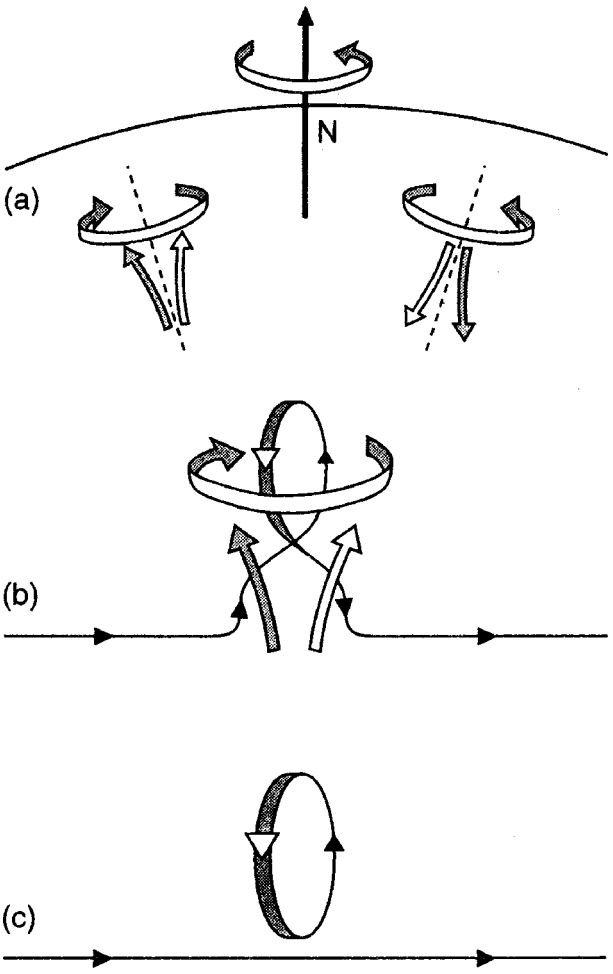

FIG. 7. Cartoons describing the microscopic α effect. (a) rising (left) and sinking (right), eddies in the northern hemisphere of a rotating, turbulently convecting fluid; (b) the effect of these on a horizontal field line; (c) the situation after the flux loop created shown in panel (b) has broken away from the parent field line.

We would like to be able to solve Eq. (3.31) for $\mathbf{B}^t$ and thence to obtain $\langle \mathcal{F} \rangle$ as a linear functional of $\langle \mathbf{B} \rangle$ that could be used to close Eq. (3.30). As before, this is a daunting task. One may, however, argue heuristically that, if the microscale $\mathcal{L}^t$ is sufficiently small compared with the macroscale $\overline{\mathcal{L}}$, the functional $\langle \mathcal{F} \rangle (\langle \mathbf{B} \rangle)$ at the point $\mathbf{x}$ should be well represented by the first few terms in its Taylor expansion about $\mathbf{x}$, e.g.,

$$\langle \mathcal{F} \rangle_i = \alpha_{ij} \langle B_j \rangle + \beta_{ijk} \nabla_j \langle B_k \rangle, \tag{3.32}$$

where α_{ij} and β_{ijk} depend on $\langle \mathbf{V} \rangle$ and on the statistical properties of the turbulence $\mathbf{V}^t$. According to Eq. (3.32), $\langle \mathcal{F} \rangle$ at $\mathbf{x}$ depends only on $\langle \mathbf{B} \rangle$ and its derivatives at $\mathbf{x}$. This is what is meant by a *local turbulence theory*; we shall meet it again in Sec. IV.D. The existence and importance of the first term in the expansion (3.32) was first noticed by Parker (1955). We briefly review his picture of microscale induction by "cyclonic turbulence."

Consider (in the corotating frame) turbulent convection in the northern hemisphere of a rotating sphere of compressible fluid rotating about an axis Oz. To simplify the discussion, suppose that $\langle \mathbf{V} \rangle = \mathbf{0}$. Visualize, as in Fig. 7(a), the turbulence as consisting of tiny rising and sinking "eddies," each having a brief identity before dissolving back into its surroundings. The left-hand eddy in Fig. 7(a) is rising ($V_r^t > 0$), and as it rises it expands, tending to conserve its angular momentum about the vertical as it does so. The vertical component $(\nabla \times \mathbf{V}^t)_r$ of its vorticity (relative to the rotating frame) is therefore negative, as is $V_r^t (\nabla \times \mathbf{V}^t)_r$. The right-hand eddy in Fig. 7(a) is sinking ($V_r^t < 0$), and as it does so it compresses and tends to rotate more rapidly about the vertical [$(\nabla \times \mathbf{V}^t)_r > 0$], so that again $V_r^t (\nabla \times \mathbf{V}^t)_r < 0$. Averaging over rising and falling eddies, we see that the *helicity*[18] of the turbulence, defined by

$$H = \langle \mathbf{V}^t \cdot \nabla \times \mathbf{V}^t \rangle, \tag{3.33}$$

is negative.

In understanding the inductive effects of an eddy, we suppose that its magnetic Reynolds number Rm^t is large enough for Alfvén's frozen flux theorem to be useful. The effect of the cyclonic motions on a large-scale horizontal field $\langle \mathbf{B} \rangle$ is sketched in Fig. 7(b). An upward-moving eddy makes an Ω-shaped indentation in a horizontal field line and the vertical vorticity simultaneously twists that Ω out of the plane of the paper. Now recall that, though Rm^t is large, it is not infinite, so that diffusion acts particularly strongly where the field gradients are large, as at the base of the Ω. This causes the Ω to be severed from its parent line, to form a loop of flux in a plane perpendicular to the paper, as in Fig. 7(c). A downward-moving eddy creates a flux loop of the same type. These processes are repeated throughout the fluid, and their net effect is to impose on the initial field a right-handed helical structure, just as though an electric field existed to drive current parallel to the initial field[19]:

$$\langle \mathcal{F} \rangle = \alpha \langle \mathbf{B} \rangle. \tag{3.34}$$

Steenbeck and Krause (1966) christened this the "alpha effect," for no better reason than that they used the letter α to describe the proportionality. But the name has stuck. It has spawned an entirely new field of study, *mean-field electrodynamics*, which investigates in greater depth how $\langle \mathcal{F} \rangle$ depends on the strength and statistical properties of the turbulence [see Moffatt (1978) and Krause and Rädler (1980)].

On comparing the *Ansatz* (3.34) with Eq. (3.32), we see that the latter implies that $\alpha_{ij} = \alpha \delta_{ij}$, which requires that the turbulence be pseudoisotropic, i.e., turbulence having statistics that are independent of direction but

[18]This felicitous term is due to Moffatt (1969). The quantity itself was first introduced by Steenbeck and Krause (1966), who gave it the more forbidding German name *Schraubensinn*, which might be translated as "sense of screws."

[19]From $H < 0$, we therefore have $\alpha > 0$, and similarly, $\alpha < 0$ in the southern hemisphere where $H > 0$. These pseudoscalars tend to have opposite signs. The use of α elsewhere in this review to mean the coefficient of volume expansion should not cause confusion.

that are not invariant under coordinate reflection. (In truth, not even the cyclonic turbulence described above is like that.) Isotropy requires that $\beta_{ijk}=-\overline{\eta}^t\epsilon_{ijk}$ where $\overline{\eta}^t$ is a turbulent magnetic diffusivity. When $\overline{\eta}^t \gg \overline{\eta}$, the α effect *Ansatz* leads, not to Eq. (3.1), but to an induction equation for $\langle\mathbf{B}\rangle$ of the form

$$\partial_t\langle\mathbf{B}\rangle=\boldsymbol{\nabla}\times(\langle\mathbf{V}\rangle\times\langle\mathbf{B}\rangle+\alpha\langle\mathbf{B}\rangle)-\boldsymbol{\nabla}\times(\overline{\eta}^t\boldsymbol{\nabla}\times\langle\mathbf{B}\rangle). \tag{3.35}$$

Cowling's theorem does not apply to this equation, and in principle it can have nontrivial axisymmetric solutions when $\alpha\neq 0$.

D. Large-scale helicity and α effect

Although the Earth's core is undoubtedly turbulent, it is unlikely, in view of the large magnetic diffusivity of the fluid, that Rm^t is large. This implies that microscale induction is not very significant, and Eq. (3.1) is more realistic than Eq. (3.35). Our reason for discussing cyclonic turbulence was not geophysical realism, but to introduce in a simple way the concepts of helicity and the α effect and to show how they arise naturally in rotating convection. In fact, convective motions *of every scale* are helical in a rotating fluid, and they create $\bar{\boldsymbol{\mathcal{E}}}$ by something like an α effect, though one that is nonlocal and not simply related to helicity. We believe that the geodynamo (though not every dynamo in nature) is maintained principally by large-scale flows. The successful Ponomorenko motion (3.14) is of large scale and helical, and the same is true of the Dudley and James models.[20]

The *Ansatz*

$$\tilde{\boldsymbol{\mathcal{E}}}=\alpha\tilde{\mathbf{B}} \tag{3.36}$$

[cf. Eq. (3.34)] is not so easily defended when $\tilde{\boldsymbol{\mathcal{E}}}$ is produced nonlocally by $\mathbf{V}'$ and $\mathbf{B}'$, but an interesting class of large-scale motions with helicity that generate a local α effect was discovered by Braginsky (1964a, 1964b). He had a very attractive idea: axisymmetric $\mathbf{B}$ is impossible (i.e., requires infinite Rm), but perhaps nearly axisymmetric dynamos can work if Rm is large enough. He supposed that $\mathbf{V}'/\tilde{V}_\phi=O(Rm^{-1/2})$, which produced $\mathbf{B}'/\tilde{B}_\phi=O(Rm^{-1/2})$ by Eq. (3.18) and therefore an $\tilde{\boldsymbol{\mathcal{E}}}_\phi$ of order Rm^{-1}. He found, in analogy with the turbulent α effect, that $\tilde{\boldsymbol{\mathcal{E}}}=\alpha\tilde{B}_\phi\mathbf{1}_\phi$, so that Cowling's theorem is again evaded; nearly axisymmetric flows can maintain a dynamo in which $\tilde{\mathbf{B}}_p$ is of order $\tilde{B}_\phi/Rm$. Braginsky computed α explicitly in terms of the assumed $\mathbf{V}'/\tilde{V}_\phi$. In this way he provided the first mathematical justification of Parker's ideas and could also compute what were, in a sense, the first 3D kinematic geodynamos (Braginsky, 1964c). Soward (1972) later made use of asymptotic techniques based on $Rm\to\infty$ to create a powerful, pseudo-Lagrangian alternative to Braginsky's method. He rederived Braginsky's results and found a direct connection between Braginsky's α and the helicity of the flow; see also Chap. 8 of Moffatt (1978). This approach also explains why Braginsky's α is local, in the sense defined above, even though $\mathbf{V}'$ is a large-scale flow; see also Soward (1990).

The *Ansatz* (3.36) provides a simple and popular way of constructing 2D mean-field dynamos (Roberts, 1972) by a two-stage process:

step 1: A is created from B by the $\tilde{\mathcal{E}}_\phi=\alpha B$ source in Eq. (3.22);

step 2: B is created from A through the source $s\mathbf{B}_p\cdot\boldsymbol{\nabla}\zeta+(\boldsymbol{\nabla}\times\tilde{\boldsymbol{\mathcal{E}}})_\phi=[\boldsymbol{\nabla}(sA)\times\boldsymbol{\nabla}\zeta+\boldsymbol{\nabla}\times(\alpha\boldsymbol{\nabla}\times A\mathbf{1}_\phi)]_\phi$ in Eq. (3.23).

Clearly α is essential in step 1, but there are three possibilities in step 2. If $(\boldsymbol{\nabla}\times\tilde{\boldsymbol{\mathcal{E}}})_\phi$ is large compared with $s\mathbf{B}_p\cdot\boldsymbol{\nabla}\zeta$, step 2 relies on α for a second time, so that such models are called "α^2 dynamos." If $s\mathbf{B}_p\cdot\boldsymbol{\nabla}\zeta$ is large compared with $(\boldsymbol{\nabla}\times\tilde{\boldsymbol{\mathcal{E}}})_\phi$, then B is created by the ω effect, and the model is an "$\alpha\omega$ dynamo." When α and ω effects are equally significant in step 2, it is an "$\alpha^2\omega$ dynamo." The terms α^2 dynamo, $\alpha\omega$ dynamo, etc. are also used in Sec. VI to describe how a 3D dynamo model maintains the axisymmetric part $\tilde{\mathbf{B}}$ of its field $\mathbf{B}$.

Many useful kinematic dynamos operating with 3D large-scale motions have been produced by numerical integration, without any appeal to mean-field electrodynamics or the Braginsky-Soward theory; see, for example, Love and Gubbins (1996). It is fashionable to say that the kinematic dynamo problem is solved, despite the fact that it is still a nontrivial operation to extract $\mathbf{B}$ from an arbitrarily specified $\mathbf{V}$.

IV. DYNAMICAL THEORY

A. The full (primitive) equations

The main motivation for this section is to explain how the full MHD theory of the core can be reduced to realistic but manageable proportions. A more complete analysis has been given by Braginsky and Roberts (1995). Readers interested only in a basis for numerical simulations may wish to move forward to Sec. IV.E.

The starting point is the set of primitive equations:

$$\partial_t\rho=-\boldsymbol{\nabla}\cdot(\rho\mathbf{V}), \tag{4.1}$$

$$\rho d_t\mathbf{V}=-\boldsymbol{\nabla}P+\rho\mathbf{g}-2\rho\boldsymbol{\Omega}\times\mathbf{V}+\rho\mathbf{F}^B+\rho\mathbf{F}^\nu, \tag{4.2}$$

$$\rho d_t S=-\boldsymbol{\nabla}\cdot\mathbf{I}^S+\sigma^S, \tag{4.3}$$

$$\rho d_t\xi=-\boldsymbol{\nabla}\cdot\mathbf{I}^\xi, \tag{4.4}$$

$$\boldsymbol{\nabla}\cdot\mathbf{B}=0, \tag{4.5}$$

$$\partial_t\mathbf{B}=\boldsymbol{\nabla}\times(\mathbf{V}\times\mathbf{B})-\boldsymbol{\nabla}\times(\eta\boldsymbol{\nabla}\times\mathbf{B}), \tag{4.6}$$

where $d_t=\partial_t+\mathbf{V}\cdot\boldsymbol{\nabla}$ is the motional (or Lagrangian) derivative in the chosen reference frame, which is usually fixed to the mantle. Equations (4.1) and (4.2) express conservation of total mass and momentum. The latter is no more than the usual Navier-Stokes equation in the

[20] Strictly speaking, helicity is not essential for a dynamo to function, but it certainly helps; see Gailitis (1993).

rotating frame, with the buoyancy force $\rho\mathbf{g}$ and Lorentz force $\rho\mathbf{F}^B=\mathbf{J}\times\mathbf{B}$ included, where $\mathbf{B}$ is determined by Eqs. (4.5) and (4.6), the topic of Sec. III. The rotation of the frame has introduced not only a Coriolis force $-2\rho\boldsymbol{\Omega}\times\mathbf{V}$ but also a centripetal acceleration $-\boldsymbol{\Omega}\times(\boldsymbol{\Omega}\times\mathbf{r})$, which is absorbed into the Newtonian gravitational acceleration to create the "effective" gravitational field $\mathbf{g}=-\boldsymbol{\nabla}U$. The effective gravitational potential U satisfies

$$\nabla^2 U=4\pi G\rho-2\Omega^2, \tag{4.7}$$

where G is the constant of gravitation. The Poincaré force $-\dot{\boldsymbol{\Omega}}\times\mathbf{r}$ has been ignored (but would have to be restored if we were to include the luni-solar precession; see Sec. II.A). The viscous force is

$$\rho\mathbf{F}^{\nu}=\boldsymbol{\nabla}\cdot\overleftrightarrow{\boldsymbol{\pi}}^{\nu},\quad \text{where}\quad \pi^{\nu}_{ij}=2\rho\nu_M(e_{ij}-\tfrac{1}{3}e_{kk}\delta_{ij}), \tag{4.8}$$

where $e_{ij}=\frac{1}{2}(\nabla_i V_j+\nabla_j V_i)$ is the rate of strain tensor. Equation (4.3) governs the evolution of entropy, $\mathbf{I}^S$ being the entropy flux and σ^S the rate of entropy production. Equation (4.4) when combined with Eq. (4.1) ensures mass conservation for the individual constituents of the alloy; $\mathbf{I}^{\xi}$ is a mass flux proportional to the small difference between the velocity of the light constituent and that of the heavy.

Energy conservation is expressed by

$$\partial_t u^{\text{total}}+\boldsymbol{\nabla}\cdot\mathbf{I}^{\text{total}}=q^R, \tag{4.9}$$

where u^{total} is the total energy density and $\mathbf{I}^{\text{total}}$ is the total energy flux, which includes the heat flux $\mathbf{I}^q$. The radioactive heat source q^R is the only volumetric source of energy. Equations (4.1)–(4.8) must imply Eq. (4.9), which is the case only if

$$\mathbf{I}^q=T\mathbf{I}^S+\mu\mathbf{I}^{\xi}, \tag{4.10}$$

$$T\sigma^S=q^R+q^J+q^{\nu}-\mathbf{I}^S\cdot\boldsymbol{\nabla}T-\mathbf{I}^{\xi}\cdot\boldsymbol{\nabla}\mu, \tag{4.11}$$

where

$$q^J=\mu_0\eta\mathbf{J}^2,\quad q^{\nu}=e_{ij}\pi^{\nu}_{ij} \tag{4.12}$$

are the Joule heating and the viscous regeneration of heat; they are both non-negative. The final two terms in Eq. (4.11) arise from diffusion of heat and composition; this combination must be non-negative too: $q^t\geqslant 0$ where

$$q^t\equiv-\mathbf{I}^S\cdot\boldsymbol{\nabla}T-\mathbf{I}^{\xi}\cdot\boldsymbol{\nabla}\mu. \tag{4.13}$$

We shall not need the general expressions for $\mathbf{I}^S$, $\mathbf{I}^{\xi}$, and σ^S arising from molecular diffusion; they may be found in, for example, Chap. VI of Landau and Lifshitz (1987). We give below alternative expressions for turbulent diffusion, and this has motivated the otherwise idiosyncratic notation q^t in Eq. (4.13).

B. The reference state

The reference state is hydrostatic with uniform S and ξ; see Sec. II.C. Reference state variables carry an overbar. We have

$$\boldsymbol{\nabla}\overline{P}=-\overline{\rho}\boldsymbol{\nabla}\overline{U}, \tag{4.14}$$

$$\boldsymbol{\nabla}\overline{S}=\mathbf{0}, \tag{4.15}$$

$$\boldsymbol{\nabla}\overline{\xi}=\mathbf{0}. \tag{4.16}$$

Applying $\boldsymbol{\nabla}\times$ to Eq. (4.14), we see that $\overline{\rho}=\overline{\rho}(\overline{U})$ and that therefore $\overline{P}$ and all other thermodynamic variables are constant on each equipotential surface $\overline{U}=\text{const}$. Since the inner core boundary is a phase boundary, it too is an equipotential surface.[21] We shall briefly return in Sec. IV.D to the full generality of Eqs. (4.14)–(4.16), but elsewhere shall assume spherical symmetry. All reference state variables then depend spatially on r alone, the Ω^2 term in Eq. (4.7) is disregarded, and Eqs. (4.14)–(4.16) become

$$\partial_r\overline{P}=-\overline{g\rho},\quad \partial_r\overline{S}=0,\quad \partial_r\overline{\xi}=0, \tag{4.17}$$

where $\overline{g}=-\overline{g}_r>0$. These imply

$$\partial_r\overline{\rho}=-\overline{\rho g}/\overline{u_S^2},\quad \partial_r\overline{T}=-\overline{\alpha^S g},\quad \partial_r\overline{\mu}=-\overline{\alpha^{\xi}g}. \tag{4.18}$$

Parameters such as $\overline{\alpha^S}$ and $\overline{\alpha^{\xi}}$ depend spatially on r. The reference state used in the simulations to be described in Sec. VI was based on the preliminary reference Earth model (PREM) of Dziewonski and Anderson (1981).

Because the core evolves in time as the Earth cools, the reference state must be continually updated. One should not lose sight of the fact that the reference state is merely a mathematical convenience and has no profound physical meaning. One reference state would not, even in an immobilized core, evolve into another reference state. To see this, we first discard $\overline{\mathbf{I}^{\xi}}$ as negligible. Heat conduction down the adiabat in the reference state would then give (see, for example, Landau and Lifshitz, 1987)

$$\overline{\mathbf{I}^S}=\overline{\mathbf{I}^q}/\overline{T},\quad \overline{\mathbf{I}^q}=-\overline{K}_M\boldsymbol{\nabla}\overline{T},\quad \overline{\sigma^S}=\overline{K}_M\boldsymbol{\nabla}\overline{T}/\overline{T})^2+q^R/\overline{T}, \tag{4.19}$$

where radioactive sources q^R have been included (in case any exist). The right-hand side of Eq. (4.3) would therefore be

$$\overline{\sigma}^S_-=\overline{\sigma}^T_-+q^R/\overline{T},\quad \text{where}\quad \overline{\sigma}^T_-=\overline{T}^{-1}\boldsymbol{\nabla}\cdot(\overline{K}_M\boldsymbol{\nabla}\overline{T}). \tag{4.20}$$

Since $\overline{\sigma}^T_-$ depends on r, the assumed r independence of $\overline{S}$ in the initial reference state would, according to Eq. (4.3), be lost. [It may be noted for future reference that $\overline{\sigma}^T_-$ is negative, even though $\overline{\sigma}^S>0$; this is what we expect for a cooling core ($\dot{\bar{S}}<0$).]

C. The anelastic equations

The convection equations are obtained by expanding about the reference state by writing

[21] This statement is true, only insofar as the solid inner core can be treated hydrostatically: see Sec. II.B.

$$S=\overline{S}+S_c,\quad \mathbf{I}^S=\overline{\mathbf{I}}^S+\mathbf{I}_c^S,\quad \rho=\overline{\rho}+\rho_c,\ldots. \tag{4.21}$$

We have seen in Sec. II.C that $S_c/\overline{S}$, $\xi_c/\overline{\xi},\ldots$ are of order 10^{-8}. We may therefore confidently linearize the thermodynamic variables about their reference values, as we essentially did in Sec. II.C. All other nonlinearities are retained. Since[22] $\overline{\mathbf{V}}=\overline{\mathbf{B}}=\mathbf{0}$, we may omit c from $\mathbf{V}$, $\mathbf{B}$, and $\mathbf{J}$.

The core is cooling and (in the absence of q^R) it is driven into motion *only* by that cooling; it is imperative to incorporate this into the theory. Because the evolution of the core is slow, a ready-made mathematical technique can be used: the method of multiple time scales. See, for example, Bender and Orszag (1978), Chap. 11. All variables are functions of a reference time variable $\overline{t}$, and all convection variables are also functions of a convective time variable t_c, where $\overline{t}/t_c=O(10^8)$. We write

$$\partial_t=\partial_{\overline{t}}+\partial_t^c. \tag{4.22}$$

Then, for example, since $\partial_t^c\overline{S}=0$ and $\partial_{\overline{t}}S_c=O(10^{-8})\partial_t^c S_c$,

$$\partial_t S=(\partial_{\overline{t}}+\partial_t^c)(\overline{S}+S_c)\approx\partial_t^c S_c+\dot{\overline{S}}, \tag{4.23}$$

where the overdot is used (exclusively) for $\overline{t}$ derivatives. The two terms on the right-hand side of Eq. (4.23) are similar in magnitude, because $S_c/\overline{S}=O(10^{-8})$.

The governing equations (4.1)–(4.6) become

$$\boldsymbol{\nabla}\cdot(\overline{\rho}\overline{\mathbf{V}})=0, \tag{4.24}$$

$$\partial_t(\overline{\rho}\overline{\mathbf{V}})+\boldsymbol{\nabla}\cdot(\overline{\rho}\overline{\mathbf{V}}\mathbf{V}-\overline{\overline{\pi}}^{\nu}-\overline{\overline{\pi}}^{B})=-\overline{\rho}\boldsymbol{\nabla}\Pi+C\overline{\rho}\,\overline{\mathbf{g}}-2\overline{\rho}\overline{\boldsymbol{\Omega}}\times\mathbf{V}, \tag{4.25}$$

$$\partial(\overline{\rho}S_c)+\boldsymbol{\nabla}\cdot(\overline{\rho}S_c\mathbf{V}+\mathbf{I}_c^S)=-\overline{\rho}\dot{\overline{S}}+\overline{\sigma}_-^S+\sigma^D, \tag{4.26}$$

$$\partial(\overline{\rho}\xi_c)+\boldsymbol{\nabla}\cdot(\overline{\rho}\xi_c\mathbf{V}+\mathbf{I}_c^{\xi})=-\overline{\rho}\dot{\overline{\xi}}, \tag{4.27}$$

$$\boldsymbol{\nabla}\cdot\mathbf{B}=0, \tag{4.28}$$

$$\partial_t\mathbf{B}=\boldsymbol{\nabla}\times(\mathbf{V}\times\mathbf{B}-\overline{\eta}\boldsymbol{\nabla}\times\mathbf{B}), \tag{4.29}$$

where $\Pi=P_c/\overline{\rho}+U_c$ is the reduced pressure, U_c is the perturbation in gravitational potential created by ρ_c, and

$$C=-\overline{\alpha}^S S_c-\overline{\alpha}^{\xi}\xi_c \tag{4.30}$$

is the CO density; see Eq. (2.14). It is of order 10^{-8}; see Sec. V.B. The Lorentz force $\rho\mathbf{F}^B$ has been expressed as the divergence of the magnetic stress tensor:

$$\overline{\rho}\overline{\mathbf{F}}^B=\boldsymbol{\nabla}\cdot\overline{\overline{\boldsymbol{\pi}}}^B,\quad \text{where}\quad \pi_{ij}^B=\mu_0^{-1}(B_iB_j-\tfrac{1}{2}B^2\delta_{ij}). \tag{4.31}$$

[The steps from Eq. (4.2) to Eq. (4.25) are not immediate; see Braginsky and Roberts (1995).] In addition to $\overline{\sigma}_-^S$ defined by Eq. (4.20), entropy is produced convectively at the rate

$$\sigma^D=q^D/\overline{T},\quad \text{where}\quad q^D=q^J+q^{\nu}. \tag{4.32}$$

The approximation (4.24) for mass conservation is known as the *anelastic equation*. It filters out sound (seismic) waves, which are uninteresting since they cross the core in minutes rather than in the decades to millenia of geomagnetic phenomena.

D. Core turbulence

Four molecular diffusivities appear in core MHD: the kinematic viscosity ν_M, the magnetic diffusivity η, the thermal diffusivity κ_M, and the compositional diffusivity D_M between the two components of the alloy. (For a recent estimate of ν_M, see de Wijs *et al.*, 1998.) Three analogs of the magnetic Reynolds number (3.13) arise, namely, the Reynolds number, the Péclet number, and the mass Péclet number:

$$Re=\frac{\overline{\mathcal{UL}}}{\overline{\nu}_M},\quad Pe=\frac{\overline{\mathcal{UL}}}{\overline{\kappa}_M},\quad Mp=\frac{\overline{\mathcal{UL}}}{\overline{D}_M}. \tag{4.33}$$

We have discussed the significance of Rm in Sec. III.B. Using estimates (1.24) and (1.25), and values listed in Table I, we find that

$$Re\approx 2.5\times10^8,\quad Pe\approx 5\times10^7,\quad Mp\approx 2.5\times10^{11}. \tag{4.34}$$

Given such giant numbers, it cannot be doubted that small-scale turbulent eddies exist in the fluid outer core, as they do in the Earth's atmosphere and oceans. Although these small eddies have little energy compared with that in the larger scales, they are, by many orders of magnitude, more effective in transporting heat, composition, and momentum than molecular diffusion. The computing resources that would be necessary to resolve numerically the full spectrum of turbulent length and time scales does not exist, and progress can only be made by being less ambitious. We shall therefore aim to model the macroscales by averaging Eqs. (4.24)–(4.29) over the microscale, a process that introduces turbulent fluxes of macroscale momentum, heat, and composition which have to be parametrized.

We divide each variable into a macroscale and a microscale part, as in Eq. (3.28). The average of the term $\overline{\rho}\overline{\mathbf{V}}\mathbf{V}$ in Eq. (4.25) is

$$\langle\overline{\rho}\overline{\mathbf{V}}\mathbf{V}\rangle=\overline{\rho}\langle(\langle\mathbf{V}\rangle+\mathbf{V}^t)(\langle\mathbf{V}\rangle+\mathbf{V}^t)\rangle=\overline{\rho}\langle\mathbf{V}\rangle\langle\mathbf{V}\rangle+\overline{\rho}\langle\mathbf{V}^t\mathbf{V}^t\rangle. \tag{4.35}$$

Here $\overline{\rho}\langle\mathbf{V}^t\mathbf{V}^t\rangle$ is known as the *Reynolds stress tensor*.

As in Sec. III.C, we shall develop a local turbulence theory, based on the "Reynolds analogy," the basic idea of which is that the transport of macroscale fields by chaotic, subgrid-scale "eddies" is similar to their transport by chaotic molecular motions and can therefore be represented mathematically in a similar way though with turbulent diffusion coefficients that are much greater than their molecular counterparts. In this way "eddy" transport coefficients are used to account crudely for the mixing done by the unresolved scales of motion.

[22] A velocity $\overline{\mathbf{V}}$ arises through gravitational settling; it is very tiny [$\overline{\mathbf{V}}=O(10^{-8}\mathbf{V}^c)$], and (like $\overline{\mathbf{I}}^{\xi}$) we ignore it.

Momentum transport provides the most famous application of local turbulence theory: since the stresses due to molecular viscosity $\overline{\nu_M}$ are, by Eq. (4.8), $\pi_{ij}^{\nu}=\overline{\rho}\nu_M(\nabla_i V_j+\nabla_j V_i-\frac{2}{3}\nabla_k V_k\delta_{ij})$, the last term in Eq. (4.35) can be analogously represented by

$$\pi_{ij}^{t}\equiv-\langle\overline{\rho}V_i^t V_j^t\rangle$$
$$=\overline{\rho}\nu^t(\nabla_i\langle V_j\rangle+\nabla_j\langle V_i\rangle-\tfrac{2}{3}\nabla_k\langle V_k\rangle\delta_{ij}), \tag{4.36}$$

where ν^t is the "turbulent viscosity." The Reynolds stresses then depend only on the local gradient of the macroscale flow.

The magnetic diffusivity η greatly exceeds ν_M, κ_M, and D_M, and the microscale magnetic Reynolds number $Rm=\mathcal{U}^t\mathcal{L}^t/\eta$ is small. This means (see Sec. III.D) that molecular diffusion of large-scale magnetic fields is more significant than turbulent diffusion, i.e., when we average $\mathbf{V}\times\mathbf{B}$ in Eq. (4.29) and obtain

$$\langle\mathbf{V}\times\mathbf{B}\rangle=\langle\mathbf{V}\rangle\times\langle\mathbf{B}\rangle+\langle\mathbf{V}^t\times\mathbf{B}^t\rangle, \tag{4.37}$$

the final term, $\langle\mathcal{F}\rangle=\langle\mathbf{V}^t\times\mathbf{B}^t\rangle$, is small in comparison with $\overline{\eta}\nabla\times\langle\mathbf{B}\rangle$. This does not mean that the magnetic Reynolds stress, arising from the average of $\overleftrightarrow{\pi}^B$ in Eq. (4.25), may also be neglected; $\mathbf{B}^t$ acts as an additional brake on the macroscale flow and, when we combine the turbulent kinetic and magnetic Reynolds stresses and represent them by the $\overleftrightarrow{\pi}^t$ defined in Eq. (4.36), we should increase ν^t appropriately.

The Reynolds analogy is also applied to two terms that appear when Eqs. (4.26) and (4.27) are averaged:

$$\mathbf{I}_c^{St}\equiv\langle\overline{\rho}S_c^t\mathbf{V}^t\rangle=-\overline{\rho}\kappa^t\nabla\langle S_c\rangle, \tag{4.38}$$

$$\mathbf{I}_c^{\xi t}\equiv\langle\overline{\rho}\xi_c^t\mathbf{V}^t\rangle=-\overline{\rho}\kappa^t\nabla\langle\xi_c\rangle. \tag{4.39}$$

Since turbulence should transport all passive scalars in the same way, the same turbulent diffusivity (κ^t) appears in both expressions.

The energy dissipation q^D can also be divided into macroscale and microscale parts:

$$q^D=\langle q^J\rangle+\langle q^{\nu}\rangle+q^t, \tag{4.40}$$

where

$$\langle q^J\rangle=\mu_0\overline{\eta}\langle\mathbf{J}\rangle^2,\quad\langle q^{\nu}\rangle=\langle e_{ij}\rangle\langle\pi_{ij}^{\nu}\rangle, \tag{4.41}$$

are the macroscale dissipations and

$$q^t=\langle\mu_0\overline{\eta}(\mathbf{J}^t)^2+e_{ij}^t(\pi_{ij}^{\nu})^t\rangle \tag{4.42}$$

is the *turbulent dissipation*. Braginsky and Roberts (1995) showed that, since $\overline{\nu}_M\ll\overline{\eta}$, the viscous turbulent dissipation in Eq. (4.42) is negligible compared with the ohmic.

Braginsky and Roberts (1995; Appendix C) deduced an alternative expression for q^t based on Eq. (4.13) which demonstrated that the energy loss (4.42) can be replaced directly by the rate of working of the buoyancy force and not by the turbulent cascade of classical shear flow turbulence. They showed that

$$q^t=\overline{\rho}\kappa^t\overline{\mathbf{g}}\cdot(\overline{\alpha}^S\nabla\langle S_c\rangle+\overline{\alpha}^{\xi}\nabla\langle\xi_c\rangle). \tag{4.43}$$

If $\overline{\alpha}^S$ and $\overline{\alpha}^{\xi}$ are constants, this can be written as

$$q^t=-\overline{\rho}\kappa^t\overline{\mathbf{g}}\cdot\nabla\langle C\rangle. \tag{4.44}$$

Although κ^t and ν^t depend on position and time through the local strength of the turbulence, we expect that in the main body of the core they will be $O(\mathcal{U}^t\mathcal{L}^t)$. If we take $\mathcal{L}^t=10^4$ m and $\mathcal{U}^t=10^{-4}\,\mathrm{m\,s^{-1}}$ as typical, we obtain $\kappa^t\approx\nu^t\approx1\,\mathrm{m^2\,s^{-1}}$, which may be compared with the tiny molecular diffusivities listed in Table I. We may now, with one exception, *remove the molecular fluxes of momentum, entropy, and composition* in favor of the corresponding turbulent fluxes.[23] The one exception is the conduction of heat down the adiabat, which cannot be ignored because $\overline{T}/\langle T_c\rangle\sim10^8$.

E. Working equations and boundary conditions

We summarize our final, working equations that govern the large-scale fields in the Earth's core, the equations used in the simulations reported in Sec. VI. The notation will be simplified: the angle brackets denoting the mean fields will be omitted but implied, and ν and κ will be turbulent diffusivities, no longer carrying a bar or a superscript ^{t}; the overbar, and the subscript $_c$, will also be omitted except where confusion might arise. We have

$$\nabla\cdot(\rho\mathbf{V})=0, \tag{4.45}$$

$$d_t\mathbf{V}=-\nabla\Pi+C\mathbf{g}-2\boldsymbol{\Omega}\times\mathbf{V}+\mathbf{F}^B+\mathbf{F}^{\nu}, \tag{4.46}$$

$$\rho d_t\xi_c+\nabla\cdot\mathbf{I}^{\xi}=-\rho\dot{\bar{\xi}}, \tag{4.47}$$

$$\mathbf{I}^{\xi}=-\rho\kappa\nabla\xi_c, \tag{4.48}$$

$$\rho d_t S_c+\nabla\cdot\mathbf{I}^S=-\rho\dot{\bar{S}}+\overline{\sigma}_-^S+\sigma^D, \tag{4.49}$$

$$\mathbf{I}^S=-\rho\kappa\nabla S_c, \tag{4.50}$$

$$\nabla\cdot\mathbf{B}=0, \tag{4.51}$$

$$\partial_t\mathbf{B}=\nabla\times(\mathbf{V}\times\mathbf{B})-\nabla\times(\eta\nabla\times\mathbf{B}), \tag{4.52}$$

$$C=-\alpha^S S_c-\alpha^{\xi}\xi_c, \tag{4.53}$$

$$\rho F_i^{\nu}=\nabla_j\pi_{ij}^{\nu}, \tag{4.54}$$

$$\pi_{ij}^{\nu}=2\rho\nu(e_{ij}-\tfrac{1}{3}e_{kk}\delta_{ij}), \tag{4.55}$$

$$\sigma^D=q^D/T, \tag{4.56}$$

$$q^D=q^J+q^{\nu}+q^t, \tag{4.57}$$

$$q^J=\mu_0\eta\mathbf{J}^2,\quad q^{\nu}=e_{ij}\pi_{ij}^{\nu},\quad q^t=\rho\kappa\mathbf{g}\cdot(\alpha^S\nabla S_c+\alpha^{\xi}\nabla\xi_c). \tag{4.58}$$

[23]The molecular diffusivities are conceptually important in boundary layers. It is clear from Eq. (4.38), for instance, that $\kappa^t=0$ on the core-mantle boundary because $\mathbf{V}^t=\mathbf{0}$ there. The total diffusivity $\kappa^{\mathrm{total}}=\kappa^t+\overline{\kappa}_M$ is nonzero, however. As r increases within a thin thermal layer on the CMB, κ^{total} decreases and $\partial_r\langle S_c\rangle$ increases in compensation, so that $I_r^S=-\kappa^{\mathrm{total}}\partial_r\langle S_c\rangle$ does not change. Since we are not particularly interested in the boundary layer, we ignore it and apply Eq. (4.38) throughout the core, right up to its boundaries, and we similarly ignore the boundary layers of $\langle\xi_c\rangle$.

As usual, $\mu_0\mathbf{J}=\nabla\times\mathbf{B}$, $\rho\mathbf{F}^B=\mathbf{J}\times\mathbf{B}$, and $e_{ij}=\frac{1}{2}(\nabla_i V_j+\nabla_j V_i)$; Eq. (4.20) gives $\overline{\sigma}^S_-$. Also $\Pi=P_c/\rho+U_c$.

Solutions to Eqs. (4.45)–(4.58) are subject to boundary conditions; those governing $\mathbf{B}$ were dealt with in Sec. III. The velocity should obey the no-slip conditions

$$\mathbf{V}_{\mathrm{CMB}}=\mathbf{0}, \tag{4.59}$$

$$\mathbf{V}_{\mathrm{SIC}}=\mathbf{\Omega}_{\mathrm{SIC}}\times\mathbf{r}, \tag{4.60}$$

where $\mathbf{\Omega}_{\mathrm{SIC}}$ is the angular velocity[24] of the solid inner core. This is determined by solving the equation of motion for the inner core (considered as a rigid body) as it moves under $\mathbf{\Gamma}$, the sum of the magnetic, viscous, topographic, and gravitational torques to which it is subjected. The topographic torque arises because, in reality, the inner core boundary does not have an axisymmetric figure; it has ϕ-dependent bumps, on which the hydrodynamic pressure creates a torque.

We observed in Sec. IV.B that the ICB is more generally a surface of constant $\overline{U}$ rather than of constant r. The most obvious departure from spherical symmetry is the equatorial bulge of about 3 km created by the centrifugal force. As for a spinning top, the bulge provides a restoring force; the axis of rotation of the SIC does not tip over progressively under the action of Γ_x and Γ_y, but precesses about Oz. Here, as in the simulations described in Sec. VI, let us consider only the z components of $\mathbf{\Gamma}$ and $\mathbf{\Omega}_{\mathrm{SIC}}$, together with the $r\phi$ (and ϕr) stress components. The magnetic stresses on the ICB are so large compared with the viscous and topographic stresses that (in the absence of a gravitational torque) they must, paradoxically, integrate almost to zero in the computation of Γ, and Ω_{SIC} must adjust itself to bring that about. This consequence of Lenz's law led to a prediction (see Sec. VI) that the SIC is rotating in a prograde direction relative to the mantle at a few degrees per year. This conclusion was later questioned by Buffett (1997), who pointed out that mass in the mantle is not distributed with perfect spherical symmetry, and the mantle inhomogeneities make $\overline{U}$ in the core (weakly) ϕ dependent. Since the ICB is an equipotential, ϕ-dependent bumps are created on it that are directly linked to the inhomogeneities in the mantle that create them. The gravitational interaction between the bumps and the imperfections tends to lock the rotation of the SIC to that of the mantle.

Bumps on the SIC are not avoided even when we return to our simplifying assumption of a spherically symmetric reference state. Although $\overline{r}_{\mathrm{ICB}}$ is then a function only of $\overline{t}$ in the reference state, the ICB advances more rapidly wherever cold descending convection currents impinge on it, and more slowly where hot rising currents leave it, and bumps are created on the ICB (Glatzmaier and Roberts, 1998). Correspondingly, the radial components of $\mathbf{I}^\xi$ and $\mathbf{I}^S$ vary with θ and ϕ on the ICB. It is convenient to generalize the definition of the overbar to mean the horizontal average of even convective quantities and to write $\mathbf{I}^\xi=\overline{\mathbf{I}}^\xi+\mathbf{I}^{\xi h}$, $\mathbf{I}^S=\overline{\mathbf{I}}^S+\mathbf{I}^{Sh}$, and

$$r_{\mathrm{ICB}}=\overline{r}_{\mathrm{ICB}}(\overline{t})+r^h_{\mathrm{ICB}}(\theta,\phi,t_c,\overline{t}), \tag{4.61}$$

where the superscript h stands for the horizontally varying part. We then find that

$$\overline{I}^\xi_r=\rho^-\Delta\overline{\xi}\,\dot{\overline{r}}_{\mathrm{ICB}},\ \text{at}\ r=\overline{r}_{\mathrm{ICB}}, \tag{4.62}$$

$$\overline{I}^S_r=\rho^-\Delta\overline{S}\dot{\overline{r}}_{\mathrm{ICB}},\ \text{at}\ r=\overline{r}_{\mathrm{ICB}}. \tag{4.63}$$

Suppose that there is no mass exchange across the core-mantle boundary; then $r_{\mathrm{CMB}}=\mathrm{const}$, if the slow but inevitable contraction of the Earth as it cools is ignored. We then have

$$\overline{I}^\xi_r=0,\ \text{at}\ r=r_{\mathrm{CMB}}, \tag{4.64}$$

$$\overline{I}^S_r=(\overline{I}^q_r-I^{\mathrm{ad}}_r)/T,\ \text{at}\ r=r_{\mathrm{CMB}}. \tag{4.65}$$

Conditions (4.62) and (4.64) ensure conservation of the light constituents, the fluxes of ξ at the SIC being precisely what is required to account for the volumetric source on the right-hand side of Eq. (4.47). Similarly, the difference between the total flow of S from the CMB implied by Eq. (4.65) and the total flow of S into the FOC across the ICB, as given by Eq. (4.63), is the integral over the FOC of the right-hand side of Eq. (4.49).

To find $\dot{\overline{r}}_{\mathrm{ICB}}$, we must apply the condition $T(\overline{r}_{\mathrm{ICB}})=T_l(\overline{P}_{\mathrm{ICB}},\overline{\xi})$ of phase equilibrium, where $T_l(P,\xi)$ is the liquidus, assumed known. The proper implementation of this condition is lengthy. The detailed argument is given by Braginsky and Roberts (1995). Suffice it to say here that, to a good geophysical approximation, it implies

$$\dot{\overline{S}}=-c_P\Delta_*\dot{\overline{r}}_{\mathrm{ICB}}/\overline{r}_{\mathrm{ICB}}, \tag{4.66}$$

where Δ_* is dimensionless and depends in a complicated way on the latent heat (which is rather uncertain) and the depression of the freezing point due to alloying (which is even more uncertain). The error in the resulting value, $\Delta_*=0.05$, is hard to estimate but is probably large. If q^R and $\mathcal{Q}_{\mathrm{CMB}}$ are known, we can obtain $\overline{I}^S_r$ from Eq. (4.65) and can then determine the mean rate $\dot{\overline{r}}_{\mathrm{ICB}}$ of advance of the inner core boundary from Eqs. (4.49), (4.63), and (4.66).

[24]Equation (4.59) is a consequence of our choice of reference frame. The core exerts magnetic, topographic, viscous, and gravitational torques on the mantle that cause $\mathbf{\Omega}$ to change, resulting in variations in the length of day (Sec. I.C). The magnetic torques arise because the mantle is not, as we have supposed, electrically insulating, although its conductivity is small. The main torque on the mantle by the fluid outer core may arise indirectly, through the magnetic stresses exerted by the FOC on the inner core boundary and transmitted to the mantle by a gravitational torque acting as a catalyst; see Buffett (1996). Whatever its cause, it must be correctly incorporated into simulations such as those of Sec. VI. This is done by replacing the reference frame fixed in the mantle by the reference frame in which the total angular momentum of the Earth is zero. The relative motion between these frames is very small. Instead of Eqs. (4.59) and (4.60), Kuang and Bloxham (1997) require that the FOC create no viscous stress on CMB and ICB; see Sec. VII.B.

The boundary conditions on the horizontally varying fields are similar:

$$I_r^{\xi h}=\rho^- \Delta\overline{\xi}\partial_t r_{\rm ICB}^h, \text{ at } r=\overline{r}_{\rm ICB}, \tag{4.67}$$

$$I_r^{Sh}=\rho^- \Delta\overline{S}\partial_t r_{\rm ICB}^h, \text{ at } r=\overline{r}_{\rm ICB}, \tag{4.68}$$

and, in analogy with Eq. (4.66),

$$\partial_t S^h=-c_P\Delta_* \partial_t r_{\rm ICB}^h/\overline{r}_{\rm ICB}, \text{ at } r=\overline{r}_{\rm ICB}. \tag{4.69}$$

We also have

$$I_r^{\xi h}=0, \text{ at } r=r_{\rm CMB}, \tag{4.70}$$

$$I_r^{Sh}=I_r^{q,h}/T, \text{ at } r=r_{\rm CMB}, \tag{4.71}$$

where $I_r^{q,h}$ is the horizontally varying part of the heat flux from core to mantle.

These arguments show that the sources of ξ_c and S_c on the inner core boundary are proportional to one another and to the local rate of advance of this boundary. To determine that rate self-consistently, we need to know q^R and $I_{\rm CMB}^q(\theta,\phi)$, and we need to solve the dynamo problem.

F. The Boussinesq approximation

The theory of laboratory convection commonly assumes that the reference state is uniform. This is known as the Boussinesq approximation. It is adopted in most studies of core MHD and the geodynamo because it simplifies the mathematics slightly, and that is its main purpose. In the context of core MHD, it introduces inaccuracies that are typically of order 20%. These are often viewed as tolerable in view of greater uncertainties in some of the other model parameters. More seriously, the approximation totally disregards the adiabatic gradient and adiabatic heat flux. Also, the analysis of the energy and entropy balances requires extra care; see Sec. 8 of Braginsky and Roberts (1995).

Equations (4.45) and (4.46) become

$$\boldsymbol{\nabla}\cdot\mathbf{V}=0, \tag{4.72}$$

$$\partial_t\mathbf{V}+\mathbf{V}\cdot\boldsymbol{\nabla}\mathbf{V}=-\boldsymbol{\nabla}\Pi+C\mathbf{g}-2\boldsymbol{\Omega}\times\mathbf{V}+\mathbf{J}\times\mathbf{B}/\rho_0+\nu\nabla^2\mathbf{V}. \tag{4.73}$$

Usually thermodynamic linearization (Sec. IV.C) is carried out as a perturbation from $\overline{T}$ rather than from $\overline{S}$, so that, in place of Eq. (4.53),

$$C=-\alpha T_c-\alpha_T^\xi\xi_c, \tag{4.74}$$

where $\alpha_T^\xi=-\rho^{-1}(\partial\rho/\partial\xi)_{P,T}$ is the isothermal coefficient of volume expansion.

The Boussinesq approximation may be thought of as a double limit in which $g\to\infty$ and $C\to 0$ with gC finite and nonzero. This requires that $\alpha^S\to 0$ and $\alpha^\xi\to 0$, so that it is unnecessary to distinguish between α_T^ξ and α^ξ in Eq. (4.74). Then

$$S_c=(c_P/\overline{T})T_c, \tag{4.75}$$

and expressions (4.53) and (4.74) for C coincide by Eq. (1.8). The equation governing T_c is obtained by multiplying Eq. (4.49) by the constant $\overline{T}/c_P$.

V. RMHD

A. Orders of magnitude

RMHD stands for *rotating magnetohydrodynamics*, a subject so different from MHD that it deserves its own acronym.[25] If $\boldsymbol{\Omega}=\mathbf{0}$, we shall refer to RMHD as "classical MHD" and, if $\mathbf{B}=\mathbf{0}$, we shall call it "classical rotating fluids." MHD is a subject that weds electrodynamics to hydrodynamics, the progeny resembling neither parent closely. Similarly, in RMHD, classical rotating fluids and classical MHD are married, but the offspring are again surprisingly different. RMHD, as the subject stood in 1973, was reviewed by Acheson and Hide (1973).

Two dimensionless numbers arise in the classical theory of rotating fluids, the Ekman number E and the Rossby number Ro:

$$E=\nu/\Omega\overline{\mathcal{L}}^2, \tag{5.1}$$

$$Ro=\overline{\mathcal{U}}/\Omega\overline{\mathcal{L}}. \tag{5.2}$$

These measure the viscous force $\overline{\rho}\nu\nabla^2\mathbf{V}$ and the inertial force $\overline{\rho}\mathbf{V}\cdot\boldsymbol{\nabla}\mathbf{V}$ against the Coriolis force $2\overline{\rho}\boldsymbol{\Omega}\times\mathbf{V}$. In estimating E and Ro we shall abandon estimate (1.24) and, following common practice, use instead $\mathcal{L}=r_{\rm CMB}-\overline{r}_{\rm ICB}\approx 2260$ km. We find that $Ro\approx 10^{-5}$ and $E\approx 5\times 10^{-14}$ (for $\nu=\nu_M$) or 10^{-7} (for $\nu=\nu^t\approx\eta$). The core is therefore a *rapidly rotating fluid*, defined as one in which

$$E\ll 1, \tag{5.3}$$

$$Ro\ll 1, \tag{5.4}$$

and in which therefore viscous and inertial forces are generally small compared with the Coriolis force. The ratio Ro/E is the kinetic Reynolds number Re and is large; see Eqs. (4.33) and (4.34). The geodynamo is self-excited, and therefore (Sec. III.B)

$$Rm\gtrsim O(1), \tag{5.5}$$

$$\text{where } Rm=\overline{\mathcal{U}\mathcal{L}}/\eta. \tag{5.6}$$

Thus, by inequality (5.4), the magnetic Ekman number $\eta/\Omega\overline{\mathcal{L}}^2$ is small, so that inequality (5.3) is automatically satisfied. The smallness of Ro means that from now on we shall discard $\mathbf{V}\cdot\boldsymbol{\nabla}\mathbf{V}$ in Eq. (4.73). Looking ahead to Sec. V.C, we shall recognize that the nonlinearity equilibrating the solutions is the Lorentz force and not the inertial force.

[25] It does not get one, however, except in this review. In plasma physics RMHD is an abbreviation for "reduced MHD."

There are several possible levels at which **B** could saturate, but in all of them the magnetic Rossby number is small:

$$Ro^B \ll 1, \tag{5.7}$$

$$\text{where } Ro^B = \mathcal{V}_A / \Omega \overline{\mathcal{L}}, \tag{5.8}$$

where $\mathcal{V}_A = \mathcal{B}/(\mu\rho_0)^{1/2}$ is a typical Alfvén velocity. Taking $\mathcal{B}=0.002$ T and the characteristic density ρ_0 from Table I, we find that $\mathcal{V}_A \approx 1.7$ cm s^{-1}, so that $Ro^B \approx 5 \times 10^{-4}$.

The saturation level of main interest here is that of the *strong-field dynamo* in which the Lorentz and Coriolis forces have similar magnitudes.[26] Their ratio is approximately $\mathcal{V}_A^2/2\Omega\overline{\mathcal{U}}\overline{\mathcal{L}} = \Lambda/Rm$, where

$$\Lambda = \mathcal{V}_A^2/2\Omega\eta = \mathcal{B}^2/2\Omega\mu_0\rho_0\eta \tag{5.9}$$

is the *Elsasser number*,[27] which is independent of the length scale $\overline{\mathcal{L}}$. The strong-field regime is therefore one in which

$$\Lambda = O(1), \quad \mathcal{V}_A \approx (2\Omega\eta)^{1/2}, \quad \mathcal{B} = (2\Omega\mu_0\rho_0\eta)^{1/2}, \tag{5.10}$$

which gives $\mathcal{B}=0.002$ T for the core; the characteristic current density is $\mathcal{J} = \mathcal{B}/\mu_0\overline{\mathcal{L}} = 0.004$ A m^{-2}. Also, since $\mathcal{V}_A^2 \approx 2\Omega\overline{\mathcal{U}}\overline{\mathcal{L}}$, the Alfvén number $\overline{\mathcal{U}}/\overline{\mathcal{V}}_A$ is approximately $\sqrt{Ro}$, which is small. The magnetic energy density $\mathcal{E}^B$ therefore greatly exceeds $\mathcal{E}^V$, the kinetic energy density (in the rotating reference frame): $\mathcal{E}^B/\mathcal{E}^V \approx Ro^{-1}$. In some of the simulations of Sec. VI, $\mathcal{E}^B/\mathcal{E}^K \sim 10^3$. Energy is not equipartioned.

Our plan now is to give little more than a thumbnail sketch of some of the concepts and phenomena that are significant in Sec. VI. We start in Sec. V.B with the classical theory of rotating fluids. This subject has an immense literature, and it is obviously impossible to do more than extract some of its flavor through a few simple examples. More details may be found in the classic text of Greenspan (1968), in Roberts and Soward (1978), and in several books on the fluid dynamics of atmosphere and oceans, e.g., Gill (1982), Monin (1990), and Pedlosky (1979). In Sec. V.C, we shall consider how magnetic fields change the results of Sec. V.B. In Sec. V.D, we discuss some matters of more direct relevance to dynamo theory.

Simplicity is sought in this section, and we shall initially exploit the Boussinesq approximation (Sec. IV.F); we shall usually exclude compositional buoyancy and shall replace C by $-\alpha T_c$. We shall also generally ignore the solid inner core, so that the fluid outer core fills $r < r_{\mathrm{CMB}}$.

[26]A weak-field dynamo is one in which the Hartmann number $M = \mathcal{V}_A\mathcal{L}/\sqrt{(\nu\eta)}$ is $O(1)$, meaning that Lorentz and viscous forces are similar in magnitude. This would give $\mathcal{B} \approx 0.3$ nT for the core, which is even less than the field seen at the Earth's surface (Sec. I.B).

[27]As far as we are aware, Elsasser never wrote down his number (5.9), although he did identify the scale (5.10) of $\mathcal{B}$; see Elsasser (1946).

B. Classical rotating flows

In this section we suppose that $\mathbf{B} \equiv \mathbf{0}$. Inequality (5.3) suggests that solutions should be developed asymptotically, in the limit $E \to 0$. The plan therefore is to generate a *mainstream*[28] expansion for solutions within the core, excluding boundary layers on the core-mantle boundary. The viscous force does not appear in the equation governing the leading-order mainstream solution. This lowers the differential order of the system, and we can require only that

$$V_r = 0, \text{ on } r = r_{\mathrm{CMB}}. \tag{5.11}$$

The resulting solution will not obey the conditions (4.59) on $\mathbf{1}_r \times \mathbf{V}$. It is necessary to develop a *boundary layer solution* that matches to the mainstream value of $\mathbf{1}_r \times \mathbf{V}$ at its inner edge, while satisfying condition (4.59) in full on the CMB. Initially we shall consider the mainstream only and shall return to the boundary layer later.

Let us temporarily disregard buoyancy. The surviving inertial term $\partial_t \mathbf{V}$ in Eq. (4.73) is significant only at high frequencies, as for inertial waves, which are determined by condition (5.11) and

$$\boldsymbol{\nabla} \cdot \mathbf{V} = 0, \tag{5.12}$$

$$\partial_t \mathbf{V} = -\boldsymbol{\nabla}\Pi - 2\boldsymbol{\Omega} \times \mathbf{V}. \tag{5.13}$$

This is an eigenvalue problem yielding an infinity of frequencies of order Ω, though all less than 2Ω.

Consider next low frequencies. For steady motions ($\partial_t \mathbf{V} = \mathbf{0}$) we find, by operating on Eq. (5.13) by $\boldsymbol{\nabla}\times$, that

$$2\boldsymbol{\Omega} \cdot \boldsymbol{\nabla}\mathbf{V} = \mathbf{0}. \tag{5.14}$$

This embodies the Proudman-Taylor theorem: *The slow steady motion of a rotating inviscid fluid is two-dimensional with respect to the rotation axis.*
Taking $\boldsymbol{\Omega} = \Omega \mathbf{1}_z$, we have

$$\mathbf{V} = \mathbf{V}(x,y). \tag{5.15}$$

Because the boundary is axisymmetric, the only solution (5.15) that obeys condition (5.11) is

$$\mathbf{V} = \tilde{V}_G(s,t)\mathbf{1}_\phi, \tag{5.16}$$

where (s,ϕ,z) are cylindrical coordinates; t has been included in Eq. (5.16) in view of later developments, but clearly the low-frequency inertial modes, though time dependent, have approximately the form (5.16). As in Sec. III.C, a tilde is used to denote axisymmetry. A flow of type (5.16) is important in the angular momentum balance of the Earth (Sec. I.C) and is termed *geostrophic*. It is axisymmetric, zonal, and constant on *geostrophic cylinders* $\mathcal{C}(s)$ of constant radius s. Figure 8 shows a typical geostrophic cylinder in the case when a solid inner core is present. It also shows a very significant imagi-

[28]In asymptotic theory, the mainstream would usually be called "the outer solution" and the boundary layer "the inner solution" (see, for example, van Dyke, 1964), but such descriptions are confusing in the context of the core-mantle boundary.

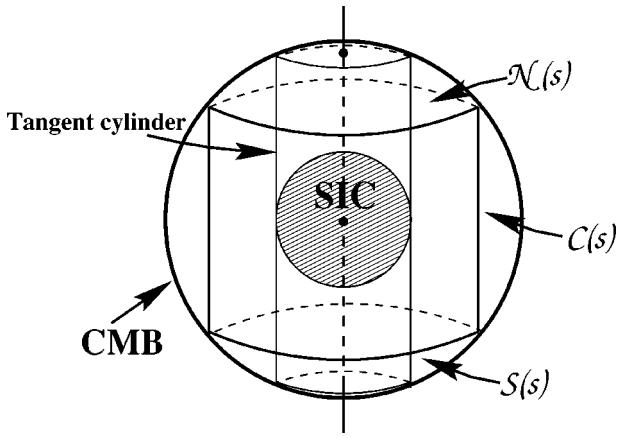

FIG. 8. Sketch of a geostrophic cylinder $\mathcal{C}(s)$ of radius s together with its northern and southern spherical end caps, $\mathcal{N}(s)$ and $\mathcal{S}(s)$. Also shown is the tangent cylinder $\mathcal{C}(r_{\rm ICB})$.

nary cylinder $\mathcal{C}(\overline{r}_{\rm ICB})$, which touches the SIC on its equator and which is therefore called the *tangent cylinder*.

We next consider the action of the buoyancy force through two examples, in the first of which $\tilde{T}_c$ is axisymmetric and is given. The steady inviscid flow driven by $\tilde{T}_c$ obeys

$$\boldsymbol{\nabla}\cdot\tilde{\mathbf{V}}=0, \tag{5.17}$$

$$\mathbf{0}=-\boldsymbol{\nabla}\tilde{\Pi}-\mathbf{g}\alpha\tilde{T}_c-2\boldsymbol{\Omega}\times\tilde{\mathbf{V}}. \tag{5.18}$$

Operating on Eq. (5.18) by $\boldsymbol{\nabla}\times$, we see that

$$2\boldsymbol{\Omega}\cdot\boldsymbol{\nabla}\tilde{\mathbf{V}}=-\alpha\mathbf{g}\times\boldsymbol{\nabla}\tilde{T}_c. \tag{5.19}$$

Since $\mathbf{g}(=-g\mathbf{1}_r)$ is radial, we recover solution (5.16) unless $\tilde{T}_c$ depends on latitude, in which case

$$\tilde{\mathbf{V}}=[\tilde{V}_T(s,z,t)+\tilde{V}_G(s,t)]\mathbf{1}_\phi, \tag{5.20}$$

where we have again included a t dependence for later convenience. The flow $\tilde{V}_T(s,z,t)\mathbf{1}_\phi$ is called the *thermal wind*. Its magnitude is $O(g\tilde{C}/\Omega)$ and, if this is to be comparable with our assumed characteristic velocity $\overline{\mathcal{U}}=5\times10^{-4}\,\mathrm{m\,s^{-1}}$, the pole-equator difference in $\tilde{C}$ must be $O(10^{-8})$. This is the origin of our estimate of C in Sec. IV.C. The corresponding $\tilde{T}_c$ is of order $10^{-4}\,\mathrm{K}$, as in our estimate of δT in Sec. II.C. The state (5.20) may be subject to asymmetric baroclinic instabilities. These are studied in, for example, Pedlosky (1979). We shall touch on their magnetic analogs in Sec. V.C.

The second example is one of convective stability and requires us to restore viscosity in the mainstream, although we continue to assume that $E\ll1$. (For simplicity, we suppose that the Prandtl number ν/κ is not small.) Imagine that heat sources are distributed uniformly in the core. If these are weak, they create only a spherically symmetric temperature distribution $T_c(r)$ that carries heat out of the core by thermal conduction. Although the associated density distribution is top heavy, the diffusion of heat and momentum prevents convective instability, but, if the heat sources are gradually increased, weak convection occurs as soon as the Rayleigh number Ra exceeds a critical value Ra_c. The Rayleigh number is a dimensionless measure of the thermal forcing, defined here by

$$Ra=g\alpha\beta\overline{\mathcal{L}}^4/\nu\kappa, \tag{5.21}$$

where β is a typical gradient of $T_c(r)$. For $Ra=Ra_c$, and also for Ra modestly in excess of Ra_c, convection takes the form of a "cartridge belt" of two-dimensional cells, often called Taylor cells, regularly spaced round the axis of rotation and drifting in longitude about that axis (Roberts, 1968; Jones *et al.*, 2000).

Taylor cells are seen clearly in Fig. 9, which is taken from the dynamo model of Kageyama and Sato (1997). Adjacent cells rotate in opposite directions (about their axes) in a sequence of cyclonic and anticyclonic vortices, with vorticity respectively parallel and antiparallel to $\boldsymbol{\Omega}$. The effect of these motions on the magnetic field will be discussed in Sec. VI.B. The name "Taylor cell" is a useful reminder of the Proudman-Taylor theorem, which the flow is trying to obey by being as 2D as possible. We see from our first example that, if $\nu=0$, small-amplitude motion must be geostrophic, since the thermal forcing $T_c(r)$ is independent of latitude. But geostrophic motions have no radial components and cannot carry heat outwards. Convection can occur only if the viscous forces are large enough to break the rotational constraint of the theorem. Thus, although Ra_c would be $O(1)$ if E were $O(1)$, the critical Rayleigh number is large when $E\ll1$; in fact $Ra_c=O(E^{-4/3})$, and the number of cells in the cartridge belt is of order $E^{-1/3}$, i.e., the scale $\mathcal{L}_\perp$ of the motions perpendicular to $\boldsymbol{\Omega}$ is $O(E^{1/3})$. Convective heat transport is mainly in the s direction, i.e., away from the rotation axis (Busse, 1970); this is significant for the simulations of Sec. VI.

We now consider the boundary layer on the CMB, which is known as an *Ekman layer*. Dimensional analysis of Eq. (4.73) correctly indicates that its thickness δ_ν is of order[29] $\sqrt{(\nu/|\Omega_r|)}\propto E^{1/2}\overline{\mathcal{L}}$, where $\Omega_r=\mathbf{1}_r\cdot\boldsymbol{\Omega}=\Omega\cos\theta$. The Ekman layer is not passive; it controls the mainstream in the sense that the geostrophic flow can only be determined through the Ekman layers. It does this through a process called *Ekman pumping*. To match the leading-order mainstream solution [which we temporarily denote by $\mathbf{V}_{\rm ms}^{(0)}$] to condition (4.59), the Ekman layer has to pump fluid radially, with a velocity of order $E^{1/2}\mathbf{V}_{\rm ms}^{(0)}$, into the mainstream. This provides a boundary

[29]There is obviously a complication at the equator of the CMB, where $\Omega_r=0$ and $\delta_\nu=\infty$. The Ekman layer has a passive singularity at the equator; δ_ν is not infinite but is of order $E^{2/5}$ (which is much greater than $E^{1/2}$ for $E\to0$); see Stewartson (1966). For an analysis of the Ekman layer, see Greenspan (1968).

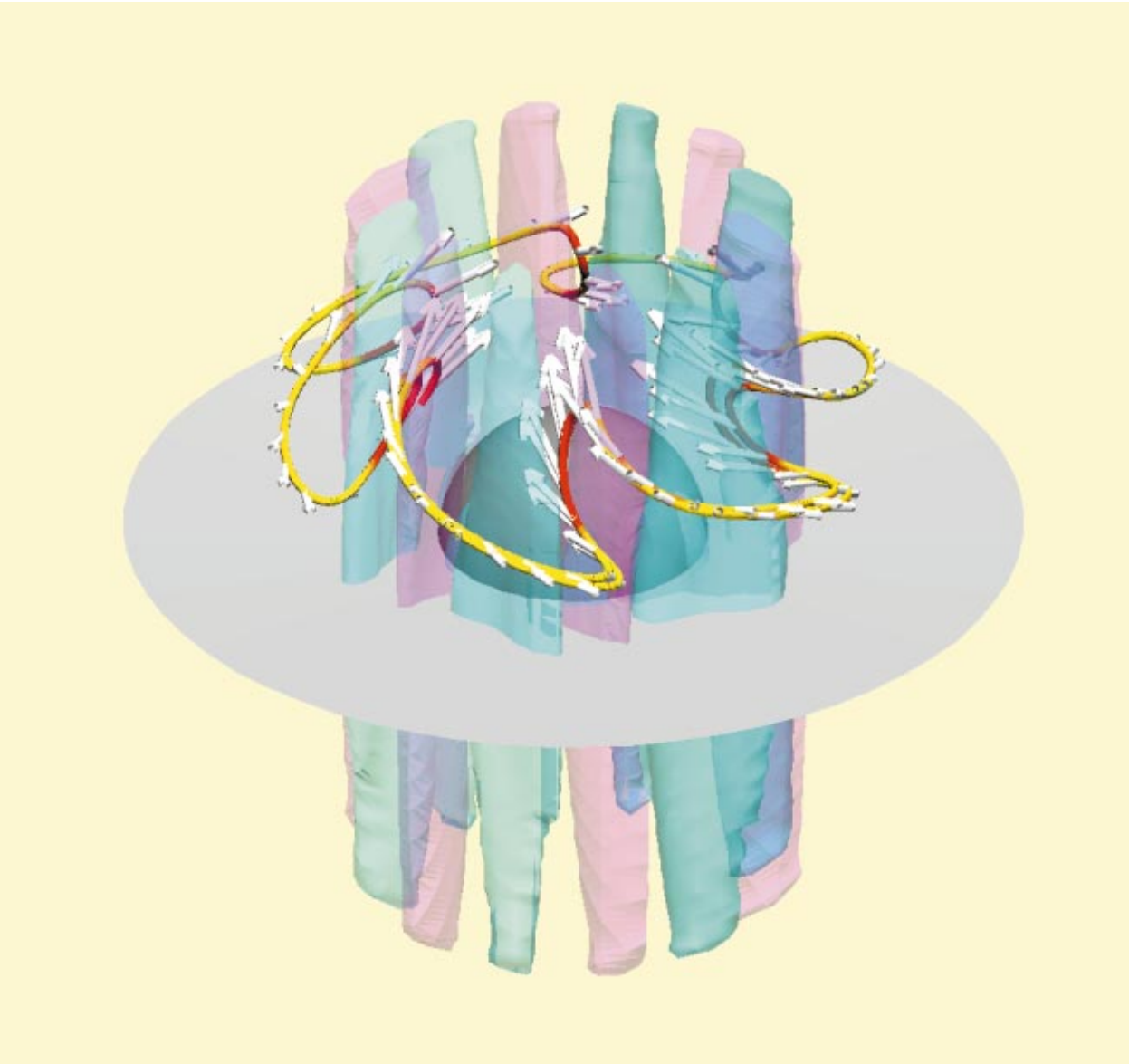

FIG. 9. The cartridge belt of Taylor cells in the rotating, convective dynamo of Kageyama and Sato (1997). Cyclonic cells are colored blue and anticylonic pink; the equatorial plane is also shown. This figure illustrates how a zonal magnetic-field line is distorted by the motion. The line is red where $-\mathbf{V}\cdot(\mathbf{J}\times\mathbf{B})$ is positive. This is where kinetic energy is transformed into magnetic energy; see Eq. (3.12). The white arrows denote $\mathbf{V}$ on the field line. From Kageyama and Sato, 1997, with permission [Color].

condition that must be obeyed by the second term, $\mathbf{V}_{\rm ms}^{(1)}$, in the expansion of the mainstream. Therefore $\mathbf{V}_{\rm ms}^{(1)}$ is $O(E^{1/2}V_{\rm ms}^{(0)})$, rather than the smaller $O(EV_{\rm ms}^{(0)})$ that Eq. (4.73) might have superficially led one to expect *a priori*. A significant application of this result is considered in Sec. V.D and in the next paragraph.

The Ekman layers adjust the rotation of a fluid to that of its boundary, by a process called *spin up* which is surprisingly rapid. Suppose that mantle and core are spinning together and that the angular velocity Ω of the mantle is then increased slightly. Eventually the core must adjust to the new angular velocity, and it does this by creating an Ekman layer that sucks fluid out of the mainstream, so drawing the preexisting z-directed vortex lines in the mainstream (as seen in the inertial frame) towards the rotation axis and increasing their density to the new requirement set by the boundary.[30] Since the rate of Ekman pumping is proportional to $E^{1/2}$, the process of spin-up is essentially complete in a time $\tau_{\rm su}$ of order $E^{-1/2}(2\pi/\Omega)$, i.e., only 3200 days$\approx$ 9 yr for $\nu=\nu^t$.

Finally, when an SIC is present, the tangent cylinder divides the FOC into three regions, the northern interior

[30]We are here appealing to the Kelvin-Helmoltz theorem, an analog of the frozen-flux theorem, according to which vortex lines in an incompressible inviscid fluid are material curves that move with the fluid. In the present case, the vortex lines are all parallel to Oz both initially and finally, and the Ekman suction essentially crowds them inwards as a whole. (The inertial waves described earlier may be visualized in the inertial frame as waves that travel along these vortex lines.)

of the tangent cylinder, the southern interior, and the exterior. The dynamics in these regions tend to be rather different, and they adjust to one another in complicated transitional regions surrounding the tangent cylinder. This was already apparent in Stewartson's (1966) solution of the "Proudman problem," which is to determine the flow that is set up when the SIC spins at a slightly different rate from the mantle; complicated "Stewartson layers" surround the tangent cylinder.

C. Magnetic effects

We now consider how the results of Sec. V.B are changed when a magnetic field $\mathbf{B}$ is present. As before, we ignore the inertial term $\mathbf{V}\cdot\boldsymbol{\nabla}\mathbf{V}$ and consider the limit $E\rightarrow 0$, focusing first on the mainstream.

As is too well known to describe here, disturbances in classical MHD are transmitted by Alfvén waves. These are dispersionless and travel, in a uniform field $\mathbf{B}_0$, with velocity $\mathbf{V}_A=\pm\mathbf{B}_0/\sqrt{(\mu_0\rho_0)}$. Rotation has a profound effect when inequality (5.7) holds. The waves are then of two distinct types: inertial waves (Sec. V.B) with frequencies of order Ω, and MAC waves.[31] This acronym highlights the forces that (together with the pressure gradient) are significant: magnetic, Archimedean, and Coriolis, though we have not yet included the Archimedean (buoyancy) force; the inertial force $\partial_t\mathbf{V}$ is conspicuous by its absence. MAC waves are dispersive; their frequencies are of order $\mathcal{V}_A^2/2\Omega\overline{\mathcal{L}^2}$, which, by inequality (5.7), are much smaller than Ω. When the inertial term $\partial_t\mathbf{V}$ is deleted from the equation of motion, a quasihydrostatic force balance remains: at leading order,

$$\mathbf{0}=-\boldsymbol{\nabla}\Pi-\mathbf{g}\alpha T_c-2\boldsymbol{\Omega}\times\mathbf{V}+\mathbf{J}\times\mathbf{B}/\rho_0. \tag{5.22}$$

The inertial forces so essential for the Alfvén wave are insignificant for the MAC wave. It is this fact that makes RMHD so different from classical MHD. Time dependence enters only through the induction equation

$$\partial_t\mathbf{B}=\boldsymbol{\nabla}\times(\mathbf{V}\times\mathbf{B}). \tag{5.23}$$

[The diffusive terms of Eqs. (4.52) and (4.73) have been ignored.] For small $\mathbf{B}-\mathbf{B}_0$, the linearized forms of Eqs. (5.22) and (5.23) provide the dispersion relation for MAC waves. Their time scales are of order

$$\tau_{\mathrm{MAC}}=2\Omega\overline{\mathcal{L}^2}/\mathcal{V}_A^2=2\Omega\mu_0\rho_0\overline{\mathcal{L}^2}/\mathcal{B}^2, \tag{5.24}$$

or about 4000 years for $\mathcal{B}=0.002$ T. This is roughly the time scale of the westward drift (Sec. I.C). Braginsky (1964d) suggested that the observed geomagnetic secular variation is a manifestation of MAC waves, an idea later developed by Hide (1966).

We now reconsider the same two examples of convective instability that were discussed in Sec. V.B, but now in the presence of an axisymmetric zonal applied field $\tilde{\mathbf{B}}_0=\tilde{B}_0(s,z)\mathbf{1}_\phi$. In the first example, the flow is driven by an axisymmetric temperature field $\tilde{T}_c(r,\theta)$, which depends on the colatitude θ. As in Sec. V.B, a zonal flow is created, but it now has three parts: a thermal wind obeying Eq. (5.19), a geostrophic flow, and a magnetic wind

$$\tilde{V}_B=\tilde{B}_0^2/2\Omega\mu_0\rho_0 s, \tag{5.25}$$

so that Eq. (5.20) is generalized to

$$\tilde{\mathbf{V}}=[\tilde{V}_T(s,z,t)+\tilde{V}_B(s,z,t)+\tilde{V}_G(s,t)]\mathbf{1}_\phi. \tag{5.26}$$

Braginsky (1967) presented a linear stability analysis of state (5.26) that assumed all forms of diffusion to be absent but that is otherwise general. If the thermal forcing $\tilde{T}_c$ is weak, the perturbations create MAC waves that travel longitudinally around the rotation axis. If it is strong, the perturbations grow without limit, according to the linear theory, but Braginsky (1964d) suggested that nonlinearities would equilibrate these perturbations at finite amplitude and that, since they are preferentially asymmetric and therefore evade Cowling's theorem (Sec. III.B), they would provide the nonzero $\bar{\mathcal{E}}_\phi$ needed to maintain the geodynamo. Unstable waves tend to travel westward (Acheson, 1972; see also Roberts and Stewartson, 1975). The shortness of the time scale (5.24) has encouraged speculations that the brevity of polarity transitions (Sec. I.C) is a manifestation of more drastic MAC instabilities. Many further studies of RMHD instabilities have been completed since 1967, several of which concern resistive instabilities such as tearing modes. The subject has been recently reviewed by Fearn (1998).

In RMHD, MAC waves take over the role of Alfvén waves almost completely. We say "almost" because there is one important class of motions for which this is untrue: torsional waves. It is easy to see that the Coriolis force associated with the geostrophic mode (5.16) is conservative and is therefore totally ineffective, since it can be absorbed into the reduced pressure Π. Weaker forces, in particular $\partial_t\tilde{\mathbf{V}}_G$, that would otherwise be neglected become significant. The torsional wave is essentially an Alfvén wave in which the geostrophic cylinders $\mathcal{C}(s)$ turn about Oz and are linked to each other by the component $B_s(s,\phi,z)$ of $\mathbf{B}$ that threads them together. The restoring force on cylinder $\mathcal{C}(s)$ depends on the integral $\mathcal{T}(s)$ of B_s^2/μ_0 over its surface; the inertia of $\mathcal{C}(s)$ is proportional to the integral $m(s)$ of ρ. The torsional wave therefore travels with the local wave speed $V_{\mathrm{tors}}(s)=\sqrt{(\mathcal{T}/m)}\approx V_A$, where V_A is a mean of the Alfvén velocity computed from $\tilde{B}_s$. This provides one of the more rapid time scales of the macroscale fields:

$$\tau_{\mathrm{tors}}=r_{\mathrm{CMB}}/\mathcal{V}_{\mathrm{tors}}. \tag{5.27}$$

If we take $B_s=2\times10^{-4}$ T, we obtain $\tau_{\mathrm{tors}}\approx 32$ yr. Torsional waves are responsible for carrying the z component of angular momentum across the core. As mentioned in Sec. I.C, several analyses of geophysical data claim to have detected them (e.g., that of Zatman and Bloxham, 1997).

[31] To call these fast and slow waves (as is often done) runs some risk of confusion with magnetoacoustic waves that are known by the same names.

Braginsky (1970) provided the complete theory of dissipationless torsional waves. Roberts and Soward (1972) showed that the waves are damped by the Ekman layers and, unless maintained, decay during a spin-up time τ_{su}. Although strictly speaking Eq. (5.22) applies only to the ageostrophic flow $\mathbf{V}-\tilde{\mathbf{V}}_G$, it may also be applied to $\tilde{\mathbf{V}}_G$ if attention is focused on time scales long compared with τ_{su}. Otherwise part of the inertial acceleration, namely, $(\partial \tilde{V}_G/\partial t)\mathbf{1}_\phi$, must be restored to Eq. (5.22). As a beneficial byproduct, the "stiffness" of numerical simulations is reduced by including $(\partial \tilde{V}_G/\partial t)\mathbf{1}_\phi$ (Jault, 1995).

Consider now the second example, the convective instability of a rotating sphere containing heat sources, but now permeated by a magnetic field. This field can be more effective than viscosity in breaking the rotational constraint. Considering the critical Rayleigh number Ra_c as a function of the field strength $\mathcal{B}$, it is found that Ra_c is smallest in the strong-field range, $\Lambda = O(1)$. The minimum Ra_c is $O(E^{-1})$, which is much smaller for $E \ll 1$ than the $O(E^{-4/3})$ critical value for $\mathcal{B}=0$. We see that the *magnetic field facilitates convection*.[32] This is not totally surprising. In the absence of field, the scale $\mathcal{L}_\perp$ of the convective motions in directions perpendicular to $\mathbf{\Omega}$ has to be small $[\mathcal{L}_\perp = O(E^{1/3}\overline{\mathcal{L}})]$ to break the rotational constraint, and such motions are energetically expensive. When $\Lambda = O(1)$, the scale of the cells is much larger $[\mathcal{L}_\perp = O(\overline{\mathcal{L}})]$, and these are less costly. (The increased scale of convection can be inferred from Fig. 9. Taylor cells, though evident, are not as numerous as they would be if $\mathbf{B}$ were zero.) The optimal case, $Ra_c = O(E^{-1})$, may be restated as $Ra_c^* = O(1)$, where

$$Ra^* = g\alpha\beta\overline{\mathcal{L}}^2/2\Omega\kappa \tag{5.28}$$

is a Rayleigh number that is independent of ν, as is the optimizing field strength $\mathcal{B}$ given by Eq. (5.10). Viscosity plays no role in the mainstream solution. Solutions for $Ra > Ra_c$ have been derived by Walker and Barenghi (1999).

Although it might seem that marginal stability calculations $(Rm=0)$ of the type just described have no direct bearing on the geodynamo $[Rm \gtrsim O(1)]$, they have proved to be a reliable guide in predicting the existence of strong-field convective dynamos such as that of Jones and Roberts (2000). A few words of caution are appropriate here. It is often said that the North-seeking property of the magnetic compass needle establishes that the Coriolis force dominates the dynamics of the core. This is an overstatement. More precisely, the Coriolis force is the only force acting that has a preferred direction. The Lorentz force is equally dominant, and, in acting to counter Coriolis forces and break the rotational constraint, it too acquires the same preferred direction. This is well illustrated by Fig. 10, which is taken from the dynamo simulation of Sakuraba and Kono (1999).

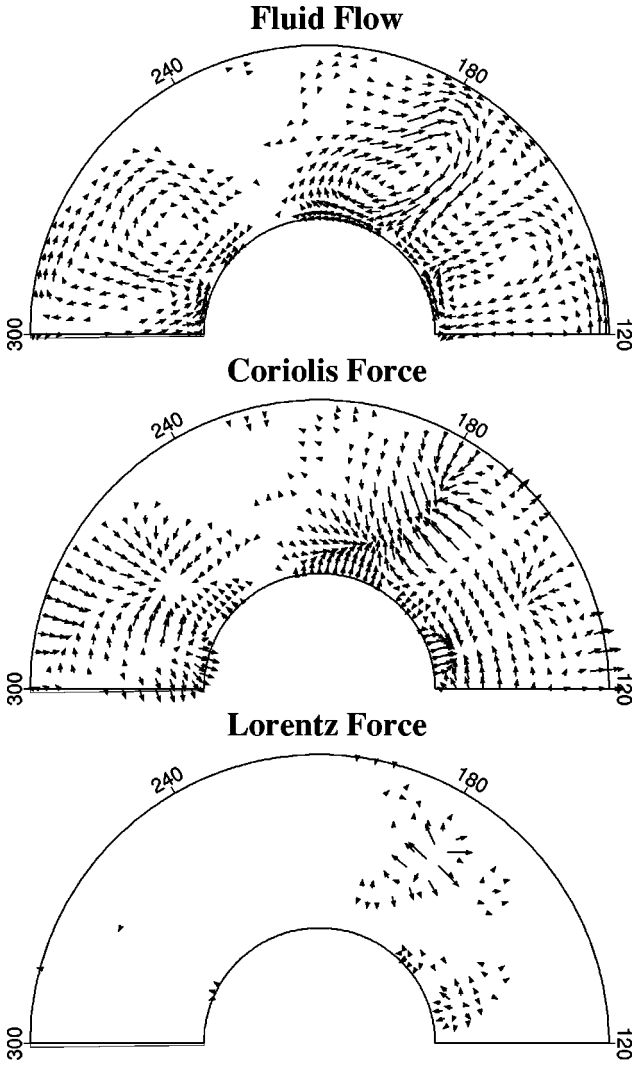

FIG. 10. Illustration of how Lorentz forces act to oppose Coriolis forces. Fluid velocity, Coriolis force, and Lorentz force are plotted in the equatorial plane. From Sakuraba and Kono, 1999, with permission.

Consider next the boundary layers. In classical MHD at high Hartmann number $M = \mathcal{V}_A\overline{\mathcal{L}}/(\nu\eta)^{1/2}$, asymptotic methods apply in which both ν and η are set to zero in determining the leading-order mainstream, and this is matched to thin "Hartmann layers" on the boundaries. In dynamo theory, however, we are almost always concerned with a mainstream in which $Rm = O(1)$ and in which therefore ohmic diffusion is not confined to boundary layers. (An exception arose in Sec. III.D.) The Ekman-Hartmann layers relevant to core dynamics therefore have the character of a magnetically modified Ekman layer rather than of a Hartmann layer; e.g., see Loper (1970).

Finally we temporarily reintroduce the SIC. The effect of a magnetic field on Stewartson (1957) layers surrounding the tangent cylinder has been analyzed by Hollerbach (1994, 1996b), who found that B_s tends to thicken them. Nevertheless, regions of large shear near

[32] It is sometimes speculated that convective dynamos have a general thermodynamic reason for their existence: a body of convecting fluid generates a dynamo field so that it can cool as rapidly as possible.

the tangent cylinder appear in the simulations of Sec. VI and seem to be significant in the dynamo mechanism. The MHD of the three regions of the fluid outer core separated by the tangent cylinder can be very different (Sec. V.B). The SIC also has another significant effect on core MHD: a large-scale magnetic field threading the SIC cannot change drastically in a time shorter than the electromagnetic time constant of the SIC, which is about 2500 years. This tends to prevent large-scale fields in the FOC from changing more rapidly than this (Hollerbach and Jones, 1993).

D. The Taylor state and model *z*

We have argued in Sec. V.C that, over time scales long compared with $\tau_{\rm su}$, inertial forces are negligible and that, at least to leading order, viscosity can also be ignored. This was the basis of our second convection example, which we emphasized was, in its optimal marginal state, independent of ν in all respects. The question arises therefore whether anelastic RMHD dynamos can be constructed which, except in boundary layers, satisfy

$$\boldsymbol{\nabla}\cdot(\rho\mathbf{V})=0, \tag{5.29}$$

$$\mathbf{0}=-\boldsymbol{\nabla}\Pi+C\mathbf{g}-2\boldsymbol{\Omega}\times\mathbf{V}+\mathbf{J}\times\mathbf{B}/\rho, \tag{5.30}$$

or the equivalent for the uniform ρ (Boussinesq) models. By integrating the ϕ component of Eq. (5.30) over the curved surface of the geostrophic cylinder $\mathcal{C}(s)$ and applying Eq. (5.29), we obtain

$$\int_{\mathcal{C}(s)}(\mathbf{J}\times\mathbf{B})_\phi dS=2\Omega\int_{\mathcal{C}(s)}\rho\mathbf{V}\cdot\mathbf{dS}$$
$$=-2\Omega\int_{\mathcal{N}+\mathcal{S}}\rho\mathbf{V}\cdot\mathbf{dS}, \tag{5.31}$$

where $\mathcal{N}(s)$ and $\mathcal{S}(s)$ are the northern and southern spherical caps at the ends of the cylinder $\mathcal{C}(s)$; see Fig. 8. By applying the boundary condition (5.11), Taylor (1963) obtained

$$\int_{\mathcal{C}(s)}(\mathbf{J}\times\mathbf{B})_\phi dS=0, \tag{5.32}$$

which is known as *Taylor's condition* or Taylor's constraint. Unless this is satisfied, Eq. (5.30) has no solution obeying condition (5.11); if it is satisfied, there is an infinity of solutions.

An alternative approach applies $\boldsymbol{\nabla}\times$ to Eq. (5.30) to obtain

$$2\Omega\partial_z\mathbf{V}=-\boldsymbol{\nabla}\times(C\mathbf{g}+\mathbf{J}\times\mathbf{B}/\rho). \tag{5.33}$$

Regarding $C\mathbf{g}+\mathbf{J}\times\mathbf{B}/\rho$ as known, we can determine V_s and V_r uniquely by two simple integrations along every line segment parallel to Oz; condition (5.11), applied at the ends of the segment where it meets the CMB, determines the two arbitrary "constants" of integration. Equation (5.29) is, in component form,

$$\rho\partial_\phi V_\phi=-\partial_s(s\rho V_s)-s\partial_z(\rho V_z). \tag{5.34}$$

This gives V'_ϕ uniquely from V'_s and V'_z, so that the asymmetric flow is completely determined. For the axisymmetric flow, there is a difficulty: when the $\tilde{V}_s$ and $\tilde{V}_z$ determined above are substituted into the right-hand side of Eq. (5.34), it is generally found to be nonzero. It is only when condition (5.32) is obeyed that the right-hand side of Eq. (5.34) is zero. When this happens, we can determine $\tilde{V}_\phi$ by integrating the ϕ component of Eq. (5.33) along the line segments, but, since there are no restrictions on $\tilde{V}_\phi$ at the ends of the segment, there is an arbitrary "constant" of integration, corresponding to an arbitrary geostrophic flow $\tilde{V}_G(s,t)\mathbf{1}_\phi$. This flow is dynamically innocuous, since its Coriolis force can be absorbed into $\boldsymbol{\nabla}\Pi$ as in Sec. V.C.

Condition (5.32) is related to the angular momentum balance about Oz. If the $\partial_t\mathbf{V}$ were restored to Eq. (5.30), one might hope that the system would respond to a failure of condition (5.32) by generating torsional waves that, if sufficiently damped, would adjust $\tilde{V}_G$ until, in a comparatively short time of order $\tau_{\rm su}$, the condition would be satisfied. The magnetic field subsequently would evolve slowly in obedience to

$$\boldsymbol{\nabla}\cdot\mathbf{B}=0, \tag{5.35}$$

$$\partial_t\mathbf{B}=\boldsymbol{\nabla}\times(\mathbf{V}\times\mathbf{B})-\boldsymbol{\nabla}\times(\eta\boldsymbol{\nabla}\times\mathbf{B}), \tag{5.36}$$

and $(\mathbf{J}\times\mathbf{B})_\phi$ would evolve slowly also. Condition (5.32) will be gradually violated unless some action is taken. From Eq. (5.36), Taylor (1963) developed an evolution equation for $\tilde{V}_G$ which ensured that condition (5.32), if satisfied initially, would be satisfied for all t. This determined the evolution of $\tilde{V}_G$ uniquely, so completing the determination of $\mathbf{V}$.

Although Taylor's prescription provides a clear-cut program for the construction of a strong-field dynamo, no successful three-dimensional dynamo has yet been found by following it; see Fearn and Proctor (1987). It was shown by Roberts and Stewartson (1975) that one should not take it for granted that the Taylor prescription will work; see also Jones and Roberts (2000). The Taylor method may run into difficulties through treating the Ekman layers as passive layers that can always be constructed (after the mainstream has been found) in such a way that conditions (4.59) are satisfied in full.

One of the tacit assumptions behind the Taylor idea is that there exists a solution of the (viscous) RMHD equations that, as $E\to 0$, has an E-independent mainstream form, as in the second convection example of Sec. V.B. Braginsky (1975, 1978) questioned this assumption and proposed an alternative, in which the mainstream solution has a geostrophic part proportional to an inverse power of E as $E\to 0$. He called this *model z* because the geostrophic flow increasingly makes the lines of force of the meridional field $\mathbf{B}_p$ almost parallel to the z axis. The idea behind model z may be clarified by regarding the large geostrophic flow, of order $E^{-1/2}(\mathbf{J}\times\mathbf{B}/2\Omega\rho)=E^{-1/2}\Lambda(\eta/\overline{\mathcal{L}})$, as the leading-order mainstream flow $\mathbf{V}^{(0)}_{\rm ms}$. Ekman pumping from $\mathcal{N}(s)$ and

$\mathcal{S}(s)$ created by this flow is of order $E^{1/2}$ times smaller (Sec. V.C), i.e., it is $O(\Lambda\eta/\bar{\mathcal{L}})$ and is a part of $\mathbf{V}_{\rm ms}^{(1)}$. Condition (5.32) no longer follows; the integral on the right-hand side of Eq. (5.31) is now in general nonzero and is of the same order as the left-hand side, to which it can be made equal, so depriving Taylor's condition of any significance. The remainder of $\mathbf{V}_{\rm ms}^{(1)}$ generally contains asymmetric parts, such as the field-generating MAC waves envisaged in Sec. V.C, and these evade Cowling's theorem.

It should by now be clear that the difficulty in solving Eqs. (5.29) and (5.30) arises from the omission of the viscous term $\mathbf{F}^{\nu}$ and is confined to the axisymmetric part $\tilde{\mathbf{V}}$ of $\mathbf{V}$. This has led to a number of investigations of axisymmetric MHD dynamos in which either C in Eq. (5.30) or $\tilde{V}_T$ in Eq. (5.26) is specified as the energy source. The aim of these models is to understand better the role of the Taylor state, model z, and indeed other types of force balance. Interest in the electrodynamics is subsidiary, but nevertheless Cowling's theorem must be evaded, and this is most often done in the simplest possible way, by including an α effect, thus leading to Eqs. (3.22) and (3.23) with $\tilde{\boldsymbol{\mathcal{E}}}=\alpha\tilde{\mathbf{B}}$. See Hollerbach (1996a) for a recent review of this area.

VI. MHD DYNAMO SIMULATIONS

A. The development of models

Here we focus only on dynamo simulations that simultaneously solve for the thermodynamic variables, the fluid flow, and the magnetic field in three dimensions (3D) with full time dependence and feedbacks. The resulting magnetic field is maintained by rotating convection for several magnetic diffusion times τ_η. This excludes many studies of mean-field and kinematic dynamos, convection in the presence of an externally applied field, and solutions in a drifting frame of reference, though all of these have materially aided the development of dynamo theory. The comparatively simple model of Childress and Soward (1972) should, however, be mentioned, since very considerable progress can be made analytically using this model; see also Soward (1974).

The Childress-Soward model is an MHD dynamo driven by convective motions in a plane layer rotating about the vertical, heated from below and cooled from above (the rotating Bénard layer). Its success rests on the fact (Sec. V.B) that, provided $\Lambda<O(1)$, the scale $\mathcal{L}_\perp$ of the motions in the (horizontal) direction perpendicular to $\boldsymbol{\Omega}$ is small compared with the depth $\bar{\mathcal{L}}$ of the layer.[33] Such microscale motions induce a macroscale field in a way similar to that described in Sec. III.C for turbulent flow, though their α effect is 2D rather than 3D, and α is a function of z. As the Rayleigh number (5.21) is increased beyond Ra_c, a bifurcation is reached at which kinematic dynamo action occurs; a further increase in Ra results in finite $\mathcal{B}$ and a concomitant increase in the horizontal scale $\mathcal{L}_\perp$ of the motions (Sec. V.C), though Λ remains small and the dynamo is of the weak field variety. Eventually, as Ra is increased further, an asymptote is reached where $\mathcal{B}\to\infty$ and $\mathcal{L}_\perp\to\bar{\mathcal{L}}$. The result $\mathcal{B}\to\infty$ is a symptom of the violation of the assumption $\mathcal{L}_\perp\ll\bar{\mathcal{L}}$ on which the analysis rests; in reality, $\mathcal{B}$ does not become unbounded, but the asymptote shows very convincingly that a strong-field regime ($\Lambda\gtrsim1$) exists in which $\mathcal{L}_\perp=O(\bar{\mathcal{L}})$; see Fautrelle and Childress (1982). The analytic method cannot follow the solution into this regime for which, as for all strong-field dynamos, numerical computation is required.

Numerical integrations of planar models were carried out by Meneguzzi and Pouquet (1989), Brandenburg *et al.* (1990), St. Pierre (1993), and Jones and Roberts (2000). That of St. Pierre (1993) was the first to reach a parameter regime in which the magnetic energy $\mathcal{E}^B$ exceeds the kinetic energy $\mathcal{E}^V$ of the convection that maintains it: $\mathcal{E}^B/\mathcal{E}^V\approx10$ (Sec. V.A). It also demonstrated how the two major forces in the problem, the Coriolis and Lorentz forces, nearly balanced each other locally (see Fig. 10 above). Planar models avoid the complication[34] of spherical geometry and are convenient for testing the effects of various physical parametrizations (Velímský and Matyska, 2000), but obviously cannot represent global modes.

Gilman and Miller pioneered spherical MHD simulations in the early 1980s with the development of a global solar dynamo model (Gilman and Miller, 1981; Gilman, 1983). This model employed the Boussinesq approximation (Sec. IV.F), which was singularly inappropriate for the interior of the Sun. Glatzmaier (1984, 1985a, 1985b) developed an alternative anelastic model (Sec. IV.C), which allowed for large variations of density with depth and which, by filtering out sound waves, allowed much larger numerical time steps than could have been taken had compressibility been fully included. These early solar dynamo models produced cycles of magnetic reversals in some ways similar to the migration of large-scale field in the solar cycle.

The first Earth-like magnetic field was generated by Glatzmaier and Roberts (1995a, 1995b) using a 3D global model designed to simulate the core MHD. The original version included only thermal buoyancy and used the Boussinesq approximation. The current version (Glatzmaier and Roberts, 1996a, 1996b, 1997, 1998;

[33] In spherical convection, the cartridge belt of Taylor cells (Sec. V.B) also defines a two-scale motion, suggesting that the Childress-Soward idea can again be usefully employed to find an MHD dynamo by mainly analytic means; see Busse (1975).

[34] Spherical models make use of a spectral transform in θ that is not fast, but planar models can make use of the fast Fourier transform in all three coordinate directions. It is therefore practical to compute planar MHD models on a workstation or a PC, truncating the Fourier modes after, for example, 64 terms in all three coordinate directions (Jones and Roberts, 2000).

Glatzmaier *et al.*, 1999) accounts for both thermal and compositional buoyancy and uses the anelastic approximation, with a reference state fitted to the Earth and convection driven by a prescribed, Earth-like, heat flux through the CMB, precisely as explained in Sec. IV above, the momentum flux $\rho\mathbf{V}$ playing a role similar to the velocity $\mathbf{V}$ in the Boussinesq approximation; cf. Eqs. (4.45) and (4.72). The magnetic field outside the core in this model had an intensity, structure, and time dependence similar to the geomagnetic field (Sec. I.C). A Boussinesq model was later developed by Kuang and Bloxham (1997, 1999) that used different velocity and thermal boundary conditions and operated in a somewhat different parameter regime but one that also produced an Earth-like magnetic field outside the core. Both of these models were able to operate with relatively small diffusion coefficients, which increased the effects of buoyancy and Coriolis forces; moreover, in rough agreement with estimates for the Earth, $\mathcal{E}^B/\mathcal{E}^V \approx 10^3$; see Sec. V.A.

The Glatzmaier-Roberts model is an improved version of Glatzmaier's original solar model; it computes the magnetic field within a finitely conducting solid inner core, the importance of which was demonstrated with a 2D mean-field model by Hollerbach and Jones (1993), and it treats the Coriolis force implicitly in the time integration, which makes it possible to operate in more extreme (less diffusive) parameter regimes. It uses the spectral transform method, the spatial resolution chosen (i.e., the number of modes retained in the spectral expansions) being dictated by the time span to be simulated. High resolution is affordable only for time spans of a few thousand years (Roberts and Glatzmaier, 2000), but more than a million years have been simulated at low resolution, using a numerical time step of about 15 days (Glatzmaier *et al.*, 1999). In this review we present results from a medium-resolution case: 49 radial (Chebyshev) levels in the fluid outer core (plus 17 in the solid inner core), 144 latitudinal levels, and 144 longitudinal levels. This corresponds to a rhomboidal truncation of spherical harmonics up to order 47 and degree 95. We set the core size, rotation rate, density profile, CMB heat flux, and magnetic diffusivity ($\eta = 2\ \mathrm{m^2\,s^{-1}}$) to Earth-like values and use viscous, thermal, and compositional eddy diffusivities to account for mixing by the unresolved turbulence (see Sec. IV.D). The diffusivity κ^t of heat and composition is taken as η; the viscous eddy diffusivity ν^t is 750 times greater. In addition, we use a "hyperdiffusivity" that increases these values (according to the square of the spherical harmonic degree) such that the diffusivity experienced by the degree 95 modes is ten times greater (five times greater for the magnetic diffusivity) than that experienced by the low-degree (large-scale) modes. This means that the Ekman number E is 5.4×10^{-6} for the large scales and 5.4×10^{-5} for the small scales. Here, and for the remainder of this review, we follow the usual practice of taking $\bar{\mathcal{L}}$ to be the radial depth of the FOC:

$$\bar{\mathcal{L}} = r_{\mathrm{CMB}} - \bar{r}_{\mathrm{ICB}} \approx 2.26\times10^6\ \mathrm{m}. \tag{6.1}$$

In order to include torsional waves, the axisymmetric inertial terms are retained, but the asymmetric accelerations are discarded.

Simulations such as these are specific to the Earth. They are expensive and do not provide a complete understanding of the fundamentals of convective dynamos in rotating spherical shells. For example, they are strongly driven and create fields on many time and length scales; they do not provide information about the bifurcation structure of the solutions as the sources of buoyancy are gradually strengthened from the marginal state. They also sample parameter space sparsely. Many other models have been studied recently,[35] especially ones in which diffusion plays a more prominent role and in which, therefore, the flow and field structures are more dominated by larger scales. Several assume that the SIC is electrically insulating. Apart from the Kageyama-Sato (1995, 1997) model, which is fully compressible, all these simulations employ the Boussinesq approximation. The Kageyama-Sato model also differs from the others by employing a perfect gas equation of state. It is therefore similar to the early solar dynamo models, e.g., those of Gilman and Miller (1981), Gilman (1983), and Glatzmaier (1984, 1985a, 1985b).

In order to reach the more geophysically realistic parameter regimes of the Glatzmaier-Roberts and Kuang-Bloxham models without their huge computational cost, a "$2\frac{1}{2}$D" Boussinesq model was developed by Jones *et al.* (1995), Sarson *et al.* (1997, 1998), Sarson and Jones (1999), Morrison and Fearn (2000), and Sarson (2000). These do what in the solar physics community used to be called *modal simulations*, in which the spatial resolution is adequate in the r and θ directions, but which retain only the longitudinal wave numbers 0 and 2 (or wave numbers 0, 2, 4, 6, and 8 in the case of Sarson, 2000). Although the longitudinal structure is coarse, the axisymmetric parts of the fields appear to be quite similar to those of the fully 3D simulations of Glatzmaier and Roberts.

B. Some results

Magnetic field is generated by twisting and shearing of existing magnetic field into new magnetic field, and by magnetic diffusion that causes field lines to break and reconnect into new topologies, as in the turbulent α effect described in Sec. III.C. Taylor cells create a large-scale α effect of the type discussed in Sec. III.D. The dynamo simulation of Kageyama and Sato (1997) illustrates this nicely; see Fig. 9. Taylor cells of rotating fluid outside the tangent cylinder have local angular velocity (vorticity) either parallel (cyclonic) or antiparallel (anticyclonic) to $\mathbf{\Omega}$. In addition, due to the spherical bound-

[35] See Kageyama and Sato (1995, 1997), Kida *et al.* (1997), Busse *et al.* (1998), Christensen *et al.* (1998, 1999), Kitauchi and Kida (1998), Grote *et al.* (1999, 2000), Kageyama *et al.* (1999), Olson *et al.* (1999), Sakuraba and Kono (1999), and Kutzner and Christensen (2000).

aries, fluid drifts along these cells, so that the motions have a left-handed helical sense in the northern hemisphere, and a right-handed sense in the southern hemisphere. They twist the zonal magnetic-field lines, whether directed eastward or westward, into right-handed helices in the northern hemisphere and left-handed helices in the southern hemisphere. The average over longitude ϕ is a meridional field $\mathbf{B}_p$ (see also Glatzmaier, 1985a, and Olson *et al.*, 1999). This completes step 1 of the two-stage process maintaining $\tilde{\mathbf{B}}$ described in Sec. III.C.

In addition, zonal field has to be generated from meridional field by step 2 of the two-stage process of Sec. III.C. Kageyama and Sato (1997) find that in their simulation the zonal field is mainly created from the meridional field by the zonal shear outside the tangent cylinder. In the terminology of Sec. III.C, $\tilde{\mathbf{B}}$ is maintained by an $\alpha\omega$-dynamo process. Olson *et al.* (1999), however, demonstrate that weakly driven convective dynamos, which are dominated by Taylor cells outside the tangent cylinder, usually sustain their $\tilde{\mathbf{B}}$ by an α^2-dynamo mechanism. Their more strongly driven (less diffusive) dynamos maintain $\tilde{\mathbf{B}}$ by an $\alpha\omega$ process, step 2 being dominated by a thermal wind shear inside the tangent cylinder. Indications of this are seen in Fig. 11 from Olson *et al.* (1999), where (in the northern hemisphere) a left-handed helical upflow in the polar region horizontally diverges below the core-mantle boundary. This correlates with enhanced convective heat flux and weak radial magnetic field at the poles. Reducing viscous, thermal, compositional, and magnetic diffusion also strengthens the dynamo process and increases the kinetic and magnetic energies. The ratio of these energies depends on the relative values of these diffusivities (Busse *et al.*, 1998).

Both the Glatzmaier-Roberts and the Kuang-Bloxham models operate with relatively small diffusion coefficients. The convective velocity is very time dependent but typically has a maximum of a few mm s^{-1}. Convection is so effective that the maximum variation in T (on a sphere of constant radius) is only about 10^{-3} K. The maximum magnetic-field intensity (in the deep interior of the core) can be as large as 50 mT and the magnetic energy (integrated throughout the core) is typically more than 2000 times greater than the kinetic energy of the convection that maintains it: $\mathcal{E}^B/\mathcal{E}^V = 2\times 10^3$; see Sec. V.A.

Large magnetic fields with large spatial gradients produce strong Lorentz forces, which need to be approximately balanced by the other major force in this problem, the Coriolis force. This was illustrated in Fig. 10 above, where the Coriolis and Lorentz forces were seen to nearly balance in one of the downwellings.

We now show results from the Glatzmaier-Roberts integrations. The simulated fluid flow outside the tangent cylinder is a combination of axisymmetric zonal and meridional circulations and nonaxisymmetric Taylor cells; see the snapshot of Fig. 12, where the equatorial projection of the flow is shown. The Taylor columns are smaller in scale, less well defined, and more time dependent than they are in more diffusive solutions. Although the patterns of the thermodynamic perturbations, fluid flow, and magnetic field are continually changing in all directions, one can identify a westward phase propagation. Even on the inner core boundary, the patterns of heat flux, composition flux, and inner core growth rate tend to propagate westward relative to the rotating frame of reference (Glatzmaier and Roberts, 1998). The phase velocity depends on location and time but is typically about 0.1° yr^{-1}, similar to the observed westward drift of the Earth's field (Sec. I.C).

The axisymmetric zonal flow outside the tangent cylinder is rather constant (Fig. 13), although there is a weak minimum in the equatorial region. Much greater variations exist inside the tangent cylinder where, relative to the mean rotation rate of the model Earth, the zonal flow is westward near the mantle and eastward near the solid inner core. This is principally a thermal wind, whose existence may be understood in the following way. The efficient Taylor column convection outside the tangent cylinder maintains that region at a fairly uniform temperature and composition compared with the less efficient convective flow inside the tangent cylinder (Fig. 13), where thermal and compositional buoyancy causes fluid near the polar axis to flow outward along that axis. Mass conservation requires the fluid to return near the tangent cylinder, to flow toward the rotation axis near the ICB and away from it near the CMB. Since the angular momentum is approximately conserved, fluid inside the tangent cylinder spins up (moves eastward) near the ICB, and spins down (moves westward) near the CMB (Fig. 13). Although the fluid near the ICB flows eastward, the patterns of thermodynamic perturbations, fluid velocity, and magnetic field there all drift westward; see above.

The radial magnetic field threads the fluid outer core and solid inner core together and provides a potentially strong magnetic torque between them, as described in Sec. IV.E. To balance (on average) the small viscous torque on the ICB, the SIC must rotate at roughly the same average rate of the fluid just above it; see Sec. IV.E. This mechanism, similar to an induction motor, is what maintains the super-rotation of the SIC predicted by Glatzmaier and Roberts (1995a, 1996b). This prediction motivated seismologists to look for, and find, evidence of inner core super-rotation (Song and Richards, 1996; Su *et al.*, 1996). The initial prediction and those original seismic estimates placed the rate at roughly 2° yr^{-1}. More recent seismic analyses (Creager, 1997; Souriau, 1998) suggest a rate of order 0.1° yr^{-1} or less. The maximum, according to the Glatzmaier-Roberts simulation described here, is about 1° yr^{-1}. Simulations (Buffett and Glatzmaier, 2000) that include a parametrized gravitational coupling (Sec. IV.E) between density variations in the mantle and an estimated topography of the inner core boundary give average super-rotation rates as small as 0.02° yr^{-1}.

Since the SIC rotates as a solid body while the zonal flow just above it does not, a local shear exists in the

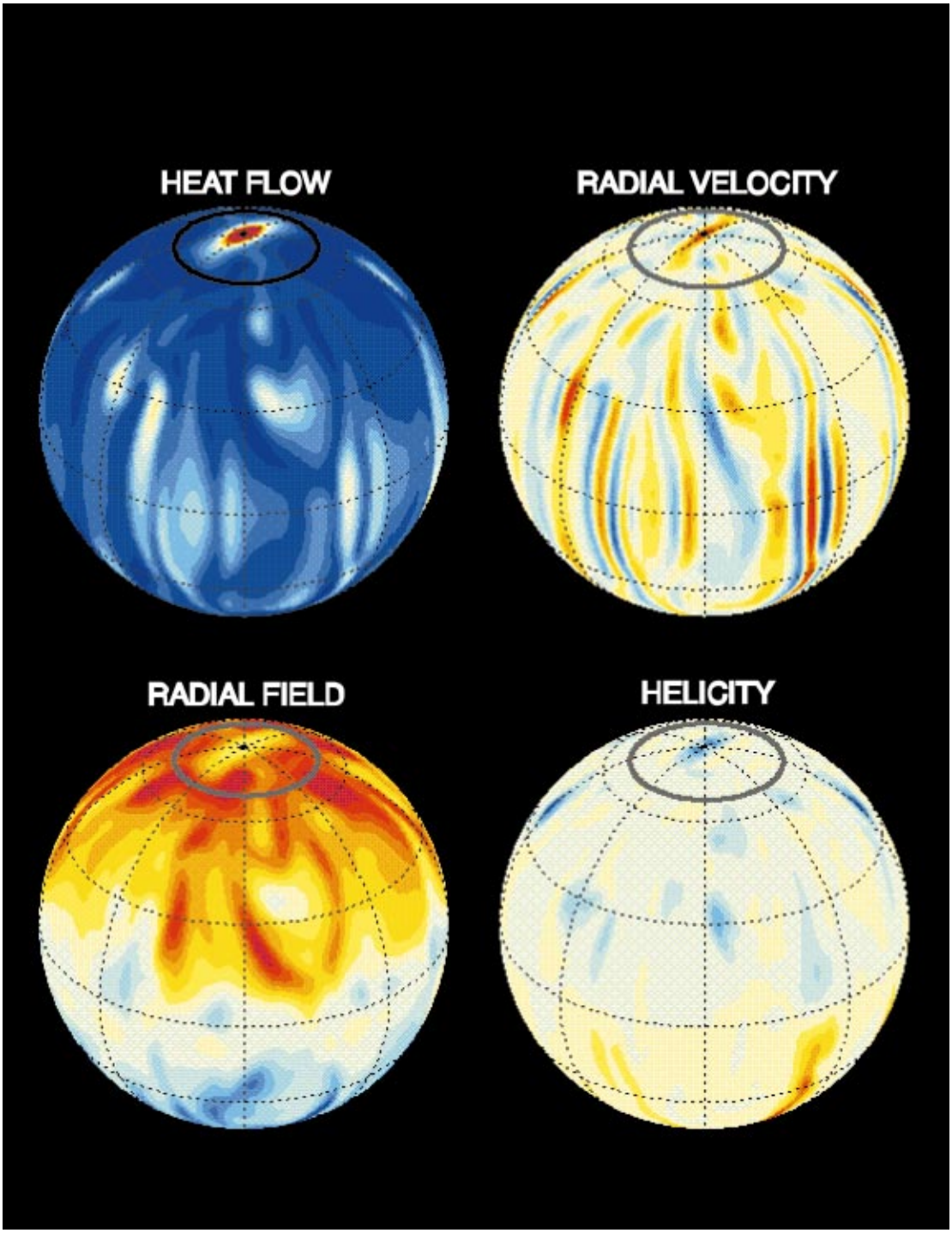

FIG. 11. Heat flux from the core, radial components of fluid velocity and magnetic field, and helicity plotted on a surface below the core-mantle boundary. Blue means outwardly directed heat flux and red inwardly directed; reds are positive, blues are negative for V_r and B_r; red helicity is right handed, blue is left handed. From Olson *et al.*, 1999, with permission [Color].

zonal flow near the ICB. Shear flow also exists across the tangent cylinder due to the transition between the different styles of convection inside and outside this cylinder. These strong shear flows, not seen in the more diffusive dynamos, are responsible for much of the zonal field generation in the Glatzmaier-Roberts simulations, which appears to maintain its $\tilde{\mathbf{B}}$ by an $\alpha\omega$ mechanism.

The Glatzmaier-Roberts geodynamo simulations were the first to demonstrate spontaneous magnetic dipole reversals. The initial reversal (Glatzmaier and Roberts, 1995b) occurred about 3.5×10^4 yr into the original simulation and took a little more than 10^3 yr to complete. Before and after the reversal the dipole polarities were opposite inside and outside (roughly) the tangent cylinder. (A somewhat similar dual-polarity configuration is seen in the modal calculations of Sarson, 2000.) We continued our simulation at this point using the anelastic model. After about 10^4 yr, the field outside the tangent

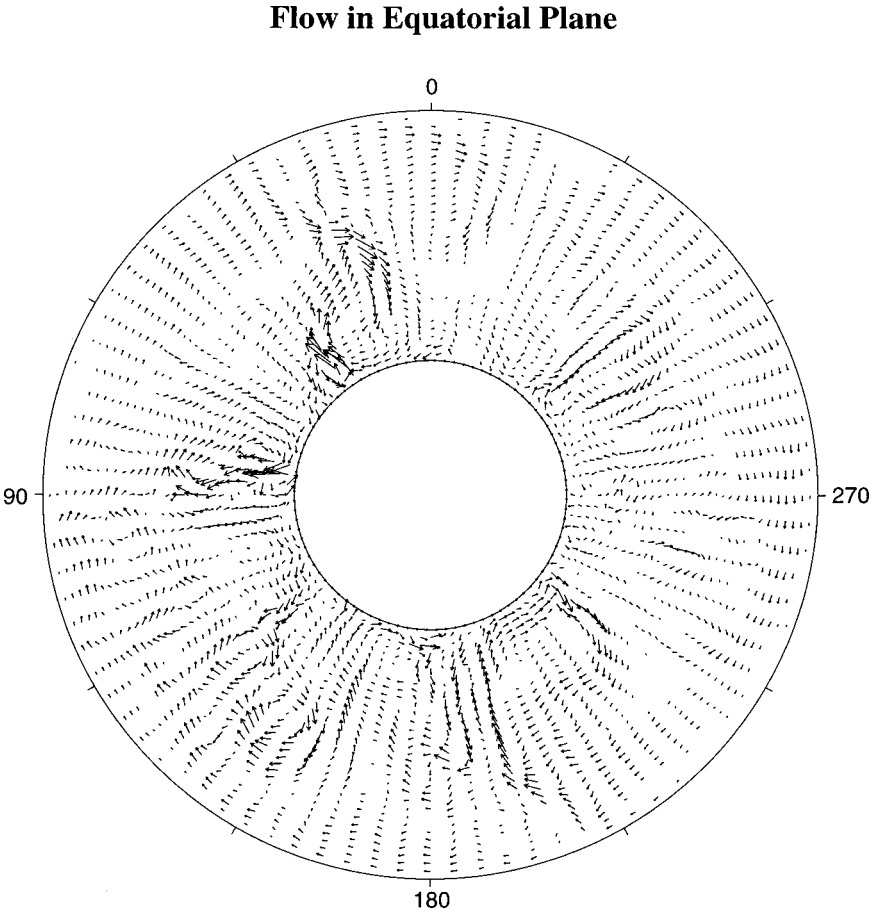

FIG. 12. Fluid velocity plotted in the equatorial plane for a snapshot from the Glatzmaier-Roberts simulation. The lengths of the arrows are proportional to the flow speed.

cylinder reversed again, leaving a single dipole polarity throughout the core (Glatzmaier and Roberts, 1996a). This new polarity configuration is apparently more stable, since, although the field was time dependent, it maintained this new polarity state for the next 2.3×10^5 yr. It then quickly reversed in less than 10^3 yr (although it took a further few thousand years for the axial dipole to become dominant again). It remained in this polarity state for the next 1.7×10^5 yr, quickly reversed back, and has been in this latest state for the remaining 10^5 yr of the simulation (Glatzmaier *et al.*, 1999). This 5.5×10^5 yr simulation (over 27 magnetic dipole diffusion times) took 16 million numerical time steps; 3×10^5 yr of this are illustrated in Fig. 14, where it can be seen that,

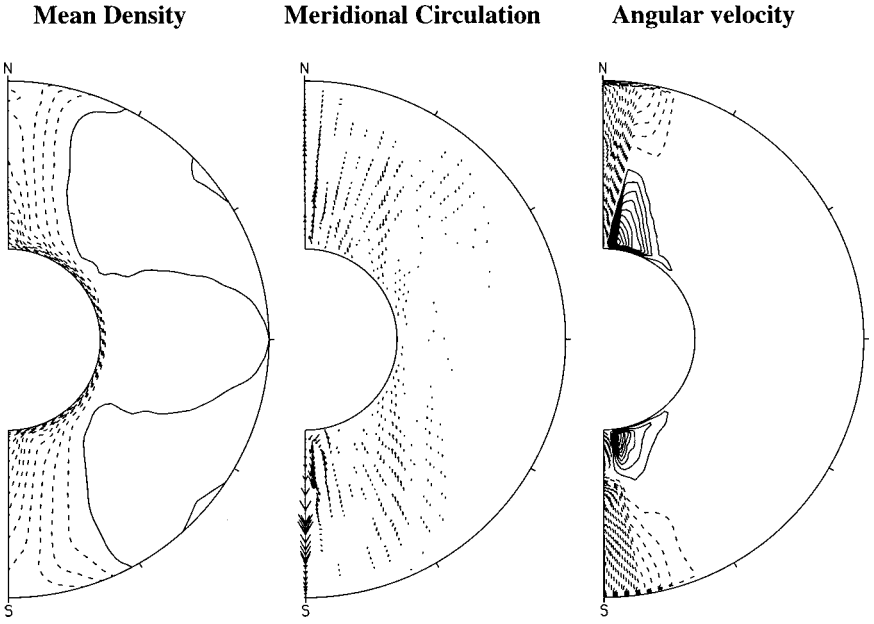

FIG. 13. Longitudinally averaged density perturbation, meridional circulation, and angular velocity (relative to the rotating frame) for a snapshot from the Glatzmaier-Roberts simulation. Solid contours are positive; broken are negative so that, for the angular velocity, solid contours represent superrotation. In the center plot, the lengths of the arrows are proportional to the meridional flow speed.

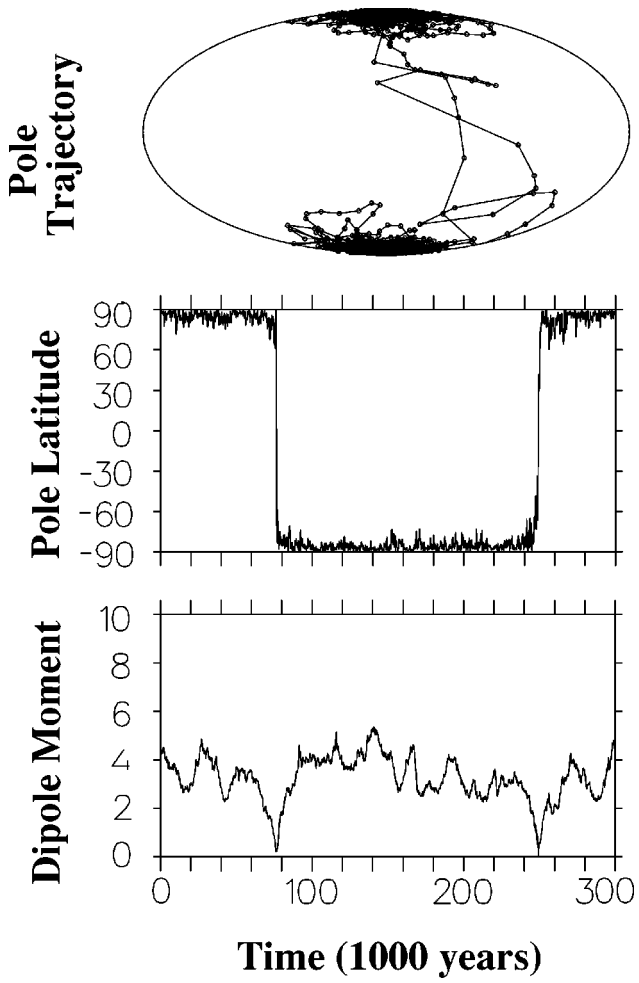

FIG. 14. 300 000 years in the middle of a 550 000-year Glatzmaier-Roberts simulation showing the evolution of the magnetic dipole (outside the core) in terms of its South-pole trajectory (in an equal-area projection with the North geographic pole at the top), its pole latitude, and its dipole moment. The South magnetic pole of the dipole is plotted once per 100 years and the dipole moment is in units of 10^{22} A m^2. From Glatzmaier *et al.*, 1999, with permission.

as in the palaeomagnetic reversal records, the dipole moment decreases significantly during reversals. The frequency of reversals and their durations in this simulation also compare well with those of the Earth. It is tempting to regard a field reversal as just another fluctuation (albeit a large one) of a system driven so strongly that it varies stochastically on all scales. The second panel of Fig. 14 makes this view hard to defend. The level of secular variation both before and after the reversal is extremely low, but is quite typical of the model at all times. A reversal occurs like a "bolt from the blue."

During the first reversal, the field reversed inside the tangent cylinder about a thousand years before it did so outside, but during the next two reversals the opposite sequence occurred. That is, when viewed from the Earth's surface, the field would appear to have completed the reversal a thousand years or so before it actually reverses deep within the core (Glatzmaier *et al.*, 1999). The four snapshots in Fig. 15 illustrate how the radial component of the field at the surface and the axisymmetric part of the field throughout the core change during a typical reversal.

Occasional, spontaneous dipole reversals have also occurred in recent modal calculations (Sarson and Jones, 1999; Sarson, 2000) and in other 3D simulations (Kagayama *et al.*, 1999); they differ in details, as they surely have in all past geomagnetic reversals. The reversals seen in the modal calculations are associated with fluctuations in the (axisymmetric) meridional circulation, possibly due to buoyancy surges originating near the inner core boundary. It is not clear, however, what triggers what, since buoyancy surges continually occur in these simulations, and the fluctuations in the meridional circulation sometimes appear after the magnetic dipole begins to decrease. We also see changes in the structure of the meridional circulation $\mathbf{V}_p$ during reversals, but these usually occur after the dipole begins to lose intensity.

Some of the fluctuations continually occurring in the Glatzmaier-Roberts simulations are strong enough to produce a field that is locally of the opposite polarity. Only once in many attempts does one survive long enough to challenge the original polarity seriously. In some of these cases the field reverses outside the tangent cylinder but not inside it. Then, instead of a complete reversal, the field outside the tangent cylinder quickly reverses back to its original polarity (Glatzmaier *et al.*, 1999). This may provide an explanation of cryptochrons (Sec. I.C). The modal calculations of Sarson (2000) also show a tendency for the surface field to reverse more frequently than the entire field inside the core.

The geomagnetic field has apparently been of constant dipole polarity during long "superchrons" (tens of millions of years). Since this is roughly the time scale for mantle convection (which is a million times slower than core convection), it has been suggested that changes in the thermal structure of the lowermost mantle (due to the accumulation of subducted lithospheric slabs) may influence the geodynamo; see Sec. II.C. The Glatzmaier-Roberts model has been used to test this hypothesis (Glatzmaier *et al.*, 1999). Eight cases were simulated, in each of which the total heat flow $\mathcal{Q}_{\mathrm{CMB}}$ from core to mantle was 7.2 TW. They differed only in the way that this heat flow was distributed over the CMB, i.e., in the choice of $I^q_{\mathrm{CMB}}(\theta,\phi)$. Spontaneous reversals occurred in all cases but one. The essence of the results was

(a) The westward drift is less disturbed when I^q_{CMB} is axisymmetric;

(b) When $I^q_{\mathrm{CMB}}(\theta)$ is unsymmetric with respect to the equatorial plane, reversals are frequent;

(c) When I^q_{CMB} is symmetric with respect to the equatorial plane $[I^q_{\mathrm{CMB}}(\theta)=I^q_{\mathrm{CMB}}(\pi-\theta)]$, and when I^q_{CMB} is greater in the polar regions than in the equatorial regions (rather than the reverse), the periods of constant polarity are longer, the duration of reversals (when they occur) is shorter, and the reversals are between states in which the field has a greater intensity and a weaker secular variation.

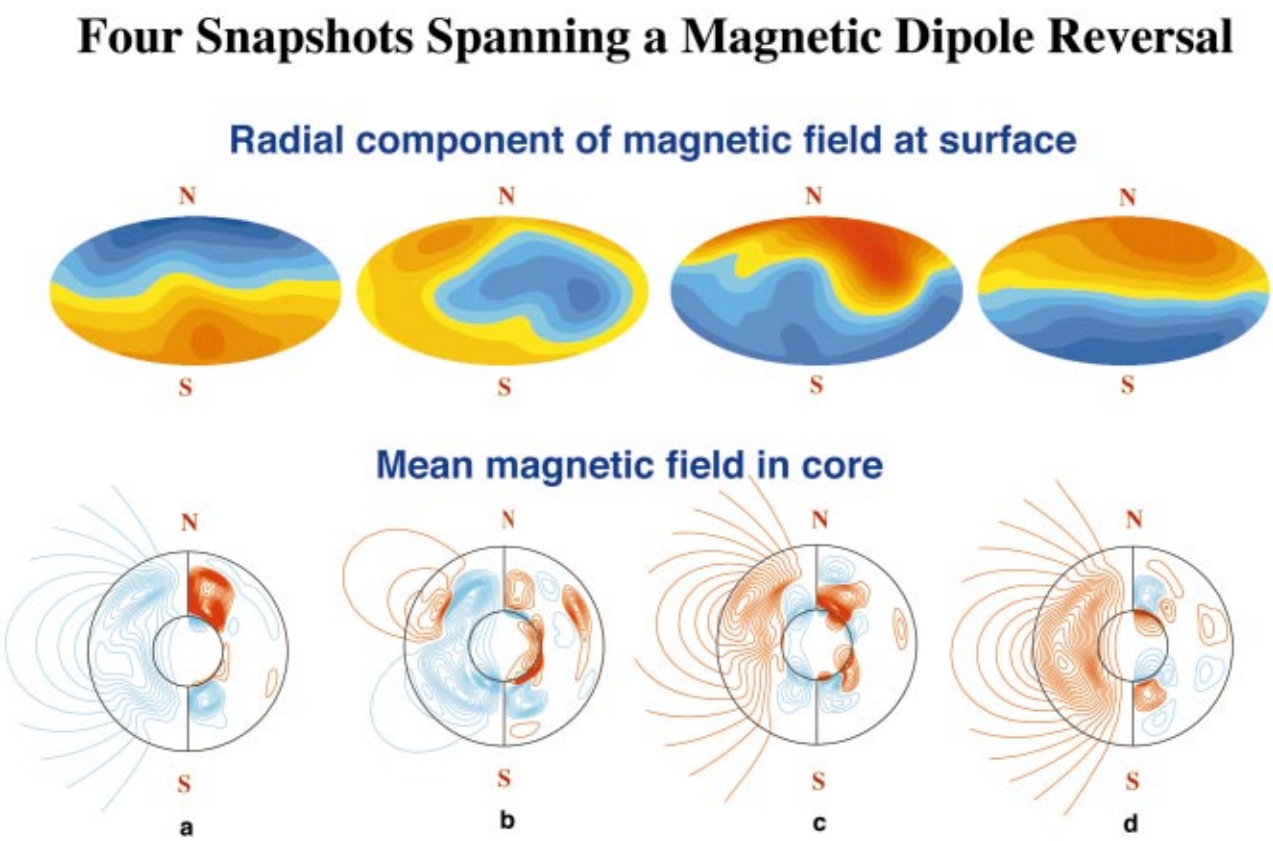

FIG. 15. Four snapshots from the Glatzmaier-Roberts simulation spanning a magnetic reversal. The top row shows the radial component of the field (red directed outward and blue inward) plotted at the surface of the model Earth. The bottom row shows the longitudinally averaged field through the core at the same times. Poloidal field is illustrated as lines of force on the left of each image; blue is clockwise directed and yellow is counter-clockwise directed. On the right of each image are contours of toroidal field; red is eastward and blue is westward. The outer circle is the core-mantle boundary; the inner circle is the inner core boundary. From Glatzmaier *et al.*, 1999, with permission [Color].

Conditions (c) promote the rise of buoyant fluid in the tangent cylinder and therefore a strong, stable, thermal wind therein. Prescribed $I^q_{\mathrm{CMB}}(\theta,\phi)$ that are less compatible with this favored dynamics seem to spawn more successful fluctuations that enhance the secular variation of the field and its reversal frequency.

VII. THE FUTURE

This final section is devoted to some contentious issues and to some unresolved matters that hopefully will be targets for future research.

A. Turbulence, diffusion, and hyperdiffusion

From a numerical point of view, the necessity for eddy diffusivities of heat, composition, and momentum represents a failure to resolve the solution adequately. If one could gradually improve the resolution, one would also gradually diminish the assumed eddy diffusivities until, when the microscale $\mathcal{L}^t$ mainly responsible for the diffusion of the macroscale fields was reached, it would no longer be necessary to invoke turbulent diffusivities at all. Braginsky and Roberts (1995) estimate that $\mathcal{L}^t$ ~ 2 km and, since the currently attainable resolution is very much coarser than this, turbulent diffusivities are a practical necessity.

It is hard to estimate the eddy diffusivities κ^t and ν^t. In addition to the heuristic approach of Braginsky and Meytlis (1990), two methods have been tried: direct numerical simulation and closure approximation. In the former, the microscale fields are solved in isolation in a small volume of the core, the macroscale fields being specified; κ^t is estimated from the statistics of the solution. See, for example, Matsushima *et al.* (1999). In the second approach, the equations governing the microscale fields ξ^t_c, S^t_c, $\mathbf{V}^t$, etc. are simplified and solved using a (possibly drastic) closure approximation, and the mean fluxes $\langle \xi^t_c \mathbf{V}^t \rangle$, $\langle S^t_c \mathbf{V}^t \rangle$, $\langle \mathbf{V}^t \mathbf{V}^t \rangle$, etc. are evaluated in terms of the macroscale fields, as described in Sec. IV.D. The resulting estimates of κ^t and ν^t are, however, no better than the closure approximation used to obtain them.

In the absence of reliable estimates of κ^t and ν^t, the usual expedient is to suppose that all diffusivities, whether for scalar or for vector fields, are the same or are comparable. Most simulations of convective dynamos are of this "equidiffusional" type, but their diffu-

sivities are many orders of magnitude greater than $\eta = 2\,\mathrm{m^2\,s^{-1}}$, so that their Ekman numbers E (viscous, thermal, and magnetic) are typically 10^{-3}–10^{-4}, rather than 5×10^{-9}. The Kuang-Bloxham model is equidiffusional, all diffusivities being (for the large scales) about $1.5\times10^{4}\,\mathrm{m^2\,s^{-1}}$, so that $E\approx4\times10^{-5}$. All diffusion time scales are therefore at least 7500 times too short relative to the rotation period of the Earth. An alternative way of describing this choice of parameters (J. Bloxham, private communication) is to say that all diffusivities are 2 $\mathrm{m^2\,s^{-1}}$ but that the accelerations experienced by the fluid outer core (and solid inner core) are artificially damped by 7500 and that the viscous forces are artificially enhanced by the same factor. In effect, Kuang and Bloxham have increased all their Ekman numbers from 5×10^{-9} to 4×10^{-5}. However, they have shown (W. Kuang, private communication and Kuang, 1999) that their viscous and inertial terms are at least an order of magnitude smaller than the Coriolis, Lorentz, and buoyancy forces (outside the boundary layers). They therefore claim that the momentum balance has not been seriously disturbed, especially since only the axisymmetric parts of the inertial terms are retained in their model. In the Glatzmaier-Roberts model, κ^t and η are both set to 2 $\mathrm{m^2\,s^{-1}}$, so the thermal and magnetic Ekman numbers are 5×10^{-9} (for the large scales). However, to resolve the Ekman boundary layers (Sec. V.B), a much larger value for ν^t, $1500\,\mathrm{m^2\,s^{-1}}$, is used.

The phrase "for the large scales" was used twice in the last paragraph. This was because the choices of diffusivities made there do not overcome the numerical difficulties faced by Earth-like simulations. With one exception, these have all required additional "hyperdiffusion," i.e., diffusivities that increase with decreasing length scale. Hyperdiffusivity allows the large (global) length scales to experience appropriately little diffusion (i.e., to be more Earth-like) and evades the small scales that would otherwise have to be numerically resolved. Solutions with hyperdiffusion appear to be somewhat more Earth-like than those that avoid hyperdiffusion by uniformly increasing the diffusivities on all scales while retaining the same numerical resolution. This may be because the total amount of diffusion is much less. The magnitude and wave-number dependence of hyperdiffusion has, however, so far been quite arbitrary, and the resulting energy spectra may be significantly different from those that would be obtained at a much higher spatial resolution using a smaller constant diffusivity. One can avoid hyperdiffusivity by drastically increasing the spatial resolution (Roberts and Glatzmaier, 2000), but such simulations are too expensive to integrate over long times and they still need an eddy viscosity that is almost three orders of magnitude larger than the other diffusivities.

The need to increase ν and to add hyperdiffusion has unfortunate repercussions on the energy arguments of Sec. II: $\mathcal{Q}^\nu$ need no longer be small, and hyperdiffusion is not allowed for in the energy balance (2.3). In a snapshot of the Glatzmaier-Roberts simulation, it was found that $\mathcal{Q}^J\approx0.3$ TW, $\mathcal{Q}^t\approx0.1$ TW, and $\mathcal{Q}^\nu\approx0.7$ TW, but $\mathcal{Q}^D$ should be approximately 2.1 TW according to Sec. II.C. The 1-TW discrepancy seems rather too large to be explained as a fluctuation and is more probably the result of the hyperdiffusion.

Two further difficulties should be mentioned. Suppose that, as argued by Braginsky (1999), there is a stable layer (an inverted "ocean") at the top of the core. How should it be simulated numerically? Recall that the energy dissipated by the turbulence is directly supplied by buoyancy forces; see Eq. (4.44). Clearly, by the second law, q^t must be positive, but, when the density distribution is bottom heavy, i.e., when the CO density C increases downwards, q^t is negative, according to Eq. (4.44). This represents a breakdown in local theory and of the *Ansätze* (4.48) and (4.50). This breakdown is not surprising: if turbulence is driven only by a locally top-heavy density distribution, it cannot arise when the distribution is locally bottom heavy. If there is turbulence in a stable layer, its cause must be different, such as baroclinic instability, or the overshoot of turbulence from an adjacent unstable layer. So far, no serious effort has been made to find a substitute for the *Ansätze* (4.48) and (4.50) inside the stable layer, and we can only hope that the ocean proves to be either nonexistent or unimportant in core MHD.

Second, we took the Reynolds analogy too far in Sec. IV.D when we assumed that, as for molecular motions, the microscale velocities are completely chaotic, and in particular have no preferred direction. Because of the effects of the Coriolis and Lorentz forces, core turbulence is expected to be highly anisotropic, the convective eddies being elongated in the directions of $\mathbf{\Omega}$ and $\mathbf{B}$; see Braginsky (1964d), Braginsky and Meytlis (1990), Braginsky and Roberts (1995), and St. Pierre (1996). This means that turbulent transport should also be enhanced in these directions, so that the isotropic laws (4.48) and (4.50) should be replaced by

$$\mathbf{I}^\xi = -\rho\overleftrightarrow{\boldsymbol{\kappa}}\cdot\boldsymbol{\nabla}\xi_c\,, \tag{7.1}$$

$$\mathbf{I}^S = -\rho\overleftrightarrow{\boldsymbol{\kappa}}\cdot\boldsymbol{\nabla}S_c\,, \tag{7.2}$$

where the diffusivity, now the tensor $\overleftrightarrow{\boldsymbol{\kappa}}$, is as before the same for ξ_c as for S_c.

Anisotropy considerably complicates momentum transfer. In principle a fourth-rank tensor $\overleftrightarrow{\boldsymbol{\nu}}$ substitutes for the scalar ν, and Eq. (4.55) is replaced by

$$\pi^\nu_{ij} = \rho\,\nu_{ijkl}e_{kl}\,. \tag{7.3}$$

Since $e_{ij}=e_{ji}$, the symmetries $\nu_{jikl}=\nu_{ijlk}=\nu_{ijkl}$ can be assumed, and the requirement $q^\nu\equiv e_{ij}\nu_{ijkl}e_{kl}\geqslant0$ of positive entropy production demands a further reduction to "only" 21 independent components that have to be estimated. There is an added complication: turbulent transport of vector fields, such as magnetic field or momentum, introduces more than simple diffusion. For example (Sec. III.C), in addition to a contribution $\eta^t\boldsymbol{\nabla}\times\mathbf{B}$ to the turbulent emf $\boldsymbol{\mathcal{F}}$, the α effect introduces a term $\alpha\mathbf{B}$, proportional to the macroscale $\mathbf{B}$ and not to its gradient. In an analogous way, studies of turbulence in the

Sun have led to the recognition of the "Λ effect" (aka the "AKA effect," standing for anisotropic kinetic alpha effect), in which

$$\pi_{ij}^{\nu} = \rho \Lambda_{ijk} \omega_k , \tag{7.4}$$

where $\boldsymbol{\omega} = \nabla \times \mathbf{V}$ is the local macroscale vorticity; see Chap. 4 of Rüdiger (1989). When this operates, as it does in solar convection, the macroscale flow cannot be solid-body rotation.

The importance of these tensor diffusivities in computer simulations of the geodynamo again depends on the spatial resolution one can afford. Presumably the more modes that are numerically resolved, the less important are the details of the transport by the remaining modes until, when the resolved part of the spectrum contains most of the energy, all anisotropic turbulent transport will be adequately represented. Until that day arrives, one can hope that, since $Ro \ll 1$, turbulent momentum transport is not significant in the core, except in boundary layers and possibly near the tangent cylinder. If so, it may not be necessary to apply the *Ansätze* (7.3) and (7.4). It is doubtful whether the *Ansätze* (7.1) and (7.2) can be similarly ignored, but so far no numerical simulations have taken them into account.

B. Boundary conditions

Away from boundaries, the eddy viscosity plays a minor role in both the Glatzmaier-Roberts and the Kuang-Bloxham models, but it is still orders of magnitude greater than what one wants. The Ekman layers on the core-mantle and inner core boundaries present the dynamo theorist with something of a dilemma. On the one hand, if he takes ν to be the molecular viscosity ν_M, he finds that δ_ν is only about 10 cm and that the pumping velocities $E^{1/2}\overline{\mathcal{U}}$ are only about $10^{-10}\,\mathrm{m\,s^{-1}}$; see Sec. V.B. He may find it hard to believe that these can be significant, and he may agree with Kuang and Bloxham (1999) that they should be ignored, and the no-slip conditions (4.59) and (4.60) replaced by the conditions that the tangential components $\pi_{r\theta}^{\nu}$ and $\pi_{r\phi}^{\nu}$ of viscous stress vanish—the so-called *viscous stress-free conditions*.

On the other hand, such a step would remove the Ekman layers that are responsible for spin-up (Sec. V.B) and for helping to create an α effect. Moreover, the use of ν_M in computing the Ekman pumping is questionable. The Ekman layers observed in the upper layers of the ocean are described by a turbulent viscosity about three orders of magnitude greater than the molecular viscosity of seawater (Hunkins, 1966). This suggests that we should similarly describe the Ekman layers in the core with the turbulent viscosity $\nu^t \approx 2\ \mathrm{m^2\,s^{-1}}$, leading to $\delta_\nu \approx 160$ m and a spin-up time τ_{su} of only about 9 yr (Sec. V.B); the viscous coupling between the fluid and its boundaries is especially potent for the geostrophic part of $\mathbf{V}$. In contrast, the viscous stress-free conditions give $\tau_{\mathrm{su}} = \infty$, and only magnetic, topographic, and gravitational torques can couple the fluid to its boundaries. This suggests that use of the viscous stress-free conditions in place of the no-slip conditions is a more serious step than one might intuitively have suspected.

No-slip conditions were used in the Glatzmaier-Roberts simulations mainly for consistency: since the transport of momentum by the unresolved eddies is included within the fluid, why ignore the stronger coupling between the fluid and the solid boundaries? Nevertheless, the eddy viscous torque on the boundaries of the Glatzmaier-Roberts simulations is too large, so the other extreme of eliminating it totally, as in the Kuang-Bloxham model, is certainly worth investigating. Test runs with the Glatzmaier-Roberts model with zero viscous torque on the boundaries produced, as in the Kuang-Bloxham solution, a smaller inner core superrotation rate and less magnetic-field generation near the inner core boundary.

A comparison of the magnetic fields generated in the Kuang-Bloxham simulation and those in the current Glatzmaier-Roberts solution (with no-slip boundaries) is made in Fig. 16. Snapshots of the radial component of the generated fields, plotted at the CMB, and the axisymmetric parts of the fields, plotted throughout the core, are displayed. Both solutions produce dipole-dominated magnetic fields at the CMB. The lower diffusion and higher resolution of the current Glatzmaier-Roberts model, however, produces a solution with a more prominent small-scale magnetic structure and a more distinct tangent cylinder effect. The zonal field is mainly confined to the interior of the tangent cylinder, whereas the meridional field is mainly outside it. The Kuang-Bloxham solution and the original (low-resolution) Glatzmaier-Roberts solution are dominated by larger-scale structures.

C. The road ahead

It will be apparent to all readers who have had the stamina to read this review through that geodynamo theory already explains, at least qualitatively, virtually every known facet of the geomagnetic field described in Sec. I.C. They will also recognize that this is remarkable in view of the approximations and uncertainties currently inherent in the theory, some more of which are adumbrated below.

First, most of the physical parameters on which simulations rely are uncertain to a greater or lesser extent, especially the strength of the radioactive heat sources in the core, the heat flow from the core to the mantle, the latent heat of crystallization of core fluid, and the depression of its freezing point by alloying. This is hardly surprising when we recall that the principal alloying element in the core is still unknown and is likely to remain so for some time to come. Interesting issues are raised by the apparent youth of the solid inner core. According to the simulation of Glatzmaier and Roberts, $\overline{\tau} \approx 1.3$ Gyr, and this is not very different from other recent

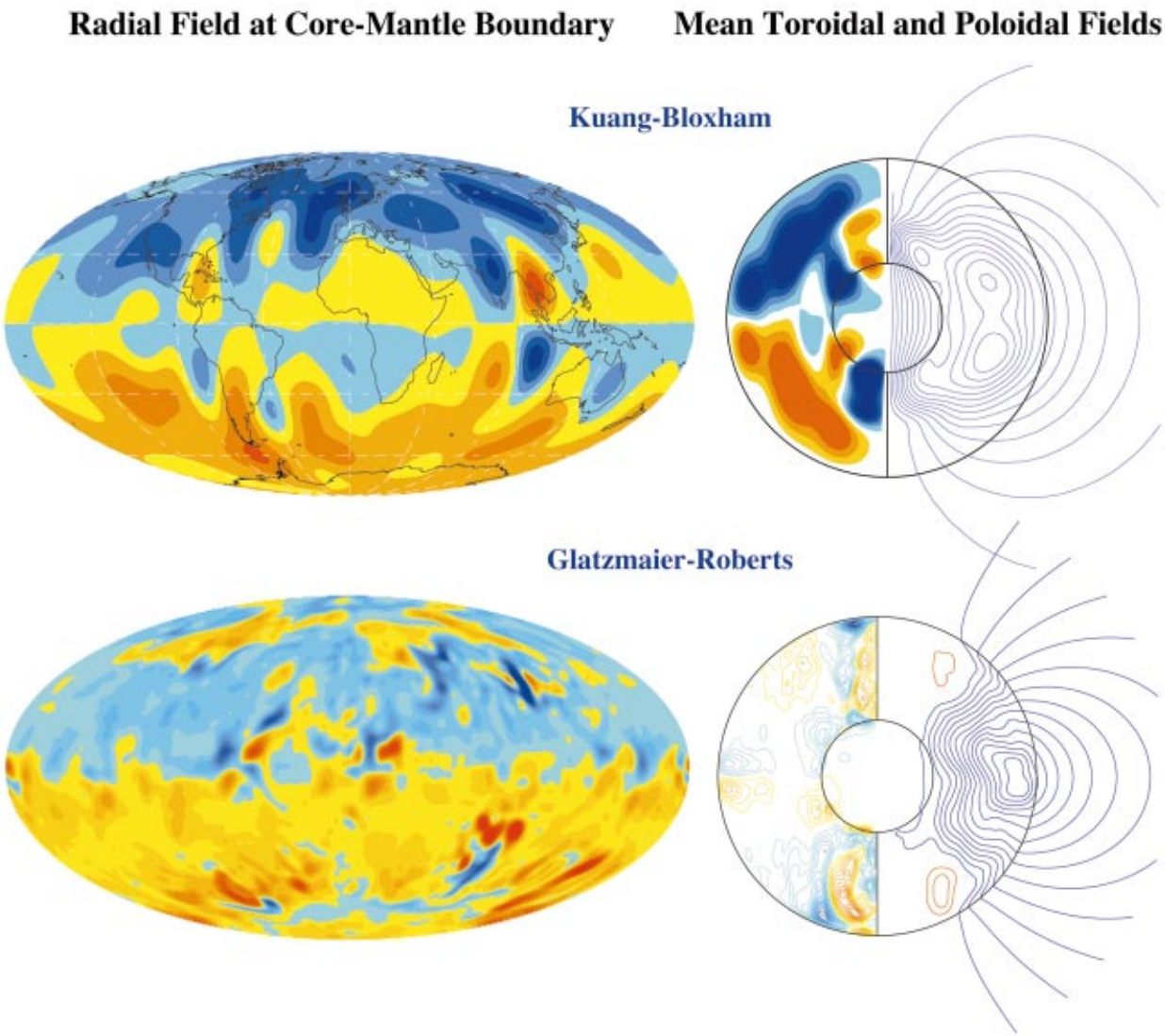

FIG. 16. Snapshots of the radial component of the magnetic field at the core-mantle boundary (in equal-area projections with red outward and blue inward) and the longitudinally averaged field throughout the core (with toroidal field contours on the left and poloidal field lines of force on the right of each image). The top row is from the Kuang-Bloxham simulation and the bottom row is from the Glatzmaier-Roberts simulation [Color].

estimates.[36] The age of the geomagnetic field exceeds 3 Gyr, however (Sec. I.C). A dynamo can certainly operate in a completely fluid core (Sakuraba and Kono, 1999), but one might have expected it to produce a qualitatively different, and perhaps weaker, magnetic field than the one observed today. Even if we took $\mathcal{Q}^D=0$, we would, if we insisted that $\mathcal{Q}^R=0$, find from Sec. III.C that $\overline{\tau}$ is only 3.7 Gyr. Moreover, $\mathcal{Q}^D=0$ is unreasonable since the convection that is needed to maintain the adiabatic state of the core must dissipate energy (and, if there is no magnetic field, this involves a very large viscous dissipation; see Sec. V.C). Is it really true that the SIC is much younger than the Earth? Or is $\mathcal{Q}^R$ significantly nonzero? Or are some of our other parameter estimates wide of the mark?

Second, spectral transform methods are currently used by virtually every modeler. Despite their many virtues, it is hard to attain the numerical resolution necessary to represent solutions in such a lightly diffused system as the core; large eddy diffusivities have to be used. Presumably, as computer technology advances and becomes cheaper, resolution will improve and smaller diffusivities will become practical. Eventually, at some time in the remote future, it will be possible to construct models using only molecular diffusivities. In the meantime, how is progress to be maintained? One possibility is to continue to parametrize the effects of the turbulent microscales on the global macroscales and to hope that

[36]Stevenson *et al.* (1983) found that $\overline{\tau}\approx 2.3$ Gyr, Buffett *et al.* (1996) that $\overline{\tau}\approx 2.8$ Gyr, and Labrosse *et al.* (1997) that $\overline{\tau}\approx 1.7$ Gyr. These authors modeled the thermal history of the Earth globally and did not set up a theory on which a detailed model could be constructed. Consequently, they omitted the turbulent dissipation, which, following Braginsky and Roberts (1995), is included by Glatzmaier and Roberts.

advances in turbulence theory will lead to improved parametrizations. A second method, currently favored by several new groups, is to use very different numerical methods that are more suitable for lightly damped systems and are more readily applied in parallel computation than spectral transform methods. Some exploratory work has already been done in this direction, but only for 2D mean-field models (Braginsky and Roberts, 1994; Jault, 1995).

Improved numerical techniques should help answer other puzzles, such as the roles of Taylor's constraint and model z in geodynamo theory (Sec. V.D). Current Earth-like models cannot provide an unequivocal answer because their Ekman numbers E are too large, but the question has been given increasing attention over the past decade through the integration of 2D mean-field models. It appears that some models are Taylor-like, some have a model-z character, while others are of neither type; see Hollerbach (1996a).

The effect of adding new physical ingredients should be investigated. For example (Sec. II.A), the effects of the luni-solar precession of the Earth's mantle needs to be studied with 3D geodynamo simulations.

Finally, models similar to the geodynamo models reviewed here form a basis for the study of dynamos in other planets and satellites in our solar system and in planets now being discovered around other stars, and we may expect new research in this direction also.

Geodynamo simulations have made giant strides during the past decade and, with more players joining this exciting activity every year and with ever increasing computer capabilities, we are confident that many of the outstanding issues will be resolved during the first decade of the new millennium.

ACKNOWLEDGMENTS

We thank Robert Coe and David Loper for their criticisms of a draft of this review, and Weijia Kuang for supplying half of Fig. 16, and for his comments on parts of Sec. VII. We thank Maureen Roberts for producing Figs. 1, 6, 7, and 8. Our work on the geodynamo is supported by the Institute of Geophysics and Planetary Physics, the Los Alamos LDRD Program, by the University of California Research Partnership Initiatives Program, by the NSF Geophysics Program, and by the NASA HPCC/ESS Grand Challenge Program. Computing resources were provided by the NPACI, NCSA, GSFC, and the Los Alamos ACL supercomputing centers.

REFERENCES

Acheson, D. J., 1972, "On the hydromagnetic stability of a rotating fluid annulus," J. Fluid Mech. **52**, 529–541.

Acheson, D. J., and R. Hide, 1973, "Hydromagnetics of rotating fluids," Rep. Prog. Phys. **36**, 159–221.

Bender, C. M., and S. A. Orszag, 1978, *Advanced Mathematical Methods for Scientists and Engineers* (McGraw-Hill, New York).

Birch, F., 1952, "Elasticity and constitution of the Earth's interior," J. Geophys. Res. **57**, 227–286.

Blackett, P. M. S., 1947, "The magnetic field of massive rotating bodies," Nature (London) **159**, 658–666.

Braginsky, S. I., 1963, "Structure of the F layer and reasons for convection in earth's core," Dokl. Akad. Nauk SSSR **149**, 1311–1314 [Sov. Phys. Dokl. **149**, 8–10 (1963)].

Braginsky, S. I., 1964a, "Self-excitation of a magnetic field during the motion of a highly conducting fluid," Zh. Eksp. Teor. Fiz. SSSR **47**, 1084–1098 [Sov. Phys. JETP **20**, 726–735].

Braginsky, S. I., 1964b, "Theory of the hydromagnetic dynamo," Zh Eksp. Teor. Fiz. SSSR **47**, 2178–2193 [Sov. Phys. JETP **20**, 1462–1471 (1965)].

Braginsky, S. I., 1964c, "Kinematic models of the Earth's hydromagnetic dynamo," Geomagn. Aeron. (Russia) **4**, 732–747 [Geomagn. Aeron. (USA) **4**, 572–583 (1964)].

Braginsky, S. I., 1964d, "Magnetohydrodynamics of the Earth's core," Geomagn. Aeron. (Russia) **4**, 898–916 [Geomagn. Aeron. (USA) **4**, 698–712 (1964)].

Braginsky, S. I., 1967, "Magnetic waves in the Earth's core," Geomagn. Aeron. (Russia) **7**, 1050–1060 [Geomagn. Aeron. (USA) **7**, 851–859 (1967)].

Braginsky, S. I., 1970, "Torsional magnetohydrodynamic vibrations in the Earth's core and variations in day length," Geomagn. Aeron. (Russia) **10**, 3–12 [Geomagn. Aeron. (USA) **10**, 1–8 (1970)].

Braginsky, S. I., 1975, "Nearly axially symmetric model of the hydromagnetic dynamo of the Earth, I," Geomagn. Aeron. (Russia) **15**, 149–156 [Geomagn. Aeron. (USA) **15**, 122–128 (1975)].

Braginsky, S. I., 1978, "Nearly axially symmetric model of the hydromagnetic dynamo of the Earth," Geomagn. Aeron. (Russia) **18**, 340–351 [Geomagn. Aeron. (USA) **18**, 225–231 (1978)].

Braginsky, S. I., 1999, "Dynamics of the stably stratified ocean at the top of the core," Phys. Earth Planet. Inter. **111**, 21–34.

Braginsky, S. I., and V. P. Meytlis, 1990, "Local turbulence in the Earth's core," Geophys. Astrophys. Fluid Dyn. **55**, 71–87.

Braginsky, S. I., and P. H. Roberts, 1994, "From Taylor state to model-z," Geophys. Astrophys. Fluid Dyn. **77**, 3–13.

Braginsky, S. I., and P. H. Roberts, 1995, "Equations governing Earth's core and the geodynamo," Geophys. Astrophys. Fluid Dyn. **79**, 1–97.

Braginsky, S. I., and P. H. Roberts, 2000, in *Advances in Nonlinear Dynamos*, edited by A. Ferriz Mas and M. Nuñez (Gordon and Breach, London).

Brandenburg, A., A. Nordland, P. Pulkkinen, R. F. Stein, and I. Tuominen, 1990, "Simulation of turbulent cyclonic magneto-convection," Astron. Astrophys. **232**, 277–291.

Buffett, B. A., 1996, "A mechanism for decade fluctuations in the length of day," Geophys. Res. Lett. **23**, 3803–3806.

Buffett, B. A., 1997, "Geodynamic estimates of the viscosity of the Earth's inner core," Nature (London) **388**, 571–573.

Buffett, B. A., and G. A. Glatzmaier, 2000, "Gravitational breaking of inner-core rotation in geodynamo simulations," Geophys. Res. Lett., in press.

Buffett, B. A., H. E. Huppert, J. R. Lister, and A. W. Woods, 1996, "On the thermal evolution of the Earth's core," J. Geophys. Res. **101**, 7989–8006.

Bullard, E. C., 1949, "The magnetic field within the earth," Proc. R. Soc. London, Ser. A **197**, 433–453.

Busse, F. H., 1970, "Thermal instability in rapidly rotating systems," J. Fluid Mech. **44**, 441–460.

Busse, F. H., 1975, "A model of the geodynamo," Geophys. J. R. Astron. Soc. **42**, 437–459.
Busse, F. H., 2000, "Homogeneous dynamos in planetary cores and in the laboratory," Annu. Rev. Fluid Mech. **32**, 383–408.
Busse, F. H., E. Grote, and A. Tilgner, 1998, "On convection driven dynamos in rotating spherical shells," Stud. Geophys. Geod. **42**, 1–6.
Chabot, N. L., and M. J. Drake, 1999, "Potassium solubility in metal: The effects of composition at 15 kbar and 1900° on partitioning between iron alloys and silicate melts," Earth Planet. Sci. Lett. **172**, 323–335.
Childress, S., and A. D. Gilbert, 1995, *Stretch, Twist, Fold: The Fast Dynamo* (Springer, Berlin).
Childress, S., and A. M. Soward, 1972, "Convection-driven hydromagnetic dynamo," Phys. Rev. Lett. **29**, 837–839.
Christensen, U., P. Olson, and G. A. Glatzmaier, 1998, "A dynamo model interpretation of geomagnetic field structures," Geophys. Res. Lett. **25**, 1565–1568.
Christensen, U., P. Olson, and G. A. Glatzmaier, 1999, "Numerical modeling of the geodynamo: A systematic parameter study," Geophys. J. Int. **138**, 393–409.
Cowling, T. G., 1933, "The magnetic field of sunspots," Mon. Not. R. Astron. Soc. **140**, 39–48.
Creager, K., 1997, "Inner core rotation rate from small scale heterogeneity and time-varying travel times," Science **278**, 1284–1288.
de Wijs, G. A., G. Kresse, L. Vočadlo, D. Dobson, A. Alfè, M. J. Gillan, and G. D. Price, 1998, "The viscosity of liquid iron at the physical conditions of the Earth's core," Nature (London) **392**, 805–807.
Dudley, M. L., and R. W. James, 1989, "Time-dependent kinematic dynamos with stationary flows," Proc. R. Soc. London, Ser. A **425**, 407–429.
Dziewonski, A. M., and D. L. Anderson, 1981, "Preliminary reference Earth model," Phys. Earth Planet. Inter. **25**, 297–356.
Elsasser, W. M., 1946, "Induction effects in terrestrial magnetism. Part II. The secular variation," Phys. Rev. **70**, 202–212.
Fautrelle, Y., and S. Childress, 1982, "Convective dynamos with intermediate and strong fields," Geophys. Astrophys. Fluid Dyn. **22**, 235–279.
Fearn, D. R., 1998, "Hydromagnetic flow in planetary cores," Rep. Prog. Phys. **61**, 175–235.
Fearn, D. R., and M. R. E. Proctor, 1987, "On the computation of steady, self-consistent spherical dynamos," Geophys. Astrophys. Fluid Dyn. **38**, 293–325.
Fowler, T. K., 1999, "Nuclear power—fusion," Rev. Mod. Phys. **71**, S456–459.
Gailitis, A., 1993, "Magnetic field generation by the axisymmetric conducting fluid flow in a spherical cavity of a stationary conductor," Magn. Gidrodin. **29**, 3–14 [Magnetohydrodynamics **29**, 107–115 (1993)].
Gailitis, A., O. Lielausis, S. Dementev, E. Platacis, A. Cifersons, G. Gerbeth, T. Gundrum, F. Stefani, M. Christen, H. Hänel, and G. Will, 2000, "Detection of a flow induced magnetic field eigenmode in the Riga dynamo facility," Phys. Rev. Lett. **84**, 4365–4368.
Gill, A. E., 1982, *Atmosphere-Ocean Dynamics* (Academic, New York).
Gilman, P. A., 1983, "Dynamically consistent nonlinear dynamos driven by convection in a rotating spherical shell. II. Dynamos with cycles and strong feedbacks," Astrophys. J., Suppl. Ser. **53**, 243–268.
Gilman, P. A., and J. Miller, 1981, "Dynamically consistent nonlinear dynamos driven by convection in a rotating spherical shell," Astrophys. J., Suppl. Ser. **46**, 211–238.
Gire, C., J.-L. Le Mouël, and J. Ducruix, 1983, "Evolution of the secular variation field from the beginning of the century," Nature (London) **307**, 349–352.
Glatzmaier, G. A., 1984, "Numerical simulations of stellar convective dynamos. I. The model and the method," J. Comput. Phys. **55**, 461–484.
Glatzmaier, G. A., 1985a, "Numerical simulations of stellar convective dynamos. II. Field propagation in the convection zone," Astrophys. J. **291**, 300–307.
Glatzmaier, G. A., 1985b, "Numerical simulations of stellar convective dynamos. III. At the bottom of the convection zone," Geophys. Astrophys. Fluid Dyn. **31**, 137–150.
Glatzmaier, G. A., R. S. Coe, L. Hongre, and P. H. Roberts, 1999, "The role of the Earth's mantle in controlling the frequency of geomagnetic reversals," Nature (London) **401**, 885–890.
Glatzmaier, G. A., and P. H. Roberts, 1995a, "A three-dimensional convective dynamo solution with rotating and finitely conducting inner core and mantle," Phys. Earth Planet. Inter. **91**, 63–75.
Glatzmaier, G. A., and P. H. Roberts, 1995b, "A three-dimensional self-consistent computer simulation of a geomagnetic field reversal," Nature (London) **377**, 203–209.
Glatzmaier, G. A., and P. H. Roberts, 1996a, "An anelastic evolutionary geodynamo simulation driven by compositional and thermal convection," Physica D **97**, 81–94.
Glatzmaier, G. A., and P. H. Roberts, 1996b, "Rotation and magnetism of Earth's inner core," Science **274**, 1887–1891.
Glatzmaier, G. A., and P. H. Roberts, 1997, "Simulating the geodynamo," Contemp. Phys. **38**, 269–288.
Glatzmaier, G. A., and P. H. Roberts, 1998, "Dynamo theory then and now," Int. J. Eng. Sci. **36**, 1325–1338.
Greenspan, H. P., 1968, *The Theory of Rotating Fluids* (Cambridge University, Cambridge, England).
Grote, E., F. H. Busse, and A. Tilgner, 1999, "Convection-driven quadrupolar dynamos in rotating spherical shells," Phys. Rev. E **60**, R5025–R5028.
Grote, E., F. H. Busse, and A. Tilgner, 2000, "Regular and chaotic spherical dynamos," Phys. Earth Planet. Inter. **117**, 259–272.
Gubbins, D., and P. H. Roberts, 1987, in *Geomagnetism*, **2**, edited by J. A. Jacobs (Academic, London, England), pp. 1–183.
Hide, R., 1966, "Free oscillations of the Earth's core and the theory of the geomagnetic secular variation," Philos. Trans. R. Soc. London, Ser. A **259**, 615–647.
Hide, R., 1978, "How to locate the electrically conducting fluid core of a planet from external magnetic observation," Nature (London) **271**, 640–641.
Hide, R., and S. R. C. Malin, 1979, "The size of Jupiter's electrically conducting fluid core," Nature (London) **280**, 42–43.
Hide, R., and S. R. C. Malin, 1981, "On the determination of the size of the Earth's core from observations of the geomagnetic secular variation," Proc. R. Soc. London, Ser. A **374**, 15–33.
Hollerbach, R., 1994, "Magnetohydrodynamic Ekman and Stewartson layers in a rotating spherical shell," Proc. R. Soc. London, Ser. A **444**, 333–346.
Hollerbach, R., 1996a, "On the theory of the geodynamo," Phys. Earth Planet. Inter. **98**, 163–185.

Hollerbach, R., 1996b, "Magnetohydrodynamic shear layers in a rapidly rotating plane layer," Geophys. Astrophys. Fluid Dyn. **82**, 237–253.

Hollerbach, R., and C. A. Jones, 1993, "Influence of the Earth's core on geomagnetic fluctuations and reversals," Nature (London) **365**, 541–543.

Hughes, D. W., 1993, in *Solar and Planetary Dynamos*, edited by M. R. E. Proctor, P. C. Matthews, and A. M. Rucklidge (Cambridge University, Cambridge, England), pp. 153–159.

Hunkins, K., 1966, "Ekman drift currents in the Arctic Ocean," Deep-Sea Res. **13**, 607–620.

Ivers, D. J., and R. W. James, 1984, "Axisymmetric antidynamo theorems in compressible non-uniform conducting fluids," Philos. Trans. R. Soc. London, Ser. A **312**, 179–218.

Jacobs, J. A., 1953, "The Earth's inner core," Nature (London) **172**, 297–300.

Jackson, A., J. Bloxham, and D. Gubbins, 1993, in *Dynamics of Earth's Deep Interior and Earth Rotation*, edited by J.-L. Le Mouël, D. E. Smylie, and T. Herring, Geophys. Mongr. Sec. No. 72, IUGG Vol. 12 (Am. Geophys. Union, Washington, D.C.), p. 97.

Jault, D., 1995, "Model z by computation and Taylor's condition," Geophys. Astrophys. Fluid Dyn. **79**, 99–124.

Jault, D., G. Gire, and J.-L. Le Mouël, 1988, "Westward drift, core motions and exchanges of angular momentum between core and mantle," Nature (London) **333**, 353–356.

Jones, C. A., A. W. Longbottom, and R. Hollerbach, 1995, "A self-consistent convection-driven geodynamo model, using a mean-field approximation," Phys. Earth Planet. Inter. **92**, 119–141.

Jones, C. A., and P. H. Roberts, 2000, "Convection-driven dynamos in a rotating plane layer," J. Fluid Mech. **404**, 311–343.

Jones, C. A., A. M. Soward, and A. I. Mussa, 2000, "The onset of thermal convection in a rapidly rotating sphere," J. Fluid Mech. **405**, 157–179.

Kabantsev, A. A., V. B. Reva, and V. G. Sokolov, 1999, "Experimental verification of the MHD dynamo in the axisymmetric linear machine," Fusion Technol. **35**, 185–189.

Kageyama, A., M. M. Ochi, and T. Sato, 1999, "Flip-flop transitions of the magnetic intensity and polarity reversals in the magnetohydrodynamic dynamo," Phys. Rev. Lett. **82**, 5409–5412.

Kageyama, A., and T. Sato, 1995, "Computer simulation of a magnetohydrodynamic dynamo II," Phys. Plasmas **2**, 1421–1431.

Kageyama, A., and T. Sato, 1997, "Generation mechanism of a dipole field by a magneto-hydrodynamic dynamo," Phys. Rev. E **55**, 4617–4626.

Kida, S., K. Araki, and H. Kitauchi, 1997, "Periodic reversals of magnetic field generated by thermal convection in a rotating spherical shell," J. Phys. Soc. Jpn. **66**, 2194–2201.

Kitauchi, H., and S. Kida, 1998, "Intensification of magnetic field by concentrate-and-stretch of magnetic flux lines," Phys. Fluids **10**, 457–468.

Kono, M., and H. Tanaka, 1995, in *The Earth's Central Part: Its Structure and Dynamics*, edited by T. Yukutake (Terrapub, Tokyo, Japan), pp. 75–94.

Krause, F., and K.-H. Rädler, 1980, *Mean-field Magnetohydrodynamics and Dynamo Theory* (Pergamon, Oxford, England).

Kuang, W., 1999, "Force balances and convective state in the Earth's core," Phys. Earth Planet. Inter. **116**, 65–79.

Kuang, W., and J. Bloxham, 1997, "An Earth-like numerical dynamo model," Nature (London) **389**, 371–374.

Kuang, W., and J. Bloxham, 1999, "Numerical modeling of magnetohydrodynamic convection in a rapidly rotating spherical shell: Weak and strong field dynamo action." J. Comput. Phys. **153**, 51–81.

Kutzner, C., and U. Christensen, 2000, "Effects of driving mechanisms in geodynamo models," Geophys. Res. Lett. **27**, 29–32.

Labrosse, S., J.-P. Poirier, and J.-L. Mouël, 1997, "On the cooling of Earth's core," Phys. Earth Planet. Inter. **99**, 1–17.

Landau, L. D., and E. M. Lifshitz, 1987, *Fluid Mechanics*, 2nd Edition (Pergamon, Oxford, England).

Langel, R. A., 1987, in *Geomagnetism*, Vol. I, edited by J. A. Jacobs (Academic, London), pp. 249–512.

Langel, R. A., and R. H. Estes, 1982, "A geomagnetic field spectrum," Geophys. Res. Lett. **9**, 250–253.

Langel, R. A., and R. H. Estes, 1985, "The near-Earth magnetic field at 1980 determined from MAGSAT data," J. Geophys. Res. **90**, 2495–2509.

Larmor, J., 1919, "How could a rotating body such as the Sun become a magnet?" Rep. Brit. Assoc. Adv. Sci. 159–160.

Le Mouël, J.-L., and V. Courtillot, 1981, "Core motions, electromagnetic core-mantle coupling and variations in earth's rotation: new constraints from geomagnetic secular variation impulses," Phys. Earth Planet. Inter. **24**, 236–241.

Le Mouël, J.-L., J. Ducruix, and C. H. Duyen, 1982, "The worldwide character of the 1969–1970 impulse of the secular variation rate," Phys. Earth Planet. Inter. **28**, 337–350.

Le Mouël, J.-L., T. R. Madden, J. Ducruix, and V. Courtillot, 1981, "Decade fluctuations in geomagnetic westward drift and earth rotation," Nature (London) **290**, 763–765.

Loper, D. E., 1970, "On the unsteady hydromagnetic perturbations at the Earth's core-mantle interface," Phys. Earth Planet. Inter. **4**, 129–137.

Loper, D. E., 1978, "The gravitationally powered dynamo," Geophys. J. R. Astron. Soc. **54**, 389–404.

Loper, D. E., and P. H. Roberts, 1981, "A study of conditions at the inner core boundary of the Earth," Phys. Earth Planet. Inter. **24**, 302–307.

Love, J. J., and D. Gubbins, 1996, "Optimized kinematic dynamos," Geophys. J. Int. **124**, 787–800.

Lund, S. P., G. Acton, B. Clement, M. Hastedt, M. Okada, and T. Williams, 1998, "Geomagnetic field excursions occurred often during the last million years," EOS Trans. Am. Geophys. Union **79**, 178–179.

Malkus, W. V. R., 1963, "Precessional torques as the cause of geomagnetism," J. Geophys. Res. **68**, 2871–2886.

Malkus, W. V. R., 1968, "Precession of the Earth as the cause of geomagnetism," Science **160**, 259–264.

Matsushima, M., T. Nakajima, and P. H. Roberts, 1999, "The anisotropy of local turbulence in the Earth's core," Earth Planets Space **51**, 277–286.

McElhinny, M. W., 1973, *Paleomagnetism and Plate Tectonics* (Cambridge University, Cambridge, England).

Meneguzzi, M., and A. Pouquet, 1989, "Turbulent dynamos driven by convection," J. Fluid Mech. **205**, 297–318.

Merrill, R. T., M. W. McElhinny, and P. L. McFadden, 1996, *The Magnetic Field of the Earth, Paleomagnetism, the Core and the Deep Mantle* (Academic, London).

Moffatt, H. K., 1969, "The degree of knottedness of tangled vortex lines," J. Fluid Mech. **35**, 117–129.

Moffatt, H. K., 1978, *Magnetic Field Generation in Electrically Conducting Fluids* (Cambridge University, Cambridge, England).

Monin, A. S., 1990, *Theoretical Geophysical Fluid Dynamics* (Kluwer, Dordrecht).

Morrison, G., and D. R. Fearn, 2000, "The influence of Rayleigh number, azimuthal wave number and inner core radius on $2\frac{1}{2}$D hydromagnetic dynamos," Phys. Earth Planet. Inter. **117**, 237–258.

Olson, P., U. Christensen, and G. A. Glatzmaier, 1999, "Numerical modeling of the geodynamo: Mechanisms of field generation and equilibration," J. Geophys. Res. **104**, 10383–10404.

Parker, E. N., 1955, "Hydromagnetic dynamo models," Astrophys. J. **122**, 293–314.

Pedlosky, J., 1979, *Geophysical Fluid Dynamics* (Springer, New York).

Ponomarenko, Y. B., 1973, "On the theory of hydromagnetic dynamos," Zh. Prikl. Mekh. Tekh. Fiz. #6, 47–51 [J. Appl. Mech. Tech. Phys. **14**, 775–778 (1973)].

Ricard, Y., M. Richards, C. Lithgow-Bertolloni, and Y. LeStunff, 1993, "A geodynamic model of mantle density heterogeneity," J. Geophys. Res. **98**, 21859–21909.

Roberts, P. H., 1968, "On the thermal instability of a rotating-fluid sphere containing heat sources," Philos. Trans. R. Soc. London, Ser. A **263**, 93–117.

Roberts, P. H., 1972, "Kinematic dynamo models," Philos. Trans. R. Soc. London, Ser. A **272**, 663–703.

Roberts, P. H., and G. A. Glatzmaier, 2000, "A test of the frozen flux approximation using geodynamo simulations," Philos. Trans. R. Soc. London, Ser. A **358**, 1109–1121.

Roberts, P. H., and T. H. Jensen, 1993, "Homogeneous dynamos: Theory and practice," Phys. Fluids B **5**, 2657–2662.

Roberts, P. H., and A. M. Soward, 1972, "Magnetohydrodynamics of the Earth's core," Annu. Rev. Fluid Mech. **4**, 117–152.

Roberts, P. H., and A. M. Soward, 1978, eds., *Rotating Fluids in Geophysics* (Academic, New York).

Roberts, P. H., and K. Stewartson, 1975, "On double-roll convection in a rotating magnetic system," J. Fluid Mech. **68**, 447–466.

Roberts, P. H., and M. Stix, 1971, *The Turbulent Dynamo. A Translation of a Series of Papers by F. Krause, K.-H. Rädler and M. Steenbeck* (Report TN/IA-60, National Center for Atmospheric Research, Boulder, Colorado).

Rüdiger, G., 1989, *Differential Rotation and Stellar Convection: Sun and Solar-type Stars* (Gordon and Breach, New York).

Sakuraba, A., and M. Kono, 1999, "Effect of the inner core on the numerical solution of the magnetohydrodynamic dynamo," Phys. Earth Planet. Inter. **111**, 105–121.

Sarson, G. R., 2000, "Reversal models from dynamo calculations," Philos. Trans. R. Soc. London, Ser. A **358**, 921–942.

Sarson, G. R., and C. A. Jones, 1999, "A convection driven geodynamo reversal model," Phys. Earth Planet. Inter. **111**, 3–20.

Sarson, G. R., C. A. Jones, and A. W. Longbottom, 1997, "The influence of boundary region heterogeneities on the geodynamo," Phys. Earth Planet. Inter. **101**, 13–32.

Sarson, G. R., C. A. Jones, and A. W. Longbottom, 1998, "Convection-driven geodynamo models of varying Ekman number," Geophys. Astrophys. Fluid Dyn. **88**, 225–259.

Song, X., and P. Richards, 1996, "Seismological evidence for differential rotation of the Earth's inner core," Nature (London) **382**, 221–224.

Souriau, A., 1998, "New seismological constraints on differential rotation of the inner core from Novaya Zemlya events recorded at DRV, Antarctica," Geophys. J. Int. **134**, F1–F5.

Soward, A. M., 1972, "A kinematic theory of large magnetic Reynolds number dynamos," Philos. Trans. R. Soc. London, Ser. A **272**, 431–462.

Soward, A. M., 1974, "A convection-driven dynamo I. Weak-field case," Philos. Trans. R. Soc. London, Ser. A **275**, 611–651.

Soward, A. M., 1990, "A unified approach to a class of slow dynamos," Geophys. Astrophys. Fluid Dyn. **53**, 81–107.

Stacey, F. D., 1992, *Physics of the Earth*, 3rd ed. (Brookfield, Brisbane, Australia).

Steenbeck, M., and F. Krause, 1966, "The generation of stellar and planetary magnetic fields by turbulent dynamo action," Z. Naturforsch. A **21A**, 1285–1296. (English translation in Roberts and Stix, 1971).

Stevenson, D. J., 1984, "The energy flux number and three types of planetary dynamo," Astron. Nachr. **305**, 257–264.

Stevenson, D. J., T. Spohn, and G. Schubert, 1983, "Magnetism and thermal evolution of the terrestrial planets," Icarus **54**, 466–489.

Stewartson, K., 1957, "On almost rigid rotations," J. Fluid Mech. **3**, 17–26.

Stewartson, K., 1966, "On almost rigid rotations, Part 2," J. Fluid Mech. **26**, 131–144.

Stieglitz, R., and U. Müller, 2000, "Experimental demonstration of a homogeneous two-scale dynamo," Phys. Fluids (to be published).

St. Pierre, M. G., 1993, in *Theory of Solar and Planetary Dynamos*, edited by M. R. E. Proctor, P. C. Matthews, and A. M. Rucklidge (Cambridge University, Cambridge, England), pp. 295–302.

St. Pierre, M. G., 1996, "On the local nature of turbulence in Earth's outer core," Geophys. Astrophys. Fluid Dyn. **83**, 293–306.

Su, W., A. M. Dziewonski, and R. Jeanloz, 1996, "Planet within a planet: Rotation of the inner core of the Earth," Science **274**, 1883–1887.

Taylor, J. B., 1963, "The magnetohydrodynamics of a rotating fluid and the Earth's dynamo problem," Proc. R. Soc. London, Ser. A **274**, 274–283.

van Dyke, M., 1964, *Perturbation Methods in Fluid Mechanics* (Academic, New York).

Vanyo, J. P., 1991, "A geodynamo powered by luni-solar precession," Geophys. Astrophys. Fluid Dyn. **59**, 209–234.

Velímský, J., and C. Matyska, 2000, "The influence of adiabatic heating/cooling on magnetohydrodynamic systems," Phys. Earth Planet. Inter. **117**, 197–207.

Verhoogen, J., 1961, "Heat balance of the Earth's core," Geophys. J. R. Astron. Soc. **4**, 276–281.

Vidale, J. E., and P. S. Earle, 2000, "Fine-scale heterogeneity in the Earth's inner core," Nature (London) **404**, 273–275.

Walker, M. R., and C. F. Barenghi, 1999, "Nonlinear magnetoconvection and the geostrophic flow," Phys. Earth Planet. Inter. **111**, 35–46.

Zatman, S., and J. Bloxham, 1997, "Torsional oscillations and the magnetic field within the Earth's core," Nature (London) **388**, 760–763.